Cobalt(III) Corroles as Electrocatalysts for O2 Reduction: Reactivity of a Monocorrole, Biscorroles, and Porphyrin–Corrole Dyads

Laurent Fremond

Catalysis of the Electroreduction of Dioxygen by Cobalt(III) Corrole.

Reactivity of Monocorrole, Biscorrole and Porphyrin–Corrole Dyads.

A Dissertation

Presented to

the Faculty of the Department of Chemistry

University of Houston

In Partial Fulfillment

of the Requirements for the Degree of

Doctor of Philosophy

By

Laurent Frémond

August 2007

Catalysis of the Electroreduction of Dioxygen by Cobalt(III) Corrole.

Reactivity of Monocorrole, Biscorrole and Porphyrin−Corrole Dyads.

_____

Laurent Frémond

Approved:

_____

Dr. Karl M. Kadish, Chairman

_____

Dr. Xiaolian Gao

_____

Dr. Randolph P. Thummel

_____

Dr. Roman S. Czernuszewicz

_____

Dr. Arnold M. Guloy

_____

Dr. John L. Bear
Dean, College of Natural Sciences and Mathematics

Acknowledgements

I would like to thank Professor *Karl M. Kadish* and Professor *Roger Guilard* for giving me the opportunity to work on this research project. I greatly appreciated the freedom I had in the execution of the project.

I would like to thank Dr. *Fabien Burdet*, Dr. *Claude Gros* and Dr. *Jean-Michel Barbe* from the Université de Bourgogne for synthesizing the compounds whose studies are described in this dissertation.

I am also thankful to Dr. *Zhongping Ou* and Dr. *Jianguo Shao* for their initial contribution to the project contained within this dissertation.

Professor *Fred C. Anson* and Dr. *Shunnian Shi* from the Californian Institute of Technology are also acknowledged for helpful discussions.

I am also thankful for financial support provided by the Robert A. Welch Foundation.

Finally, I want to thank all the members of the laboratory for the valuable services they provided. I am in particular grateful to *Rachel*, *Minh*, *Rojer*, *Swarna*, *Wenbo*, *Ou*, *Shao* and *Eric*. It was a real pleasure to know you.

Catalysis of the Electroreduction of Dioxygen by Cobalt(III) Corrole.

Reactivity of Monocorrole, Biscorrole and Porphyrin–Corrole Dyads.

A Dissertation

Presented to

the Faculty of the Department of Chemistry

University of Houston

In Partial Fulfillment

of the Requirements for the Degree of

Doctor of Philosophy

By

Laurent Frémond

August 2007

Abstract

A series of Co(III) corrole complexes were tested as catalysts for the electroreduction of dioxygen to water. Cyclic voltammetry and rotating ring–disk electrode voltammetry were both used to examine the catalytic activity of the cobalt complexes in acidic media. Altogether twenty-nine related compounds were examined.

A simple monocorrole represented as $(Me_4Ph_5Cor)Co$, a face-to-face biscorrole complex, $(BCY)Co_2$, linked by an anthracene (A), biphenylene (B), 9,9-dimethylxanthene (X), dibenzofuran (O) or dibenzothiophene (S) bridge and a face-to-face porphyrin–corrole, $(PCY)Co_2$, containing a Co(II) porphyrin (P) and a Co(III) corrole (C) linked by one of the above rigid spacers (with Y = A, B, X, O) provided a direct four-electron pathway for the reduction of O_2 to H_2O.

The catalytic reactivity of seven heterobinuclear cofacial porphyrin–corrole complexes (PCY)MClCoCl, M being either an iron(III) or manganese(III) ion were examined and compared on one hand to related dyads with a single Co(III) corrole macrocycle linked to a free-base porphyrin with the same set of linking bridges, $(PCY)H_2Co$, and on the other hand to dicobalt porphyrin–corrole dyads having the formula $(PCY)Co_2$. The data indicates that the $E_{1/2}$ values where electrocatalysis is initiated is related to the initial site of electron transfer, which is the Co(III)/Co(II) porphyrin reduction process in the case of $(PCY)Co_2$ and the Co(IV)/Co(III) corrole reduction in the case of $(PCY)MnClCoCl$, $(PCY)FeClCoCl$ and $(PCY)H_2Co$. The overall data also suggests that the catalytically active form of the biscobalt dyad in $(PCY)Co_2$ contains a Co(II) porphyrin and a Co(IV) corrole.

Finally, a series of dicobalt cofacial porphyrin–corrole dyads bearing substituents at the *meso* positions of the corrole ring were tested for the electroreduction of dioxygen. The examined compounds are represented as $(PMes_2CY)Co_2$, where Y = 9,9-dimethylxanthene (X), dibenzofuran (O), or diphenylether (Ox). The catalytic behavior of the three investigated cofacial porphyrin–corrole dyads was compared to two cobalt corrole complexes possessing different *meso*-substituents, $(F_5PhMes_2Cor)Co$ and $(TPFCor)Co$ with F_5PhMes_2Cor = 10-(pentafluorophenyl)-5,15-bis(2,4,6-trimethylphenyl)corrole and TPFCor = 5,10,15-tris(pentafluorophenyl)corrole, respectively. The overall data shows that *meso*-substitution of porphyrin-corrole dyads disfavors the four-electron pathway and a Co(IV)/Co(III) corrole reduction process is involved in the reduction of dioxygen.

Table of Contents

Title   **Page**

Abbreviations and Symbols

A electrode area (cm^2)

BPPG   basal-plane pyrolytic graphite

B   biscorrole

C^* bulk oxygen concentration ($mol\ dm^{-3}$)

C   general notation for trianionic corrole macrocycle

CV   cyclic voltammetry

D diffusion coefficient of O_2 ($cm^2\ s^{-1}$)

DP   diporphyrin

EPPG   edge-plane pyrolytic graphite

Et   ethyl group

E applied electrode potential measured with respect to the saturated calomel electrode (SCE)

E^0 standard potential (V)

$E_{1/2}$ half-wave potential (V)

F Faraday constant (96,485 C eq^{-1})

i current (μA)

i_{Lev} Levich current (μA)

i_{lim} limiting current (μA)

i_R ring current (μA)

i_D disk current (μA)

j	current density (mA cm^{-2})
j_{lim}	limiting current density (mA cm^{-2})
j_k	kinetic current density (mA cm^{-2})
k	pseudo-first order rate constant for the catalyzed reaction
k^0	heterogeneous electron transfer rate constant (cm s^{-1})
n	number of electrons exchanged per molecule of O$_2$ reduced
n_{app}	apparent number of electrons exchanged per molecule of O$_2$ reduced
Me	methyl group
OEP	2,3,7,8,12,13,17,18-octaethylporphyrin dianion
ORR	oxygen reduction reaction
P	general notation for dianionic porphyrin macrocycle
PC	porphyrin–corrole
Ph	phenyl group
RDE	rotating disk electrode
RRDE	rotating ring–disk electrode
SCE	saturated calomel electrode
TPP	5,10,15,20-tetraphenylporphyrin dianion
α	transfer coefficient for O$_2$ reduction
Γ	surface concentration (mol cm^{-2})
ν	kinematic viscosity (cm^2 s^{-1})
ω	rotation rate of the electrode (rad s^{-1})

List of Figures

xviii

List of Tables

Chapter 1: Introduction

The molecular oxygen reduction reaction (ORR) is one of the most important reactions in electrochemical energy conversion[1] (such as hydrogen-oxygen fuel cells and metal-air batteries) and biological energy conversion.[2] This reaction provides the maximum energy when the oxygen molecule is directly reduced to water (eq. 1). An ideal electrocatalyst for fuel cell applications should reduce oxygen by four electrons directly to water in acidic media (eq. 1) at a potential near the thermodynamic value of 1.23 V and avoid formation of potentially destructive intermediates such as superoxide or hydrogen peroxide (eq. 2). A platinum-based oxygen cathode in a fuel cell has a working potential below 0.8 V so that there is a 400 mV potential loss. This large overpotential loss has generally been attributed to the adsorption of high-energy reaction intermediates, mainly Pt-OH,[3] which slow down the overall reaction.[4] The inhibition of O_2 reduction caused by OH^- adsorption on Pt is still the most limiting factor in the energy conversion efficiency of the proton exchange membrane fuel cell (PEMFC).

$$O_2 + 4H^+ + 4e^- \rightleftharpoons 2H_2O \qquad E^0 = 1.23 \text{ V} \qquad \text{(eq. 1)}$$

$$O_2 + 2H^+ + 2e^- \rightleftharpoons H_2O_2 \qquad E^0 = 0.68 \text{ V} \qquad \text{(eq. 2)}$$

From the catalytic point of view, the ORR on a Pt electrode has attracted the most attention because Pt and Pt-alloys are still the most active catalysts for low-temperature fuel cells. Significant research efforts are actively pursuing a better catalyst for the ORR, or trying to reduce the amount of Pt catalyst needed for fuel cell operation. Many kinds of catalysts such as nanoparticles,[5] inorganic and organometallic complexes,[6] transition metal oxides,[7] alloys,[8-10] enzymes,[11-13] quinones,[14-16] pyrazine derivatives[17] and viologens[18] have been investigated with a view toward increasing the efficiency of the electrochemical reduction of O_2. Among these catalysts, metal complexes with

2

macrocyclic ligands such as porphyrins and phthalocyanines that contain four nitrogen donors (i.e., metal-N_4 chelates), adsorbed on carbon and heat treated, are expected to be alternates to the conventional carbon-supported platinum catalyst[19] and a great deal of effort is focused on understanding mechanistic aspects of the electrocatalytic reduction of dioxygen by these molecular catalysts.[20-25]

The first report of a metal macrocyclic complex as an oxygen reduction catalyst was made by Jasinski in 1964.[26] He observed that cobalt phthalocyanine dispersed on graphite was an effective catalyst for dioxygen reduction in alkaline solution. Since that time, a wide variety of macrocyclic complexes have been studied as possible electrocatalysts for the reduction of O_2.[6] Cobalt and iron derivatives have attracted the greatest attention. These catalysts have been observed to reduce O_2 to H_2O_2 and/or H_2O. In all known examples of monomeric catalysts, H_2O_2 is either the final product or an intermediate in the formation of H_2O. Until recently, the direct four-electron reduction of O_2 to H_2O has only been observed for dimeric dicobalt cofacial porphyrins which reduce oxygen at very positive potentials without H_2O_2 formation.[27]

The catalysis of multielectron redox reactions involving small gaseous molecules such as O_2 is extraordinary challenging from a kinetic point of view despite the fact that the thermodynamic potentials for the overall multielectron change may be favorable. In nature, metalloenzymes efficiently transform dioxygen, nitrogen or hydrogen during multielectron redox reactions. For instance, cytochrome c oxidases (cyt. c) [Enzyme Commission number E.C. 1.9.3.1], which are the terminal enzymes of the respiratory chains of both eukaryotic mitochondria and bacteria,[2,28] catalyze the four-electron, four-

proton reduction of molecular oxygen to water (eq. 3) without releasing one-electron or two-electron reduced products ($O_2^{-\bullet}$ and H_2O_2, respectively).[2]

$$4\text{cyt. } c \text{ Fe(II)} + 4\text{H}^+ + O_2 \rightarrow 4\text{cyt. } c \text{ Fe(III)} + 2H_2O \qquad \text{(eq. 3)}$$
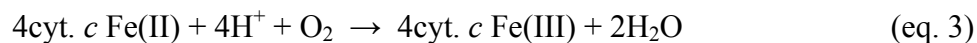
Large membrane-bound metalloenzymes such as cytochrome c oxidases harness the free energy from oxygen reduction to pump protons across the cytoplasmic or mitochondrial membranes.[28] The resulting proton concentration and electrostatic potential gradient generated across the membranes drive the synthesis of ATP (adenosine triphosphate),[2,28] the universal energy source for many cellular processes. Heme-copper oxidases catalyze 95% of molecular oxygen reduction in the biosphere.[29] Understanding the structure and function of this enzyme superfamily has been the focus of intense biochemical, spectroscopic,[30] X-ray crystallographic,[31-33] and biomimetic modeling studies.[2,27,30,34-37] The X-ray structures of cytochrome c oxidases have revealed that the catalytic site of the enzyme is a bimetallic complex of heme a and Cu (Fe_{a3}/Cu_B) (Figure 1-1).

A number of synthetic Fe_{a3}/Cu_B analogues have been synthesized to mimic the coordination environment of the Fe/Cu core as well as the catalytic function of the four-electron reduction of O_2.[30,37] The use of models that mimic a protein active site (prosthetic group) is normally prompted by the desire to eliminate any influence of the polypeptide backbone surrounding the active site in real biological molecules, which may obscure its physico-chemical properties. The first synthetic analogue for the oxygen binding site in cytochrome c oxidases was reported by Collman et $al.$[38] The authors also
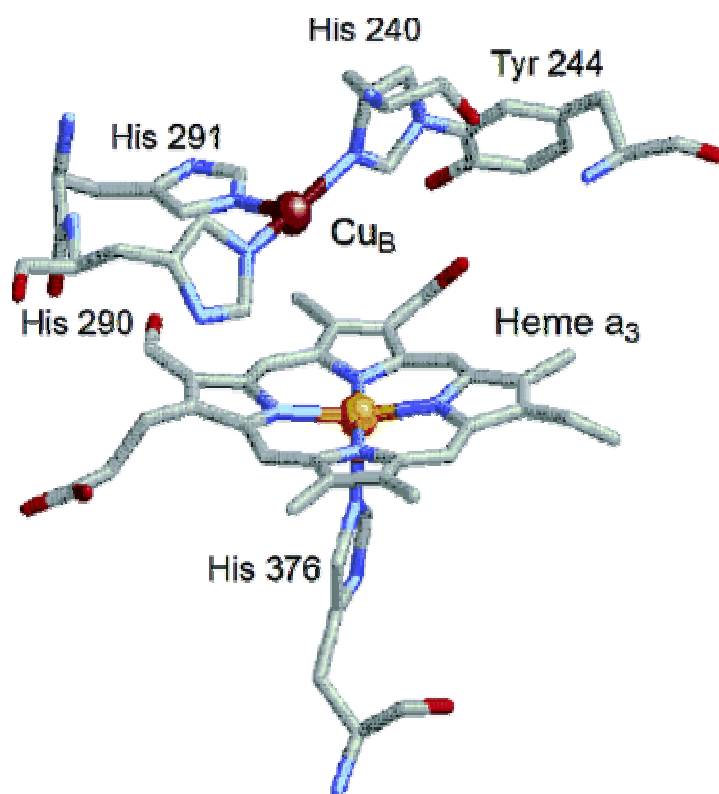
Figure 1-1. Structure of the fully reduced (heme a_3/Cu_B) active site of bovine cytochrome *c* oxidase. The O_2 binding and reduction site of cytochrome *c* oxidase contains a high-spin histidine-ligated heme (heme a_3) and a tricoordinated copper atom (Cu_B) in close proximity, Fe…Cu = 5.19 Å. (Reproduced from ref. 32).

reported a functional model of the enzyme that consisted of a copper(I) complex covalently bound above a cobalt(II) porphyrin[36] or an iron(II) porphyrin[29,39,40] in a well-defined geometry. The model compounds catalyze the selective and complete four-electron, four-proton conversion of dioxygen to water at pH 7.3 without releasing partially reduced peroxide (or superoxide) intermediates. The mechanism by which cytochrome c oxidase effects the four-electron reduction of O_2 to water without releasing the two-electron reduced species (H_2O_2) has yet to be understood. Comparison of the catalytic reactivities of the biomimetic complexes in the FeCu and Cu-free forms indicate that Cu does not significantly affect the turnover frequency or the stability of the catalyst and does not improve catalysis.[40-43] The O_2 binding to Fe at one end and to Cu at the other is not necessary, and only the iron porphyrin itself has been reported to be essential for the four-electron reduction of O_2.[37]

It has been shown that metallo-diporphyrins are potentially good functional models of cytochrome c oxidases[27,37,44,45] since dicobalt bisporphyrins efficiently electrocatalyze the direct four-electron reduction of O_2 to water[27,34] as well as π-stacked monocobalt porphyrins adsorbed on graphite electrodes.[46-51] The first simplified functional model of cytochrome c oxidases with activity as a four-electron catalyst, (FTF4)Co$_2$ where FTF4 = face-to-face porphyrin dimer with linking groups of four atoms, was the subject of many studies devoted to understand the key steps of the catalytic reduction of dioxygen.[52] Available evidence supports the idea that the catalytic reaction pathway involves O_2 binding in the well-defined cavity between the cofacial metalloporphyrin and undergoes reduction without the intermediate release of H_2O_2 from the cavity.[34] Another class of efficient four-electron dioxygen reduction catalysts includes complexes of singly linked

dicobalt cofacial bisporphyrins, occasionally referred to as "pillared" diporphyrins (DP) where the two macrocycles are bridged by anthracene (DPA) or by biphenylene (DPB).[34,53-55] More recently, cofacial bisporphrins anchored by xanthene (DPX) and dibenzofuran (DPD) pillars were examined.[56-58] The direct four-electron reduction of dioxygen by these systems is based on the ability of the bridge to provide a bimetallic cleft of proper size and flexibility (Pacman effect) to efficiently accommodate reaction intermediates during catalysis.[59] In addition, cofacial Pacman porphyrins containing one cobalt and one Lewis acidic metal were prepared and studied.[60,61] Among some of them, (DPA)CoLu(acac), (DPB)CoLu(acac) and (DPA)CoSc(OH) where Lu(III) or Sc(III) replace Co(III), have shown to promote the direct reduction of dioxygen to water.[61]

One large drawback of the bisporphyrin systems, in addition to the multi-step, high-cost and tedious syntheses of the bimetallic complexes, is the fact that the mixed-valent Co(II)/Co(III) species, is catalytically active toward O_2 reduction, needs to be chemically or electrochemically generated *via* a one-electron oxidation of the starting biscobalt(II,II) species. Therefore, the synthesis of cofacial dimers leading directly to mixed-valence Co(II)/Co(III) complexes represents a challenge.

The chemistry of corroles has been considerably developed during the past fifteen years. This interest stems from their ability to coordinate metal ions in higher oxidation states than porphyrins due to the reduced size of the macrocyclic cavity compared to porphyrins and the presence of three NH groups as compared to two in the porphyrins. At this time more than twenty metal ions have been inserted into the corrole cavity.[62] Some metallocorroles have been shown to possess catalytic activity for epoxidation,[63] cyclopropanation[64] or aerobic oxidations.[65] However, their catalytic behavior towards the

reduction of dioxygen had not been examined in detail. To understand the effect of corrole macrocyles on the multielectron reactivity of dicobalt cofacial systems towards dioxygen, Guilard and coworkers have synthesized a series of cobalt(III) corrole complexes in which the nature and the length of the macrocycle-macrocycle connectivity is varied (Figure 1-2).[66-70]
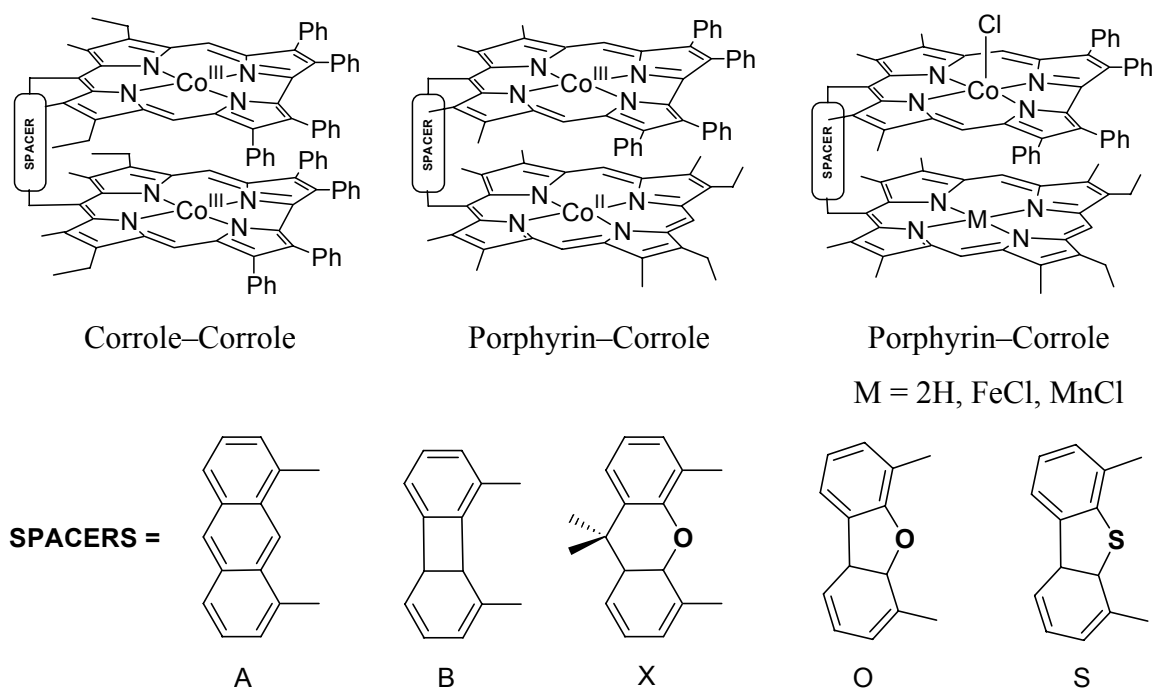
Figure 1-2. Structures of biscorroles and porphyrin–corroles with different spacers.

The main difference between the cobalt corroles and previously studied cobalt porphyrins is the oxidation state of the metal ion. The uncharged mono- and bisporphyrins contain Co(II) ions while the neutral porphyrin-corrole dyads, contain a Co(III) corrole linked to a Co(II) porphyrin. In contrast, the biscorrole dyads contain only Co(III) ions. Early studies from the Guilard/Kadish group indicated that the mixed valent

Co(II)/Co(III) porphyrin-corrole dyad (PCA)Co$_2$ (A = anthracenyl bridge) coordinates strongly O$_2$ in air-saturated organic solution to give a μ-superoxo adduct at low temperature as evidenced by its fifteen-line ESR spectrum.[71] A similar dicobalt face-to-face anthracenyl bridged bisporphyrin, (DPA)Co$_2$,[54,72,73] is able to catalyze the four-electron electroreduction of O$_2$ in acidic media and it was of interest to examine the catalytic properties of the cobalt corrole derivatives.

Outline of the Dissertation

The aim of this dissertation is to investigate the electrochemical properties and catalytic behavior toward O$_2$ of cobalt corrole as well as biscorrole and porphyrin–corrole systems covalently linked by a rigid spacer in a cofacial configuration. The nature of the bridge, the effect of the substituents and the influence of both the macrocycle and the metal ions and their relationship with the selectivity of the oxygen reduction are investigated.

Chapter 2 starts with a brief introduction to cobalt porphyrins and cobalt corroles and gives their main electronic and spectroscopic properties along with their binding properties in nonaqueous solutions. The second part of this chapter reviews their use for electrochemical oxygen reduction. Emphasis is placed on the reduction of O$_2$ at bare electrodes and the catalytic reduction of O$_2$ by metalloporphyrins.

Chapter 3 presents the chemicals used (solvents, supporting electrolytes) as well as the compounds which have been investigated in this thesis. The electrochemical techniques used to examine these compounds are briefly reviewed.

The discussion of the research carried out in the context of the present dissertation

starts with *Chapter 4*. Three series of cobalt(III) corroles are tested as catalysts for the electroreduction of dioxygen to water. One is a simple monocorrole represented as $(Me_4Ph_5Cor)Co$, one a face-to-face biscorrole linked by an anthracene (A), biphenylene (B), 9,9-dimethylxanthene (X), dibenzofuran (O) or dibenzothiophene (S) bridge, $(BCY)Co_2$ (with Y = A, B, X, O or S) and one a face-to-face bismacrocyclic complex, $(PCY)Co_2$, containing a Co(II) porphyrin and a Co(III) corrole also linked by one of the above rigid spacers (Y = A, B, X, or O). Cyclic voltammetry and rotating ring–disk electrode voltammetry were both used to examine the catalytic activity of the cobalt complexes in acid media.

Chapter 5 deals with the electrocatalytic reduction of dioxygen by three face-to-face linked porphyrin-corrole represented as $(PCY)H_2Co$ where Y = X, A, or B. The compounds are investigated as to their ability to catalyze the electroreduction of dioxygen in aqueous 1 M $HClO_4$ or HCl when adsorbed on a graphite electrode.

In *Chapter 6*, a series of heterobinuclear cofacial porphyrin–corrole dyads containing a Co(IV) corrole linked by one of four different spacers in a face-to-face arrangement with an Fe(III) or Mn(III) porphyrin are examined as catalysts for the electroreduction of O_2 to H_2O and/or H_2O_2 when adsorbed on the surface of a graphite electrode in air-saturated aqueous solutions containing 1 M $HClO_4$. The examined compounds are represented as $(PCY)M^{III}ClCo^{IV}Cl$ where P = a porphyrin dianion, C = a corrole trianion and Y = a biphenylene (B), 9,9-dimethylxanthene (X), dibenzofuran (O) or anthracene (A) spacer. The catalytic behavior of the seven investigated dyads in the two heterobimetallic (PCY)MClCoCl series of catalysts is compared on one hand to related dyads with a single Co(III) corrole macrocycle linked to a free-base porphyrin with the

10

same set of linking bridges, $(PCY)H_2Co$, and on the other to dicobalt porphyrin-corrole dyads of the form $(PCY)Co_2$ which are shown to efficiently electrocatalyze the four electron reduction of O_2 at a graphite electrode in acid media.

In *Chapter 7*, a series of dicobalt cofacial porphyrin–corrole dyads bearing substituents at the *meso* positions of the corrole ring are tested for the electroreduction of dioxygen to water in air-saturated aqueous solutions containing 1 M $HClO_4$. The examined compounds are represented as $(PMes_2CY)Co_2$, where Y = 9,9-dimethylxanthene (X), dibenzofuran (O), or diphenylether (Ox). The catalytic behavior of the three investigated cofacial porphyrin–corrole dyads is compared to two cobalt corrole complexes possessing different *meso*-substituents, $(F_5PhMes_2Cor)Co$ and $(TPFCor)Co$ with F_5PhMes_2Cor = 10-(pentafluorophenyl)-5,15-bis(2,4,6-trimethylphenyl)corrole and TPFCor = 5,10,15-tris(pentafluorophenyl)corrole, respectively.

Chapter 8 summarizes the important findings of this dissertation.

Chapter 2: Background

2.1 Porphyrin and Corrole Macrocycles

2.1.1 The Four-Orbital Model

Figure 2-1 shows the structures of porphyrin and corrole macrocycles whose atoms are labeled according to the IUPAC numbering system.[74,75] The geometry of the π aromatic systems of porphyrin and corrole is planar with D_{4h} and C_{2v} symmetry, respectively. Porphyrins are rigid tetrapyrrolic macrocycles that, after the loss of the inner protons, can serve as dianionic ligands (porphyrinato ligands), presenting four nitrogen atoms in a square-planar arrangement to metal ions located in their center. There are 12 positions on the peripheral porphyrin ring which can be substituted by an electron-withdrawing or electron-donating group. Generally, substitution occurs at the four identical *meso* positions (which refer to the carbon methinyl bridge), or at the eight identical β positions on the pyrrole rings, but many compounds with substitution at both positions are also known.

Corroles are "contracted porphryins", *i.e.*, they are tetrapyrrolic, fully conjugated macrocycles containing three methine bridges and one direct pyrrole–pyrrole bond (Figure 2-1). The genesis of this macrocycle is related to Johnson's approach to the synthesis of Vitamin B_{12}, because the corrole ring was proposed as a precursor of the cobalt corrin core of the B_{12} coenzyme.[76] Both porphyrins and corroles contain aromatic 18 π-systems that are in conjugation with two or one peripheral double bonds, respectively. The 18 π-system in the contracted framework of corroles is maintained by the change of the oxidation state of one nitrogen atom. Three pyrrole-type nitrogen atoms and one imine-type nitrogen atom thus line the central cavity of a corrole as compared to

13

two nitrogen atoms of each type in a porphyrin. Consequently, corroles are slightly smaller trianionic N_4-donors as compared to the dianionic N_4-donating porphyrins.
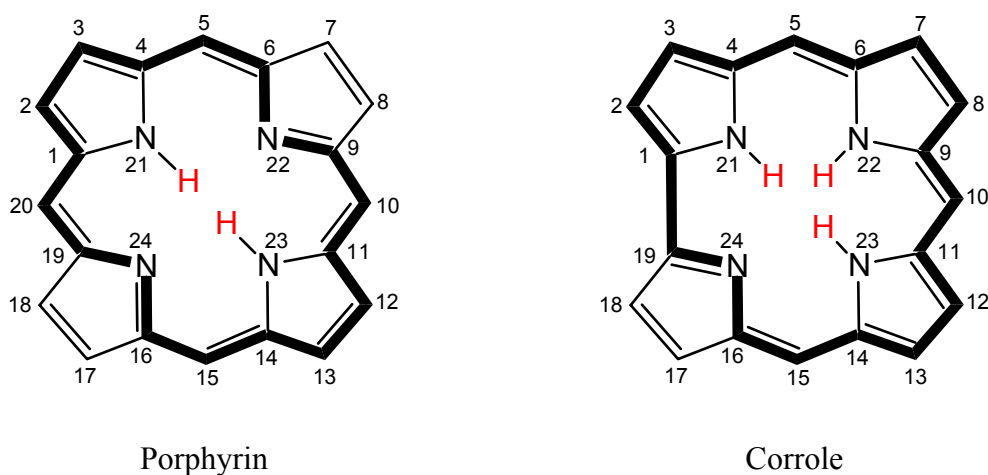
Porphyrin   Corrole

Figure 2-1. Structures of porphyrin and corrole highlighting their aromatic 18 π-electron systems.

Gouterman first proposed the four-orbital model in 1961 to explain the electronic spectra of porphyrins and metalloporphyrins (Figure 2-2).[77] The HOMOs were calculated to be two near-degenerate π orbitals (a_{1u} and a_{2u}), while the LUMOs were calculated to be a set of degenerate π^* orbitals (e_g). The a_{1u} orbital has nodes at all four *meso* positons whereas the a_{2u} orbital has high coefficients at these sites. The electronic absorption spectrum of a typical porphyrin consists of a strong transition at about 400 nm (the Soret band or B band) and a weak transition at about 550 nm (the Q band). The B and the Q bands arise from the coupling of the two π-π^* transitions (configurational interaction).[78,79] The Q bands are the result of the transition dipoles nearly canceling each other out, therefore resulting in a weaker absorbance whereas the higher energy Soret

transition results from a linear combination of the two transitions with reinforcing transition dipoles and is therefore very intense. The number and type of electron-donating or electron-withdrawing substituents at the β-pyrrole and *meso* positions of the tetrapyrrolic macrocycles can greatly affect the magnitude of the HOMO-LUMO gap.[80,81] This will also result in a shifting of the UV-visible Soret bands of the macrocycle. In addition to electronic perturbation of the substituents around the π ring system, the steric repulsion between the porphyrin ring and bulky substituents can lead to a "ruffling" of the macrocycle. The resulting deformation of the planar π-conjugated ring system will affect the optical and electrochemical properties of the macrocyle in solution as observed for zinc complexes containing substituted tetraphenylporphyrin[81] and dodecaphenyl-porphyrin.[82]

Gouterman's four-orbital model can also be applied to corrole systems (C_{2v} symmetry).[83] There are two HOMOs, a_2 and b_1, which are near-degenerate, and two LUMOs, also a_2 and b_1. The a_2 and b_1 HOMOs of the corrole are close analogues of the a_{1u} and a_{2u} porphyrin HOMOs, respectively, *i.e.*, the a_2 corrole orbital has very little to no amplitude at the *meso* positions, while the b_1 has a large amplitude at these positions, as does the porphyrin a_{2u} orbital. Comparisons between corrole and porphyrin spectra indicate that the four-orbital model can be used to interpret electronic transitions between the frontier orbitals.[84] These transitions generate intense Soret bands located at low wavelengths and relatively low intensity Q-bands at higher wavelengths.
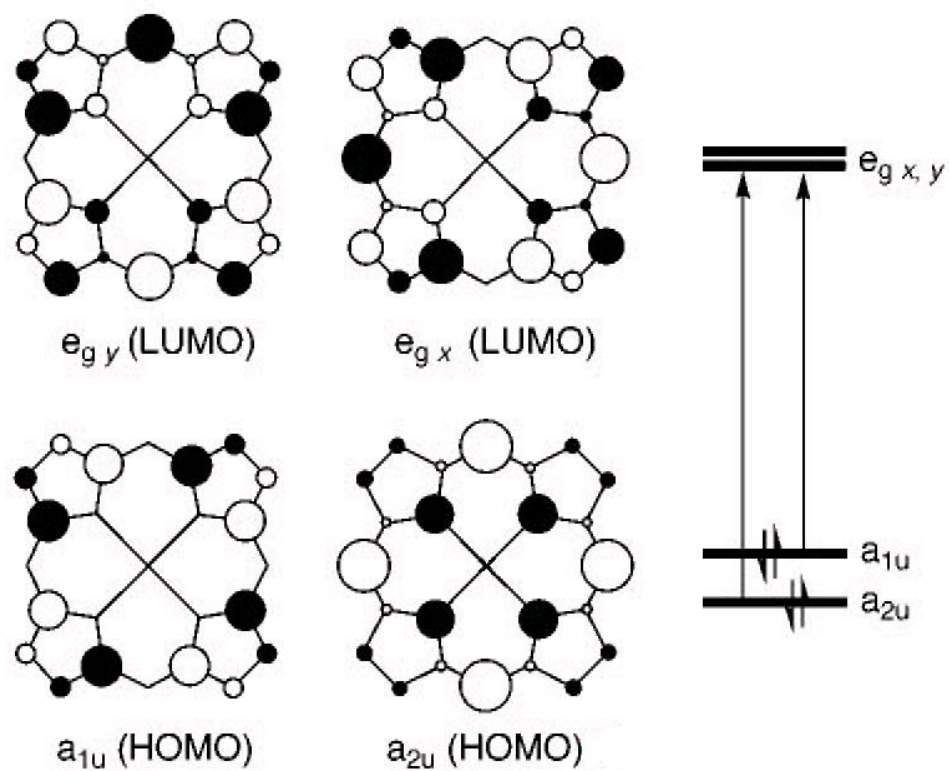
Figure 2-2. Porphyrin HOMOs (bottom row) and LUMOs (top row) in a D_{4h} symmetry.[77]

2.1.2 Redox Properties of Metal Complexes of Porphyrin and Corrole

Macrocycles

Porphyrins and corroles contain an extensive 18 π-electron aromatic system and form stable complexes with a variety of metal ions.[85] The metal complexes of these macrocycles in solution can bind one or two axial ligands and undergo metal-centered, macrocycle-centered, and/or axial ligand-centered redox reactions.[80,86,87] The measurement of redox potentials for these compounds can provide information on the frontier molecular orbitals of both tetrapyrrolic ligands as well as the degree of interaction between the metal and the π orbitals of the ligand. The measured redox potentials often depend on the type and oxidation state of the central metal ion, the nature of the macrocycle and substitution on the macrocycle periphery, as well as the type and number of axial ligands and the solvents conditions.[88] Fine tuning of the redox potentials has often been achieved by varying these factors.

In an electrochemical experiment, the HOMO represents the orbital from which an electron is removed (oxidation) and the LUMO represents the orbital to which an electron is added (reduction). Therefore, the difference between the first oxidation and first reduction potential, $E_{1/2}(\text{Ox1}) - E_{1/2}(\text{Red1})$, can be related to the HOMO-LUMO gap. This piece of data will provide an important link between electrochemical, spectroscopic and structural properties of the molecule. There are two main sites of electron transfer from/to the HOMO or LUMO levels on metal complexes of tetrapyrroles. One involves oxidation and reduction of the conjugated macrocyclic ring and results in production of π-cation radicals or π-anion radicals. The other involves electron transfer to or from the

metal ion and results in a change in the metal oxidation state.[81] For instance, the electrochemistry of tetraphenylporphyrin (TPP) or octaethylporphyrin (OEP) macrocycles indicates that both compounds are stepwise oxidized or stepwise reduced by two electrons at the π-ring system to give π-cation radicals and dications or π-anion radicals and dianions. A similar HOMO-LUMO gap of 2.25 ± 0.15 V is observed for both macrocycles and this constant separation in potentials between half-wave potentials has often been used as a diagnostic criteria to distinguish macrocycle-centered reactions from metal-centered ones.

In 1992, Kadish and coworkers[89] reported the first comprehensive study involving both the electrochemical oxidation and reduction of metallocorroles. Electrochemical studies of corroles[62] have demonstrated significant shifts in $E_{1/2}$ for reduction or oxidation of these species as compared to metalloporphyrins containing the same metal central ion. The metallocorroles are generally harder to reduce and easier to oxidize than metalloporphyrins with the same central metal ion and this is due to the fact that the formal charge on the macrocycle is -2 in the case of porphyrin and -3 in the case of corroles. The corroles in many cases will also undergo three ring-centered oxidations, giving a corrole trication as compared to only two ring-centered oxidations in the case of the analogous porphyrins, which form only dications under the same solution conditions.[62,67] The electrochemically determined HOMO-LUMO gap was measured as 2.20 ± 0.15 V for a series of 10 different octaethylcorroles which is similar to the HOMO-LUMO gap observed for planar porphyrins containing octaethylporphyrin (OEP) or tetraphenylporphyrin (TPP) macrocycle (*vide supra*).[80]

2.1.3 Cobalt Corrole and Cobalt Porphyrin Complexes

2.1.3.1 Electronic structure

The structural differences between corroles and porphyrins is reflected in their altered metal-coordination properties. The smaller trianionic corrolato ligand has a greater ability to stabilize higher central metal oxidation states than the larger dianionic porphyrinato ligand. This property has driven an intense investigation of transition metal corrole complexes. A number of different monomeric corroles and metallocorroles have been synthesized[90,91] and their electrochemical properties have also been examined extensively.[62,67,81] Cobalt corroles are by far the most studied metallocorrole complexes. Several papers relative to these derivatives have appeared in the literature,[26,62,67,70,92-97] since the pioneering work of Johnson and coworkers in the early 1970s.[76]

Due to its strong ligand field, a corrolato macrocycle stabilizes the Co(III) oxidation state whereas porphyrins stabilize cobalt atoms in the +2 oxidation state.[62,67,81] The cobalt atom in [(corrolato)$^{3-}$Co^{III}] complexes (Co^{3+} d^6) is isoelectronic with the iron atom in Fe(II) porphyrin complexes (Fe^{2+} d^6). A quantitative study of the structure and electronic properties of cobalt corroles using density functional theory showed that the Co d configuration is in the ground state $^3A_{2g}$ is $(d_{xy})^2$ $(d_{z^2})^2$ $(d\pi_1)^1$ $(d\pi_2)^1$ $(d_{x^2-y^2})^0$ (where the orbitals labeled as $d\pi_1$ and $d\pi_2$ refer to the $d_{xz} + d_{yz}$ and $d_{xz} - d_{yz}$ combinations).[98] The singlet state ($S = 0$) shows the same configuration, with an antiparallel alignement of the electrons in the last two π orbitals. This is the same ordering of spin states and the same metal d configuration as were found for Fe(II) porphyrins,[99,100] the only difference being

the smaller energy differences between the spin states of Fe porphyrin. Therefore, both spin states ($S = 0$ or 1) might be easily observed in solution for Co(III) corroles depending on the solvent nature.[95]

2.1.3.2 Cobalt(IV) corrole complexes

One important feature of tetrapyrrolic ligands is their "non-innocent", *i.e.*, redox-active nature. The large electron-rich π-systems of tetrapyrrolic ligands are readily capable of providing an electron to the central metal which reduces the formal oxidation state of the metal and generates a ligand π-cation radical. In the case of the singly oxidized cobalt(III) corrole complexes giving [(corrolato)Co]$^+$, a reversible intramolecular electron transfer, or valence tautomerism,[101] between the cobalt ion and the redox-active ligand (Figure 2-3) could generate two electronic isomers in solution (valence tautomers) with different charge distributions.
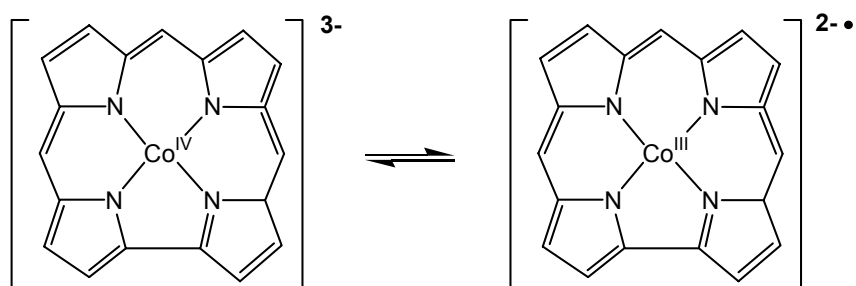
Figure 2-3. Redox equilibrium of [(corrolato)Co^{IV}]$^+$ complexes.

The oxidized cobalt complex observed may be a true Co(IV) complex with a trianionic corrolato ligand [(corrolato)$^{3-}$Co^{IV}]$^+$ or a Co(III) complex with a dianionic radical corrolato ligand [(corrolato)$^{2-•}$Co^{III}]$^+$. The type of axial ligand bound to the metal

center can change the site of electron transfer and one example is given for the case of (OEC)Co^{III} (Figure 2-4, OEC is the trianion 2,3,7,8,12,13,17,18-octaethylcorrole) and (OEC)Co^{IV}(C$_6$H$_5$) in CH$_2$Cl$_2$.[62,102] The σ-bonded complex has spin density on the cobalt d$_{yz}$ orbital (Co(IV) character) and on the macrocycle (π cation radical character).[103] The complex undergoes a Co(IV)/Co(III) transition at $E_{1/2} = -0.23$ V in CH$_2$Cl$_2$, 0.1 M TBAP, but this metal-centered process is not observed for (OEC)Co which formally contains a Co(III) ion and is oxidized to a Co(III) π-cation radical as opposed to a Co(IV) species under the same solution conditions.[62]

(OEC)Co   (Me$_6$Et$_2$Cor)Co
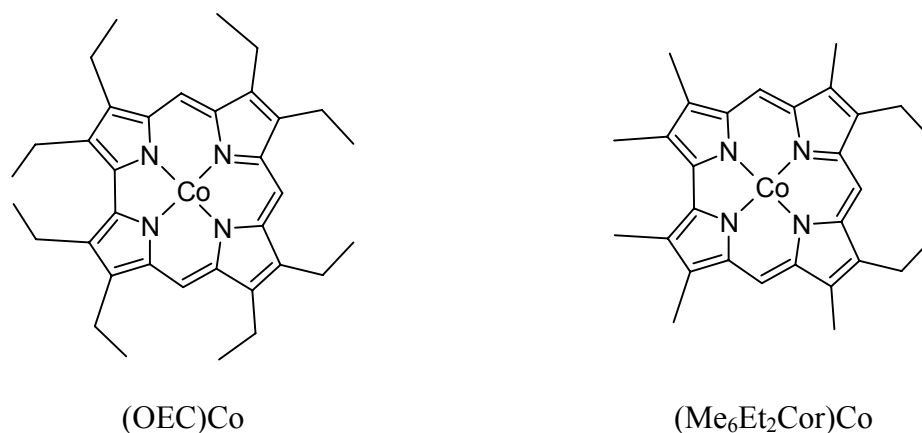
Figure 2-4. Structures of alky-substituted cobalt corroles.

Other examples of high-valent cobalt(IV) corroles have been reported[70,97,104] and the structure of one of the derivatives determined by X-ray diffraction.[70] Electrochemistry experiments, carried out on a large variety of cobalt metallocorroles, have demonstrated that the +4 oxidation state is easily available and readily stabilized by the binding of anionic halides (see below).

2.1.3.3 π-π interaction in supramolecular dimers and pyridine-binding properties of cobalt(III) corroles

Most radicals dimerize to form a two-center, two-electron bond. However, many delocalized radicals associate to form cofacially aligned π-dimers or π-stacks in condensed phases.[105] The principal driving force for π-dimerization arises from orbital overlap of SOMOs with π-symmetry which are delocalized over several atoms, and the strength of π-dimerization tends to be low (often reversible in solution) compared to σ-bond formation. The unconventional bonding in π-dimers has attracted considerable interest, and radical ion π-stacks are of central importance to a range of solid-state charge transport and magnetic phenomena.

Metallocorroles form π-stacked dimers in the solid state.[62,69,106] They are also able to form singly or doubly oxidized π-π dimers upon the abstraction of one or two electrons in CH_2Cl_2 or other noncoordinating media.[92,107,108] One example is given for the case of (OEC)M (M = Co, Ni, Cu) which exists as a monomeric species in its neutral or singly reduced forms but dimerizes after electrooxidation in CH_2Cl_2.[107] The first two oxidations of the Co, Ni, and Cu corroles involve the reversible stepwise abstraction of 1.0 electron per two (OEC)M units and lead to $[(OEC)M]_2^+$ and $[(OEC)M]_2^{2+}$, which are assigned as π-π dimers containing oxidized corrole macrocycles and divalent central-metal ions on the basis of the electrochemical and spectroscopic data.[107] The ESR spectrum of $[(OEC)Co]_2^+$ in frozen CH_2Cl_2 at 77 K has a major line at $g_\perp = 2.40$ with a weak signal at $g_\parallel = 1.89$ and is typical of a Co(II) ion in a square planar geometry. The doubly oxidized

dimer, $[(OEC)Co]_2^{2+}$, is ESR silent in CH_2Cl_2 or PhCN, thus suggesting that the two unpaired electrons of the two Co(II) ions in $[(OEC)Co]_2^{2+}$ are coupled.

The electrochemical behavior of (OEC)Co is similar to what was later reported for alkyl- and aryl-substituted Co(III) corroles.[92,108] The investigated compounds contain methyl, ethyl, phenyl, or substituted phenyl groups at the eight β-positions of the corrole macrocycle. Each cobalt corrole undergoes four reversible oxidations in CH_2Cl_2 containing 0.1 M tetra-n-butylammonium perchlorate and exists as a dimer in its singly and doubly oxidized forms. The difference in potential Δox(2–1) between the first two oxidations is associated with the degree of interaction between the two corrole units of the dimer. The largest Δox(2–1) value of the investigated compounds was obtained for $(Me_6Et_2Cor)Co$ (0.62 V) (Figure 2-5) and this can be associated with a strong interaction between the two equivalent redox centers in the singly oxidized compound.[108]

A detailed electrochemical study of dimer formation as a function of solvent and corrole macrocyclic structure was reported.[92] A series of alkyl- and aryl-substituted cobalt(III) corroles with four, five or seven β-substituted phenyl groups were examined in CH_2Cl_2, PhCN, THF, and pyridine (py) which has the largest donor number of 33.1 among the four investigated solvents. The interaction between the two macrocycles in the monooxidized dimer depends on the solvent donicity, the specific substituents on the macrocycle, and the axial binding strength of the complex. The formation of dimers occurs more easily in solvents having the lowest donor numbers (e.g., CH_2Cl_2 and PhCN)
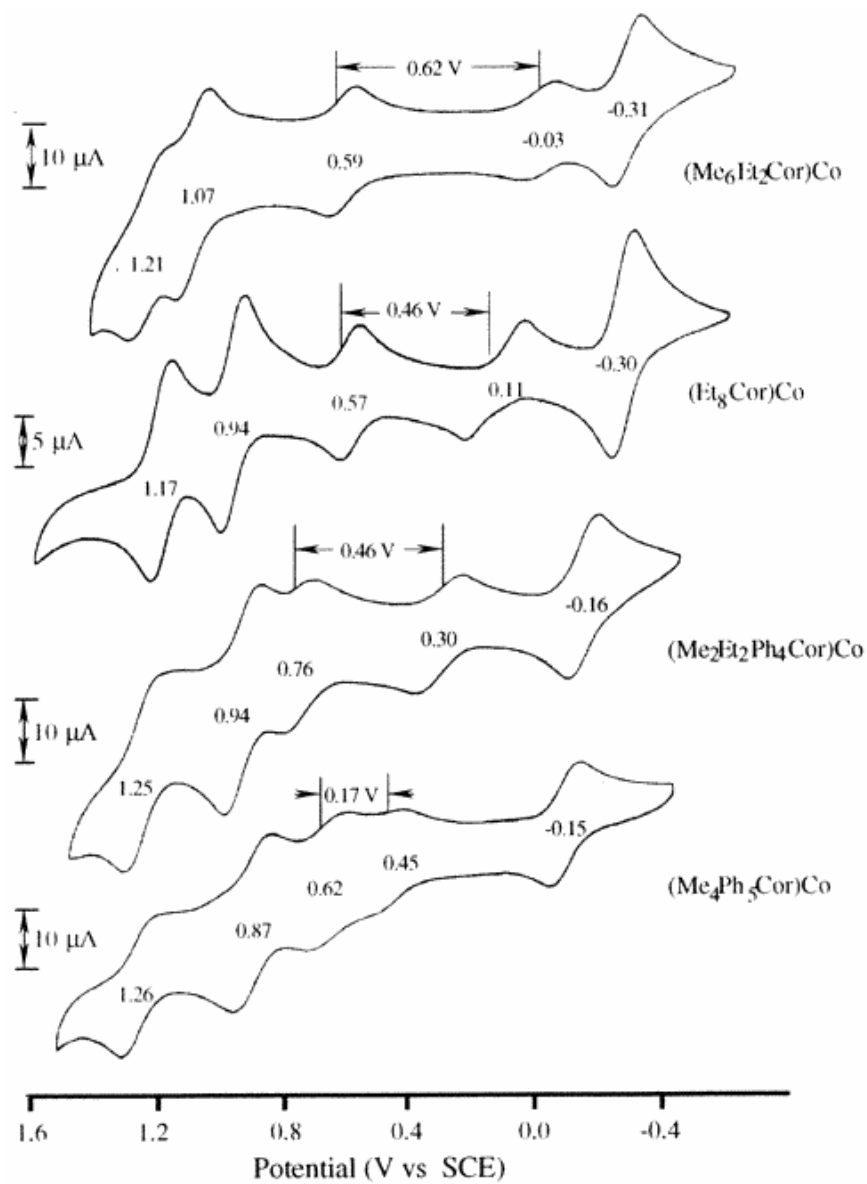
Figure 2-5. Cyclic voltammograms of 2.0×10^{-3} M (Me$_6$Et$_2$Cor)Co, 3.0×10^{-3} M (Et$_8$Cor)Co, 2.0×10^{-3} M (Me$_2$Et$_2$Ph$_4$Cor)Co, and 1.5×10^{-3} M (Me$_4$Ph$_5$Cor)Co in CH$_2$Cl$_2$, 0.1 M TBAP. (Reproduced from ref. 108).

with the only exception being the cobalt corrole compound (Me$_4$Ph$_5$Cor)Co having a phenyl group at the 10-*meso* position of the macrocycle which might hinder dimerization of the singly oxidized complex. In contrast, little or no dimerization of the same series of corroles occured in solvents with higher donor numbers (e.g., THF or pyridine), and this was explained in the case of pyridine by the formation of five- and six coordinated Co(III) complexes[108] which sterically hinder the possibility of stacking. Pyridine binding constants were obtained for all examined cobalt(III) corroles by spectroelectrochemistry and the values of log K$_1$ range from 3.78 to 5.48, while log K$_2$ values range from 2.00 to 2.38.[108] The bispyridine adduct of the neutral compounds in pyridine undergoes a reversible ring-centered one-electron oxidation to form a corrole cation radical which retains the two bound pyridine axial ligands. In contrast, the metal-centered reduction of the corroles was irreversible in pyridine and proceeds via the unreduced monopyridine adduct to give an unligated cobalt(II) corrole as the final reduction product.[92]

2.1.3.4 Reactions of cofacial cobalt biscorroles and porphyrin-corroles with pyridine, chloride and CO

The electrochemistry, ligand binding reactions, and spectroscopic properties of biscorroles and porphyrin-corrole dyads containing redox-active metal centers (see Figure 1-2 in Chapter 1) have been examined by Guilard and Kadish.[67,69-71,92,93,95-97,104,108-111] These have included bis-copper,[95] bis-nickel,[110] and bis-cobalt derivatives.[109,111] The synthesis and characterization of free-base porphyrins linked to a cobalt(III) corrole[104,112] and heterobimetallic dyads containing iron(III) or manganese(III) porphyrins linked in a face-to-face arrangement with a cobalt(IV) corrole have also been

reported.[97,104] The cobalt complexes are represented as (BCY)Co$_2$, (PCY)Co$_2$, (PCY)H$_2$Co^{III}, and (PCY)MClCo^{IV}Cl where BC = biscorrole, PC = porphyrin-corrole, M = Mn^{III} or Fe^{III}, and Y is a bridging group, either biphenylenyl (B), 9,9-dimethylxanthenyl (X), anthracenyl (A), or dibenzofuranyl (O) (Figure 1-2).

2.1.3.4.1 pyridine binding

The electrochemistry and thin-layer spectroelectrochemistry of the above (BCY)Co$_2$, (PCY)Co$_2$, (PCY)H$_2$Co^{III} and (PCY)MClCo^{IV}Cl dyads have been examined in pyridine,[67,97,109,111] a solvent known to coordinate to both the porphyrin and corrole metal centers, thus giving complexes with one to four axially bound ligands depending upon the type of metal ion in the macrocycle, the metal oxidation state, and the type of spacer linking the two macrocycles. Cobalt(III) but not cobalt(II) corrole binds pyridine, and the coordination number of Co^{III} in pyridine can be unambiguously assigned on the basis of electrochemical and spectroscopic data. An intense absorption band at 600 nm assigned to Co^{III}(py)$_2$ is observed in the UV-vis spectra of cobalt(III) corrole monomers[108] but this band is not observed for (PCB)H$_2$Co[97] which indicates that the cobalt(III) center of the dyad binds a single pyridine ligand in solution as well as in solid state, as shown by the structure of the complex.[112] In constrast, (PCX)H$_2$Co was characterized as a bispyridine adduct, (PCX)H$_2$Co(py)$_2$, in the solid state,[94] while (PCA)H$_2$Co and (PCX)H$_2$Co were shown to exist as a mixture of five- and six-coordinate cobalt(III) pyridine adducts in pyridine solutions[97] and (PCO)H$_2$Co was clearly a six-coordinate Co^{III} species in pyridine.[97] In comparison, biscobalt biscorroles and porphyrin-corrole dyads form five- and six-coordinated complexes depending on the pyridine concentration in solution. The

coordination of four pyridine molecules to the two cobalt macrocycles occurs upon going from a CH_2Cl_2/pyridine solution with 10^{-3} M pyridine to neat (12 M) pyridine in the case of (BCA)Co$_2$.[111] The pyridine binding properties of (BCB)Co$_2$, (BCO)Co$_2$, (BCX)Co$_2$ and (BCS)Co$_2$ were also examined in CH_2Cl_2/pyridine mixtures.[111] The biscorroles with shorter spacers have the two macrocycles in closer proximity to each other and thus exhibit a greater π-π interaction which results in smaller binding constants for the first ligand addition which was proposed to occur on the outside of the bismacrocycles. The same behavior is also observed for porphyrin-corroles and this is consistent with the K_1 values for pyridine binding which increase in the following order: (PCB)Co$_2$ < (PCA)Co$_2$ < (PCO)Co$_2$ for the three porphyrin-corrole dyads and (BCB)Co$_2$ < (BCS)Co$_2$ < (BCX)Co$_2$ ≈ (BCA)Co$_2$ ≈ (BCO)Co$_2$ for the five biscorrole complexes.[111]

A change in the cobalt corrole coordination number with change in the porphyrin metal oxidation state is observed both for (PCB)FeClCoCl and (PCB)MnClCoCl. The species present in pyridine are $[(PCB)Fe^{III}ClCo^{III}(py)]^+$ and $[(PCB)Mn^{III}(py)_2Co^{III}(py)]^+$, respectively. The reduction of $[(PCB)Mn^{III}(py)_2Co^{III}(py)]^+$ to $[(PCB)Mn^{II}(py)Co^{III}(py)]$ is accompanied by the appearance of a 600 nm band in the UV-vis spectra and is consistent with the addition of a second pyridine ligand to the $Co^{III}(py)$ unit of the dyad as one ligand is lost from the electrogenerated manganese(II) porphyrin, thus maintaining one pyridine ligand in the cavity. In contrast, the $[(PCB)Fe^{III}ClCo^{III}(py)]^+$ species is reduced to $[(PCB)Fe^{II}(py)_2Co^{III}(py)_2]$ which contains two pyridine ligands in the cavity.[97] In the case of the PCX, PCA and PCO derivatives, the nature of the porphyrin center (M = 2H, Fe^{III}, Fe^{II}, Mn^{III} or Mn^{II}) has no influence on the coordination number of Co^{III} which binds two pyridine ligands in solution.

2.1.3.4.2 chloride binding

The electrochemistry of Co(IV) dyads containing Mn(III) or Fe(III) porphyrins was investigated in benzonitrile and the cyclic voltammograms were generally similar to each other.[70] The reduction of (PCY)MClCoCl (M = Fe(III) or Mn(III)) in benzonitrile containing 0.1 M tetra-n-butylammonium perchlorate is followed by a rapid loss of Cl$^-$ to give the four-coordinate Co(III) corrole, which is then reoxidized to give Co^{IV}ClO$_4$ (an electrochemical EC mechanism). The dyads added to solution initially contained Co^{IV}Cl, but significant amounts of Co^{IV}ClO$_4$ could be formed prior to electron transfer, the ClO$_4{}^-$-bound species being easier to reduce than the Cl$^-$ derivative by over 300 mV.[70] Additions of TBACl to the solution result in a more reversible Co^{IV}Cl/Co^{III}Cl process between 0.09 and 0.12 V and the complete disappearance of the couple assigned to Co^{IV}ClO$_4$/Co^{III}. The Co(III)/Co(II) process is located at more negative potentials as compared to what is seen for the monomeric Co(III) macrocycle,[92,108] with the easiest metal-centered reduction being observed for dyads with the dibenzofuran (O) bridge ($E_{1/2}$ = –0.17 V) and the hardest for dyads with the biphenyl (B) bridge ($E_{1/2}$ = –0.35 V).[70] The one-electron reduction of Fe(III) to give Fe(II) is located at $E_{1/2}$ = –0.42 V (PCO) and $E_{1/2}$ = –0.44 V (PCB), respectively. In comparison, the reduction of Mn(III) to Mn(II) is located at more negative potential ($E_{1/2}$ = –0.65 V).

To further investigate the effect of Cl$^-$ on the electrode reaction of cobalt corroles, a detailed study presenting quantitative data on the binding of Cl$^-$ to both Co(IV) and Co(III) forms of the monocorrole (Me$_4$Ph$_5$Cor)Co as well as a series of three free-base porphyrin-Co(III) corrole dyads was reported.[104] The dyads are represented as (PCY)H$_2$Co (Figure 1-2) where a cobalt(III) corrole is linked to a free-base porphyrin by

28

a spacer (Y = A, X, or B). An axial binding of one or two Cl$^-$ ligands to the cobalt center of the corrole is observed for singly or doubly oxidized (PCY)H$_2$Co, *i.e.* [(PCY)H$_2$Co^{IV}]$^+$ and [(PCY$^{\bullet+}$)H$_2$Co^{IV}]$^{2+}$ respectively, with the exact stoichiometry of the reaction depending upon the spacer size and the concentration of Cl$^-$ added to solution.[104] No Cl$^-$ binding occurs for the neutral or reduced forms of the dyad, which contrasts with what is seen for the monocorrole, (Me$_4$Ph$_5$Cor)Co, where a single Cl$^-$ ligand is added to the Co(III) corrole in PhCN. The addition of one Cl$^-$ ligand to (Me$_4$Ph$_5$Cor)Co^{III} generates [(Me$_4$Ph$_5$Cor)Co^{III}Cl]$^-$ which is electrochemically oxidized to [(Me$_4$Ph$_5$Cor)Co^{IV}Cl$_2$]$^-$ in the presence of excess Cl$^-$. The doubly oxidized complex [(Me$_4$Ph$_5$Cor$^{\bullet+}$)Co^{III}]$^{2+}$, which is a Co(IV) corrole π-cation radical, can also bind two Cl$^-$ ligand in the presence of excess Cl$^-$.

1.3.4.3 CO binding

Each cobalt(III) corrole, porphyrin–corrole and biscorrole derivative was investigated as to its CO binding ability in CH$_2$Cl$_2$ by monitoring the UV−visible spectral changes as a function of the CO partial pressure.[67,108,109,111] The results of these studies indicate that each cobalt(III) center of the monocorrole, porphyrin–corrole and biscorrole coordinates with one CO molecule, thus leading to the formation of five-coordinated cobalt(III) complexes. The measured CO binding constants (log K) are 3.8 for (BCS)Co$_2$ and 3.9 (BCX)Co$_2$, and both values are comparable to the CO binding constants of (BCA)Co$_2$ and (BCB)Co$_2$ which have a log K = 3.9 and 3.6, respectively.[109] The monocorrole complex, (Me$_4$Ph$_5$Cor)Co, has a log K = 4.2.[108]

2.2. Oxygen Reduction Reaction

2.2.1 ORR in Acidic Aqueous Solutions

The complete reduction of O_2 to H_2O requires four protons and four electrons for the cleavage of two formal O−O bonds, whereas the partial reduction of O_2 to H_2O_2 requires two protons and two electrons for the cleavage of a single O−O bond. The product of the one-electron reduction of O_2, the superoxide anion, $O_2^{\bullet-}$, is highly unstable in acidic aqueous solutions where its protonated form, the peroxyl radical HO_2 (pK = 4.8),[113] decomposes to ozone, oxygen, and hydrogen peroxide.

The thermodynamic constraints on the principal pathways to the four electron reduction of oxygen in acidic media are the following[113]:

$$O_2 + 2H^+ + 2e^- \rightleftharpoons H_2O_2 \qquad E^0 = +0.68 \text{ V (NHE)}$$

$$H_2O_2 + 2H^+ + 2e^- \rightleftharpoons 2H_2O \qquad E^0 = +1.77 \text{ V (NHE)}$$

$$O_2 + 4H^+ + 4e^- \rightleftharpoons 2H_2O \qquad E^0 = +1.23 \text{ V (NHE)}$$

$$2H_2O_2 \rightleftharpoons O_2 + 2H_2O \qquad \text{(disproportionation)}$$
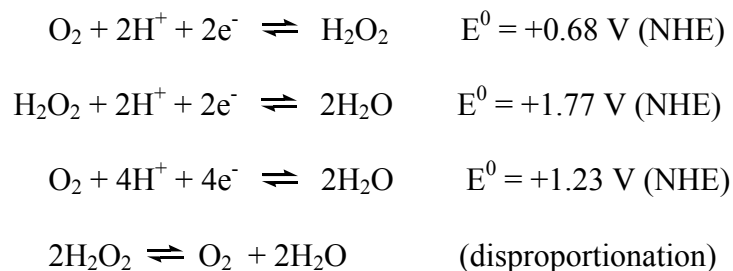
The O_2 reduction to H_2O can be accomplished indirectly in two-electron steps via hydrogen peroxide as an intermediate or directly by four electrons without H_2O_2 formation. The two-electron reduction of O_2 to H_2O_2 and the four-electron reduction of O_2 to H_2O can occur simultaneously and independently on the same electrode, as two parallel processes. The direct four electron reduction can proceed at the thermodynamic potential of +1.23 V. Consecutive two electron transfers through H_2O_2 will have a

potential governed by the first step where the standard potential is +0.68 V. A further reduction of H_2O_2 to H_2O can occur but the potential for this second step cannot exceed the thermodynamic value for its formation. H_2O_2 is a very weak acid (pK_1 = 11.6),[113] which does not lose its second proton in aqueous alkaline solutions. It is also a very powerful oxidizer (E^0 = +1.77 V) and decomposes more or less rapidly by disproportionation. When the disproportionation reaction of H_2O_2 is very fast and occurs at the surface of an electrode, the overall process is apparently the direct reduction of dioxygen to water, peroxide being an intermediate species. In terms of operating an electrochemical fuel cell, there could be a loss of more than 0.5 V in output by producing H_2O_2 as an intermediate.[114] Therefore, it is highly desirable to reduce oxygen directly to water.

Molecular oxygen is a very stable molecule and has a relatively low reactivity in spite of its high oxidizing power. Furthermore, the spin conservation principle restricts the reactions in which O_2 can participate. Dioxygen in its ground triplet state will lead to a triplet molecule when interacting with a singlet molecule.[115] However, the spin restriction can be overcome upon coordination of the O_2 molecule to a metal center which is itself paramagnetic.[116] There are now three major adsorption models in the literature[113,115] for molecular oxygen adsorption (Scheme 2-1):

- the Griffiths model in which O_2 interacts with two bonds on a single substrate atom (side-on interaction);

- the Pauling model with end-on adsorption of the oxygen molecule through a single bond (end-on interaction);

- the Yeager model, a model with two bonds interacting with two sites.

31

Griffiths   Pauling   Yeager (trans) Yeager (bridge)
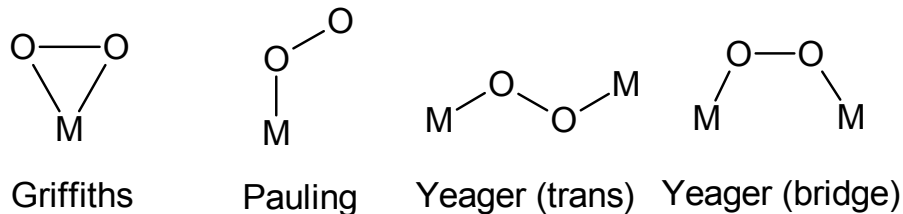
Scheme 2-1. Plausible 1:1 and 2:1 metal-dioxygen complex structures: the Griffiths model, the Pauling model, and the Yeager model (trans and bridge, respectively).

The bridge interaction in the Yeager model is likely to occur on noble metals such as Pt where O_2 is reduced to water with little or no peroxide formed. A trans configuration is likely to occur with cofacial dicobalt bismacrocycles which promote the cleavage of the O−O bond.[23]

2.2.2 ORR at Unmodified Electrodes

Despite extensive research that has been carried out in this area, a detailed mechanism of the ORR, even at Pt, is still uncertain.[4] The number of elementary steps and mechanistic routes in the reduction of O_2 to H_2O is vast, since it involves four electron transfers, four proton transfers and O−O cleavage. Adsorption of O_2 and a wide spectrum of oxygenated adsorbed intermediates probably also occur, further complicating kinetic treatment of the experimental data. Quantum mechanical calculations have been applied to determine optimal structures and adsorption energies.[117,118]

The nature and surface structure of the electrode is a fundamental aspect to consider when one or several intermediates can adsorb on the electrode surface.[119] This is

especially the case for oxygen reduction on platinum electrodes, in which four electrons are involved in the overall reduction of dioxygen to water. The high number of electrons exchanged per oxygen molecule would imply the possible existence of several adsorption intermediates, whose interaction energies with the surface will depend on the metal and its surface structure.[8]

2.2.2.1 Electrochemical reduction of oxygen at platinum

It is well-known that the ORR can proceed by a two-electron transfer pathway with the formation of hydrogen peroxide or by a four-electron process. The four-electron pathway is predominant on gold and platinum electrodes in alkaline media[120] and on platinum or platinum-based alloy electrodes in acidic media.[10,121,122]

The rotating ring-disk electrode (RRDE) technique has often been used in studies of the ORR because it provides the possibility of probing the formation of H_2O_2 accompanying oxygen reduction and therefore of determining the effective electron-transfer number, n_{eff}. The formation of H_2O_2 during the ORR at Pt-based electrodes in acid medium is presumed to occur through an alternative, parallel mechanism and is negligible at potentials outside the hydrogen adsorption region. The reaction scheme proposed by Wroblowa *et al*. has been generally accepted as the mechanism of this parallel reaction (Figure 2-6).[5]

$$k_1 \quad \text{Direct Pathway}$$

Indirect Pathway

$$O_2{}^b \xrightarrow{\text{diffusion}} O_2{}^s \underset{a_{1-}}{\overset{a_1}{\rightleftharpoons}} O_2{}^* \xrightarrow{k_2} H_2O_2{}^* \xrightarrow{k_3} H_2O$$

$$a_2 \Big\| a_{2-}$$

$$H_2O_2{}^b \xleftarrow{\text{diffusion}} H_2O_2{}^s$$
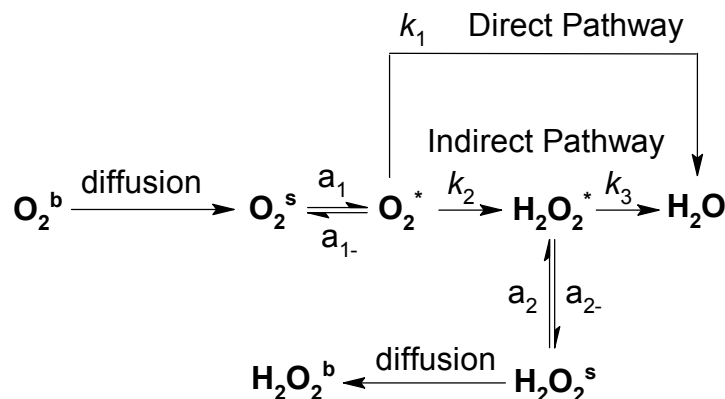
Figure 2-6. Wroblowa scheme for the pathways of the oxygen reduction reaction. The rate constants for the different steps in the scheme are indicated in the figure. b, S and * denote bulk solution, the vicinity of the electrode and the absorbed state, respectively. (Reproduced from ref. 5).

The k's and a's in Figure 2-6 are the overall rate constants for the corresponding reaction or adsorption steps, each of which may contain several elementary steps. The superscripts b, s, and * refer, respectively, to species which are in bulk solution, in the vicinity of the electrode surface, and which are adsorbed on the electrode surface. Also, it has been generally accepted that the rate-determining step in the ORR is the first electron-transfer step and that the real reaction rate is an overall result of the coupling of this step with the diffusion and adsorption of oxygen molecules.

In the so-called "peroxide pathway", as found with Hg, Au, and C electrodes, the first electroreduction step leads to the formation of a superoxide anion ($O_2{}^{\bullet-}$).[121]

$$O_2 + e^- \rightleftharpoons O_2{}^{\bullet-} \tag{eq. 4}$$

The E^0 for this reaction is –0.284 V vs NHE, well negative of the E^0 of the 4e reduction

to water, 1.23 V vs NHE. To attain the 4e$^-$ pathway to water, any hydrogen peroxide that is formed by the superoxide intermediate route would have to undergo rapid 2e$^-$ reduction to water or a decomposition to water and O_2 as the step that accomplishes O−O bond cleavage.

An alternative path (the so-called "direct pathway") involves the initial dissociative chemisorption of O_2, eq. 5, involving the splitting of the O−O bond to form adsorbed oxygen atoms (O$^•$).

$$2M + O_2 \rightleftharpoons 2MO_{ads} \qquad \text{(eq. 5)}$$

The adsorbed oxygen atoms are then electroreduced to water according to eq. 6, which actually involves a series of several elementary steps.

$$2MO_{ads} + 4H^+ + 4e^- \rightleftharpoons 2M + 2H_2O \qquad \text{(eq. 6)}$$
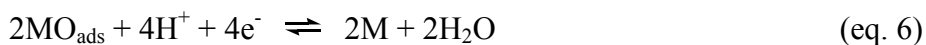
The electrolyte effects on oxygen reduction kinetics at platinum have been examined by Hsueh et al.[123] who showed that the kinetics for oxygen reduction in perchloric, phosphoric, sulfuric, or trifluoromethanesulfonic acids (all at pH = 0) and in potassium hydroxide (pH = 14) at 25°C decrease in the order KOH > H_2SO_4 ∼ CF_3SO_3H > H_3PO_4 > $HClO_4$. This order of activity reflects a negative effect of anion adsorption on ORR.[3]

2.2.2.2 Electrochemical reduction of oxygen at graphite electrodes

Carbon electrodes are of interest for electrochemical reduction of oxygen since high surface area carbon materials are used as platinum catalyst supports in fuel cell electrodes. The kinetics of O_2 reduction have been extensively investigated on glassy carbon and pyrolytic graphite.[124] Oxygen reduction reaction on carbon electrodes

proceeds predominantly as a two-electron process producing hydrogen peroxide which is an unwanted side product in fuel cells as it reduces the power efficiency. However, carbon is the electrode material of choice for the electrochemical synthesis of hydrogen peroxide, since a Nernstian response for the O_2/HO_2^- couple has been observed in alkaline solutions.[125]

The oxygen reduction reaction has been investigated on various carbon-based materials and it is well-known that the kinetics for O_2 reduction can be influenced by many factors (i.e., surface area, amount of edge plane graphite, oxygen functionalities). After decades of study, it is now well-established that surface structure has a major influence on O_2 reduction kinetics.[126] In particular, surface functionalities at edge plane defects of graphite are known to significantly increase O_2 reduction activity by acting as adsorption sites for dioxygen and other intermediates.[124] A strong interaction of oxygen with functional groups on the surface occurs during oxygen reduction on carbon and graphite. The chemical nature of active sites on carbon surfaces and how these affect electron transfer reactions have been the matter of much speculation. For instance, the electrochemical behavior of carbon materials depends strongly on electrode pre-treatment[124,126] and oxidation of the electrode leads to an increase of the O_2 reduction rate due to electrocatalysis by oxygen containing surface species.[127,128] Oxidation of carbon surfaces, which tend to increase the coverage of functional groups, also catalyzes the further reduction of hydrogen peroxide in alkaline solutions.[127] The chemical nature and surface coverage of the oxygen functionalities on carbon surfaces responsible for electrocatalysis are still not clear but quinone groups are likely candidates considering the high chemical reactivity with O_2 of the semiquinone intermediate formed in the reduction

of quinones.[124]

At unmodified graphite electrodes in neutral to alkaline media, the ORR proceeds by a two-electron reduction pathway (eq. 7) with hydrogen peroxide (HO_2^-, hydroperoxide in neutral to alkaline media) as an intermediate or final product.

$$O_2 + H_2O + 2e^- \rightleftharpoons HO_2^- + OH^- \qquad E^0 = -0.065 \text{ V (vs NHE)} \qquad \text{(eq. 7)}$$

This reaction may be followed either by a second two-electron reduction of HO_2^- to OH^- (eq. 8),

$$HO_2^- + H_2O + 2e^- \rightleftharpoons 3OH^- \qquad E^0 = 0.867 \text{ V (vs NHE)} \qquad \text{(eq. 8)}$$

or, by the rapid chemical decomposition of HO_2^- to regenerate O_2, (eq. 9).

$$HO_2^- \rightleftharpoons 1/2 O_2 + OH^- \qquad\qquad \text{(eq. 9)}$$

Although thermodynamics predict that the reduction of HO_2^- should occur at much more positive potentials than O_2 reduction, a large overpotential is generally required due to slow reduction kinetics. This, in effect, pushes the HO_2^- reduction process to potential more negative of those needed for O_2 reduction. With graphitic electrodes in the absence of additional catalysts, both successive two electron reductions of O_2 (eq. 7 and eq. 8) are observed since the slow kinetics of the chemical decomposition step (eq. 9) make hydroperoxide a stable intermediate.[124]

Although exhaustive mechanistic analysis of the ORR is difficult given the numerous possible pathways, linear sweep voltammetry can provide insights into the rate determining step (RDS) and whether an outer sphere (nonadsorptive) or inner sphere (adsorptive) pathway is observed.[128] The rate of ORR on the edge plane of pyrolytic graphite is several orders of magnitude higher than that on the basal plane and this has

been considered to result from the adsorption of the superoxide intermediate.[127,129] The low reactivity of the graphite basal plane is a result of its low density of electronic states and the lack of functional groups and adsorption sites. McCreery and coworkers[128] have proposed that, at metal-free carbon surfaces, O_2 reduction involves surface adsorption (eq. 10), with the initial electron-transfer step consisting of O_2 being reduced to superoxide (eq. 11), followed by protonation to form hydroperoxide radical (eq. 12) and subsequent reduction to hydroperoxide (eq. 13).

$$O_2 \rightarrow O_{2,ads} \qquad \text{(eq. 10)}$$

$$O_{2,ads} + e^- \rightleftharpoons O_2^{\bullet-}{}_{(ads)} \qquad \text{(eq. 11)}$$

$$O_2^{\bullet-}{}_{(ads)} + H_2O \rightleftharpoons HO_2^{\bullet}{}_{(ads)} + OH^- \qquad \text{(eq. 12)}$$

$$HO_2^{\bullet}{}_{(ads)} + e^- \rightleftharpoons HO_2^-{}_{(aq)} \qquad \text{(eq. 13)}$$

McCreery also concluded that adsorption is critical to increasing the reduction of O_2 by accelerating protonation of the superoxide ion $O_2^{\bullet-}$ (eq. 12).[127] If $O_2^{\bullet-}$ becomes more basic upon adsorption, protonation and subsequent reduction of $HO_2^{\bullet}$ are accelerated. Hence, for O_2 reduction in solutions with pH < pK $_{O_2^{\bullet-}}$, the rate determining step is the initial electron-transfer rather than the protonation of $O_2^{\bullet-}{}_{(ads)}$.[130] A pH dependence of the observed O_2 reduction potential and the apparent transfer coefficient, α_{obs}, is a key indicator in distinguishing if the adsorption pathway is predominant. Technically, the RDS shifts from eq. 11 to eq. 12 for O_2 reduction proceeding via the adsorptive pathway, yielding a value of $\alpha_{obs} = 0.5$ at neutral pH and increasing to a value near $\alpha_{obs} = 1.0$ in very alkaline conditions.[131,132] While the potential where the first electroreduction of O_2

occurs will be shifted to more positive values by a fast following reaction of $O_2^{\bullet-}$ (eq. 12),[132] one is limited in the extent of this shift by a decrease in the heterogeneous electron-transfer rate for eq. 11.

2.2.3 Homogeneous Catalysis of ORR

Numerous monomeric complexes of water-soluble Fe(II) and Co(II) porphyrins have been used as homogeneous catalysts for the electroreduction of dioxygen with the main objective of these studies being to examine mechanisms through which these metalloporphyrins catalyze the electroreduction of O_2. The electrocatalytic activity of soluble iron and cobalt porphyrins or iron and cobalt phthalocyanines have been compared.[133] It was concluded that dissolved iron porphyrins and iron phthalocyanines promote the reduction to water, H_2O_2 being often an intermediate. Monomeric cobalt porphyrins and cofacial diporphyrins are only slightly soluble in concentrated acid solutions, but the biscobalt compounds promote the four-electron reduction of O_2 under these conditions.[134] In benzonitrile, the mixed-valence $Co^{III}Co^{II}$ redox state of the biscobalt diporphyrin binds O_2 strongly.[135]

With the objective to learn more about mechanistic details for the catalytic electroreduction of O_2 by Co(II) porphyrins, water-soluble macrocyclic complexes of Co(II) have been studied by Anson and co-workers in the presence of O_2.[20,21,136,137] Cobalt complexes of tetraazamacrocycles, which include 1,4,8,11-tetraazacyclotetradecane (otherwise known as cyclam), react only slowly with O_2 in aqueous media but become more efficient catalysts for the reduction of O_2 upon

adsorption on electrode surfaces.[21] For instance, Bhugun and Anson reported that the $[(tim)Co]^{2+}$ complex (tim = 2,3,9,10-tetramethyl-1,4,8,11-tetraazacyclotetradeca-1,3,8,10-tetraene) is catalytically inactive toward O_2 when generated by electrochemical reduction of $[(tim)Co]^{3+}$ in solution.[21] However, when adsorbed on the surface of roughened graphite electrodes, the catalytic activity of the complex was enhanced. The coordination chemistry and redox reactivity exhibited by these complexes in homogeneous solutions containing O_2 have also been extensively documented by Endicott and co-workers[138-140] and Espenson and co-workers.[141] Among the features of these homogeneous catalysts for the electroreduction of O_2 are the opportunities they afford to observe the electrochemical behavior of intermediates formed during the catalytic cycle.

A mechanism for the four-electron reduction of dioxygen catalyzed by cofacial dicobalt porphyrins using one-electron reductants in the presence of perchloric acid ($HClO_4$) in benzonitrile (PhCN) was reported by Fukuzumi et al.[24,25] Comparison of the homogeneous catalytic reactivities of cofacial dicobalt porphyrins (DPY)Co_2 (with Y = A, B, D and X) and a monocobalt porphyrin, (OEP)Co, and detection of the reactive intermediates by ESR provided insights into the mechanism of O_2 reduction by this bimetallic system. Monomeric cobalt porphyrins catalyze only a two-electron reduction of O_2 by ferrocene derivatives in acidified benzonitrile whereas cofacial dicobalt porphryin complexes catalyze the four-electron reduction of O_2 under the same experimental conditions.[24] A mechanism for the catalytic four-electron reduction of dioxygen by ferrocene derivatives was proposed. In the catalytic cycle, the initial bicobalt(III) complex is reduced via a two-electron transfer process by the ferrocene

derivatives to give the Co(II)Co(II) active species, which reacts with dioxygen to produce a μ-peroxo Co(III)-O$_2$-Co(III) complex. A heterolytic cleavage of the Co(III)-O$_2$-Co(III) complex affords the high valent Co(IV) oxo species which is further reduced by ferrocene in the presence of protons to yield H$_2$O. The critical difference between the two-electron and four-electron reduction processes is competition between cleavage of the O−O bond and protonation of the oxygenated species, the O−O bond cleavage leading to a four-electron reduction of dioxygen, while protonation produces hydrogen peroxide by a two-electron reduction of dioxygen. The turnover-determining step in the dicobalt bisporphyrin-catalyzed four-electron reduction of dioxygen changes from the electron transfer to cleavage of the O−O bond of the μ-peroxo species, depending upon the electron donor ability of ferrocene derivatives. Detection of the reactive intermediates was carried out by ESR and provided valuable insights into how the four-electron reduction of dioxygen to water occurs without releasing the two-electron reduced hydrogen peroxide in the presence of biscobalt bisporphyrin systems.[142]

Fukuzumi, Guilard and coworkers also reported that the four-electron reduction of dioxygen by an acid-stable nicotinamide adenine dinucleotide (NADH) analog e.g. 10-methyl-9,10-dihydroacridine (AcrH$_2$) occurs efficiently in the presence of perchloric acid using cofacial dicobalt porphyrins as catalysts.[143] Only the two-electron reduction of O$_2$ by AcrH$_2$ takes place using monomeric cobalt octaethylporphyrin (OEP)Co under the same experimental conditions. When AcrH$_2$ is replaced by 9-alkyl-10-methyl-9,10-dihydroacridine (AcrHR: R = Me, Et, and CH$_2$COOEt), the biscobalt bisporphyrins catalyze a four-electron reduction of dioxygen by AcrHR in the presence of HClO$_4$, resulting in dehydration of AcrHR via the C(9)-H cleavage to yield H$_2$O. However, in

the case of R = Bu^t and CMe$_2$COOMe, the catalytic four-electron reduction of O$_2$ by AcrHR results in oxygenation of the alkyl group of AcrHR rather than dehydrogenation to yield 10-methylacridinium ion (AcrH$^+$) and the oxygenated products of the alkyl groups, i.e., the corresponding hydroperoxides (ROOH) and the alcohol (ROH), respectively.[143] The catalytic mechanism involves dehydrogenation vs the oxygenation of AcrHR in the two-electron and four-electron reduction of O$_2$, catalyzed by monomeric cobalt porphyrins and cofacial dicobalt porphyrins, respectively, have been discussed in relation with the C(9)-H or C(9)-C bond cleavage of AcrHR radical cations produced in the electron-transfer oxidation of AcrHR.[143]

2.2.4 ORR at Chemically Modified Electrodes (CMEs)

The electroreduction of O$_2$ on carbon surfaces is much slower than on metals such as platinum or gold. This observation has initiated a search for catalysts for the electrochemical reduction of O$_2$ on carbon electrodes under different experimental conditions. Modification of the electrode substrates with electrocatalytic materials[144] is a promising and nowadays quite common approach for the improvement of oxygen reduction by reducing the large overpotentials required. The usual approach is through immobilization of catalytic materials onto the electrode surface via chemisorption or covalent bonding.[145,146] A variety of catalysts have been used for modification of carbon electrodes in order to increase the rate of the ORR on such electrodes. These include both metal-containing catalysts like Co(II)-macrocycle complexes[6,147] and non-metal containing ones like carbon nanotubes or quinones.[124]

2.2.4.1 Mediated electron transfer at CMEs containing redox species

The objective of electrocatalysis is to drive highly efficient and selective oxidation or reduction of substrates at modest potential and under mild, clean conditions. Studies of electrocatalytic reactions utilizing chemically-modified electrodes[144-146,148-151] (CMEs) is currently an active area of research due to its great interest for the understanding of catalytic redox processes, especially those involving model complexes of metalloenzymes, and for its applications in electroanalytical chemistry.[152] Modification of electrode surfaces with electron transfer materials is widely used to prepare electrodes with electrocatalytic activity for the reduction of O_2. Porphyrins or phthalocyanines of cobalt and iron are known as effective electrocatalysts for O_2 reduction.[27,34,153] The principle of this catalytic process consists in the electrochemical generation of a low-valent form of the metalloporphyrin which converts the substrate into the desired product while regenerating the starting metalloporphyrin thus triggering a new catalytic cycle.

Figure 2-7 illustrates a typical example of an electrocatalytic reduction process at a CME. The reversible redox mediator P/Q with a standard potential of $E^0_{P/Q}$ is immobilized on an electrode to promote the irreversible reduction reaction A + e → B. The standard potential of P/Q is more positive than the irreversible potential where the direct electrochemical process to be catalyzed takes place ($E^0_{P/Q} > E^0_{A/B}$). Instead of taking place at the electrode surface, electron transfer to A occurs via the reduced form of the mediator Q generated at the electrode surface at a potential less reducing than the potential at wich the direct reduction of A occurs.
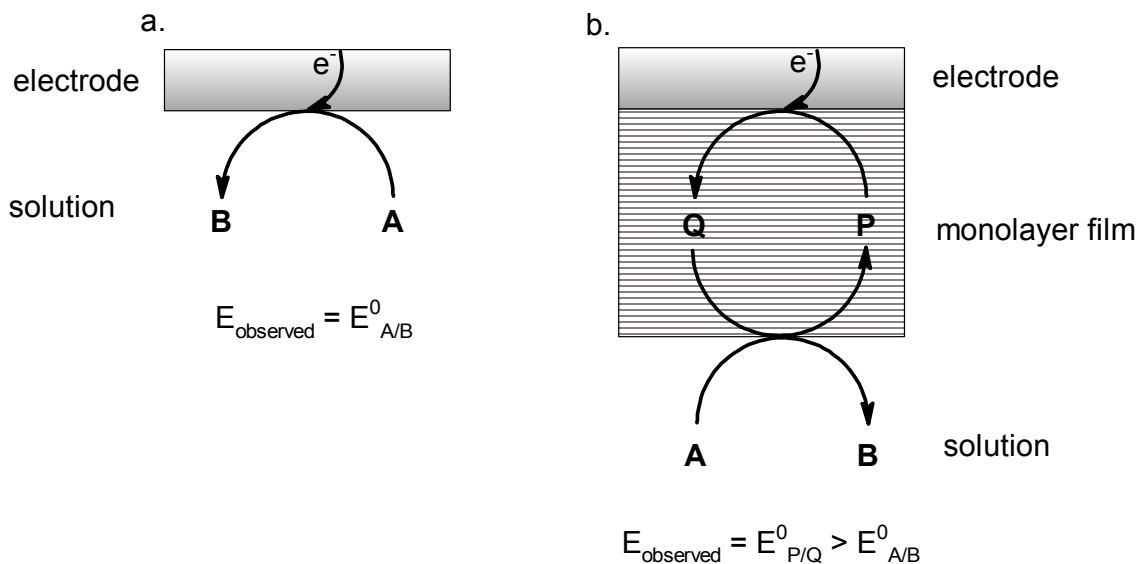
Figure 2-7. Schematic representation for the reduction reaction A → B on bare (a) and catalyzed (mediated) conditions (b). The terms P and Q correspond to the reversible mediator of oxidized and reduced states, respectively. In heterogeneous catalyzed reaction, the P/Q mediator is bonded on the electrode surface.

Mediated electron transfer of solution phase species at electrode surfaces containing immobilized redox species can be examined experimentally using a number of electrochemical techniques. The technique of rotating disk electrode voltammetry is most often applied, since in principle, the processes of reactant transport in solution, and kinetic processes at the monolayer can be separated by carrying out the voltammetric measurements over a wide range of rotation speeds. Previous theoretical work describing mediated redox catalysis at monolayers has been presented.[154-163]

2.2.4.2 ORR at quinone-modified electrodes

The heterogeneous catalytic reduction of O_2 may be represented schematically as shown below:

$$O + n\mathrm{e} \underset{k_a}{\overset{k_c}{\rightleftharpoons}} R \qquad\qquad (eq.\ 14)$$

$$R + O_2 \overset{k_h}{\longrightarrow} O + products \qquad\qquad (eq.\ 15)$$
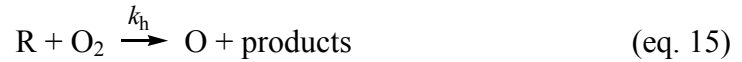
where k_c and k_a denote the formal heterogeneous electrochemical rate constants of the reversible redox reaction (eq. 14) followed by an irreversible catalytic reaction (eq. 15) where k_h represents the heterogeneous catalytic rate constant of the reaction. The term "catalytic" is employed to denote a class of reactions in which the initial electroactive species, O, is regenerated on or close to the electrode surface by a coupled chemical reaction. The products of the chemical reaction are not adsorbed or electroactive at electrode potentials in the range of interest. It is assumed that sufficient supporting electrolyte is present in solution to ensure that mass transport of the reaction constituents occurs solely by diffusion and/or convection and that the regenerative process is totally irreversible.

Electrode catalysts which promote oxygen reduction with a high efficiency and with long operating lifetimes are what is needed. The immobilization of catalytic materials is advantageous since they reduce the typically large overpotentials that are required at most electrode substrates. It has been shown that modification of the electrode surface by quinones via adsorptive attachment enhances the rate of oxygen reduction.[164] However, quinones can desorb from the surface during long-term operation, especially in alkaline

solution.[164] It is more beneficial to attach the quinone moiety covalently to the surface.[14,16,165-168]

The modification of carbon surfaces by quinones can be used to established the relationships between structure of the catalyst and the catalytic activity for oxygen reduction,[165] in particular, for H_2O_2 production.[169,170] The reactive intermediate is likely to be a semiquinone intermediate formed as the first reduction product of the surface quinone groups and there is strong evidence that O_2 reduction follows an electrochemical-chemical catalytic mechanism (EC_{cat}) on these surfaces.[165] Recent work using adsorbed anthraquinone (AQ) derivatives confirmed this mechanism at pH 4.5 and showed that the kinetics were controlled by a chemical reaction between reduced AQ and O_2.[170]

2.2.4.3 ORR at porphyrin-modified carbon electrodes

2.2.4.3.1 Monocobalt porphyrins

Since the pioneering work of Jasinski in 1964,[26] metalloporphyrins have drawn considerable interest as catalytic modifiers for carbon-based electrodes (e.g., carbon black, graphite and glassy carbon) because they are known to lower the kinetic overpotential for reduction and oxidation of small molecules. Indeed, the rich and reversible redox chemistry of metalloporphyrins is the key factor that allows them to serve as mediators in many electron transfer reactions. Among the different electrocatalytic reactions, the catalytic reduction of dioxygen is the most studied.[6] The main goal of these studies was in most cases to find a highly potent catalyst for dioxygen

reduction to substitute the noble metal Pt and to improve the oxygen (air) electrode of fuel cell systems.[171] Metal complexes of porphyrins adsorb strongly on graphite at monolayer levels, leading to chemically modified electrodes which exhibit efficient electrocatalytic activity for oxygen reduction. It is well-known that monomeric cobalt complexes usually catalyze dioxygen reduction only to hydrogen peroxide whereas iron derivatives promote the two-step, four-electron reduction of O_2 to H_2O over the full pH range.[133,172-174] However, cobalt complexes catalyze O_2 reduction to H_2O_2 with a lower overvoltage than do iron compounds; because the M^{III}/M^{II} redox potential is much higher for cobalt. In a few cases, aggregates of cobalt porphyrins adsorbed onto graphite electrodes catalyze the direct reduction of oxygen to water.[46-51] A similar behavior was reported by D'Souza *et al.*[175] for glassy carbon electrodes modified by electrostatic-assembled, tetracationic *meso*-tetrakis(*N*-methyl-4-pyridyl)porphynatocobalt and tetracationic *meso*-tetrakis(4-sulfonatophenyl)porphyrinatocobaltate films. In both cases, the authors attributed the observed catalytic efficiency to the stacked structure of the porphyrin film, allowing for the simultaneous binding of O_2 to two cobalt porphyrin sites. Similarly, cobalt porphyrins adsorbed on pyrolytic graphite and containing $[Ru(NH_3)_5]^{2+}$ or $[Os(NH_3)_5]^{2+}$ groups coordinated to *N*-pyridyl or *N*-cyanophenyl residues at the *meso* positions of the porphyrin macrocycle, catalyze the four-electron reduction of O_2 to H_2O.[22,176,177] The four-electron reduction efficiency in these cases was ascribed to back-bonding effects from the ruthenium complexes which modulate the electron transfer capability of the cobalt(II) porphyrin ring. In another study, an iron(II) porphyrin was used as the ORR catalyst and $Ru(NH_3)_6^{2+}$ as the electron carrier in a Nafion matrix.[178] Higer Ru(II) concentrations favor the 4-electron vs the 2-electron O_2 reduction pathway.

2.2.4.3.2 Bridged Cofacial Bis(metallo)porphynoids
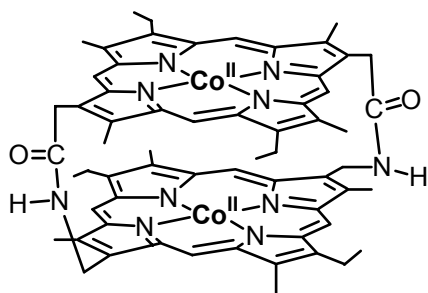
(FTF4)Co$_2$
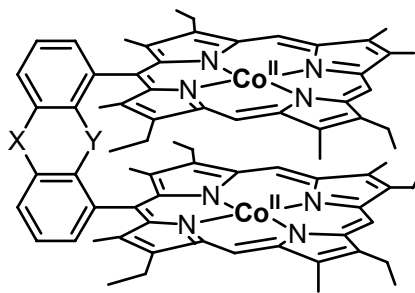
X = Y = - ; biphenylenyl ; (DPB)Co$_2$
X = Y = C ; anthracenyl ; (DPA)Co$_2$
X = CMe$_2$, Y = O ; dimethylxanthenyl ; (DPX)Co$_2$
X = - , Y = O ; dibenzofuran ; (DPD)Co$_2$

Scheme 2-2. Chemical structures of face-to-face bisporphyrins (left) and pillared
bisporphyrins (right).

Cofacial bis(metallo)porphynoids were initially prepared to study the interaction
between closely lying electroactive centers such as in the case of cytochromes, to obtain
multi-electron transfer, or to find new catalysts for the reduction or oxidation of small
substrate molecules such as O$_2$, N$_2$, or H$_2$.[179] In particular, covalently linked cofacial
cobalt bisporphyrins have been extensively studied for exploring the cooperative effect of
metal centers in promoting the four-electron reduction of O$_2$ to H$_2$O.[27,34] Cofacial
bisporphyrins can generally be grouped into two types of compounds, those linked on
opposite sides of each macrocycle with two flexible strapping units[114,179-184] ("Face-to-
Face" bisporphyrins) (Scheme 2-2) and those linked on only one side of each macrocycle
by a rigid linking unit ("pillared" bisporphyrins).[23,53,55,60,61,185-187]

2.2.4.3.2.1 Face-To-Face systems

In the field of dioxygen reduction, the rich history of cofacial metallodiporphyrins began with the synthesis of the face-to-face diporphyrins FTF4 (where FTF is for Face-To-Face diporphyrins) in which the two etio-type porphyrin units are linked at two β-pyrrolic positions of the porphyrin by amide linkages (see Scheme 2-2).[135,188-190] Experiments performed in nonaqueous media established that the biscobalt $(FTF4)Co_2^{II/II}$ complex had, in fact, a very low affinity towards dioxygen.[189] In contrast, it was shown that the monooxidized form of the dicobalt bisporphyrin $(FTF4)Co_2^{II/III}$ leading to a μ-superoxo derivative[114,191] had a very high affinity toward dioxygen[135] and catalyzed the four electron reduction of dioxygen to water when adsorbed on the graphite electrode surface.[114,183,192]

The catalytic activity of the $(FTF4)Co_2$ system can be easily determined using cyclic voltammetry (CV) or rotating ring-disk electrode (RRDE) voltammetry (Figure 2-8).[61] The technique of RRDE permits the quantitative measurement of H_2O_2 production and allows discrimination between the formation of free H_2O_2 as an intermediate or merely as a minor side product. The ring-disk electrode assembly consists of a pyrolytic graphite disk inside a concentric Pt ring. The $(FTF4)Co_2$ complex is applied to the graphite disk by irreversible adsorption. As the assembly is rotated, fresh O_2-saturated electrolyte is drawn vertically toward the disk surface and ejected radially across the disk and ring. The disk potential is controlled by a potentiostat, and the disk current-potential profile records the O_2 reduction process. At the same time, the ring is held at a potential where any H_2O_2 reaching it is rapidly oxidized to O_2. The ring current response thus monitors H_2O_2

49

production; and the ratio of disk to ring current, normalized for the collection efficiency, defines the relative contributions of the $4e^-$ and $2e^-$ reduction processes.

From the voltammograms depicted in Figure 2-8, there is no doubt left about the role of this mixed-valence compound in the catalytic reduction of oxygen to water, as the four-electron reduction is active only in the potential domain where the Co^{III}/Co^{II} redox state exists; the reduction to peroxide occurs when both cobalt centers are reduced to cobalt(II). It has been shown that the cobalt(III) atom in $(FTF4)Co_2^{II/III}$ acts as a Lewis acid center for O_2 binding and can be replaced by Lu^{III} or Sc^{III}.[61] Later on, however, it was shown that the tetra-electronic reduction process of O_2 by dicobalt bisporphyrins is not effective when the edge plane graphite is replaced by a gold electrode.[193] The participation of reactive functional groups on the graphite surface has been suggested.
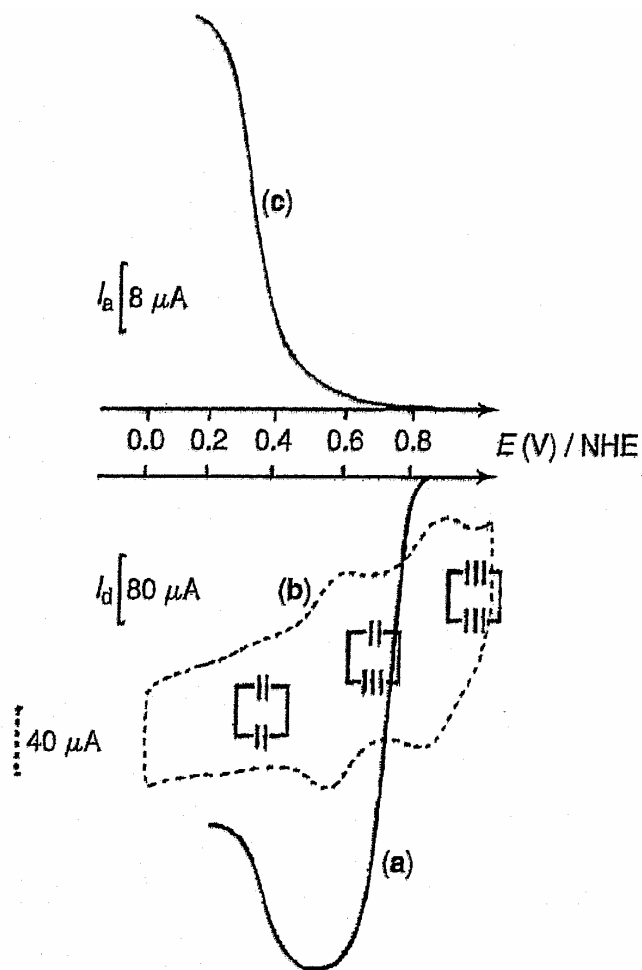
Figure 2-8. Catalysis of O_2 reduction at a ring (Pt)–disk (EPPG) electrode in contact with an aqueous 0.5 M H_2SO_4 solution, the graphite disk being modified by adsorption of a biscobalt porphyrin, $(FTF4)Co_2$.[61] (a) disk current, solution saturated with O_2 at atmospheric pressure. Rotation rate: 100 rpm; scan rate: 5 mV s^{-1}. (b) cyclic voltammetry at the EPPG disk under nitrogen. Scan rate: 100 mV s^{-1}. (c) detection of H_2O_2 on the platinum ring, $E_{ring} = 1.33$ V vs NHE.

51

2.2.4.3.2.2 Pillared systems

The cofacial bisporphyrin systems linked by a single rigid spacer are the so-called "Pacman" porphyrin systems $(DPA)H_4$, $(DPB)H_4$, $(DPX)H_4$ and $(DPD)H_4$ where DPA, DPB, DPX and DPD represent bisporphyrins (DP is for DiPorphyrin) with anthracenyl (A), biphenylenyl (B), 9,9-dimethylxanthene (X) or dibenzofuran (D) bridges (Scheme 2-2).[53,55,60,61,185-187,194] For many years, the synthesis of cofacial porphyrins had been limited to DPA and DPB bisporphyrin derivatives[34,53-55,186] where the two porphyrin units are constrained in a cofacial arrangement via a biphenylenyl (B) or anthracenyl (A) bridge.[54,195,196] Recently, Nocera and co-workers[56-58] further developed a novel one-pot method for obtaining xanthene and dibenzofuran bridges in high yield, allowing for the efficient gram-scale synthesis of cofacial "Pacman" bisporphyrins, incorporating new flexible dibenzofuran (D) or xanthene (X) spacers which display variable pocket sizes.[59,197]

The reported crystal structures of $(DPB)Co_2$,[198] $(DPA)Co_2$,[199] $(DPX)Co_2$,[59,197] and $(DPD)Co_2(2MeOH)$[59,197] indicate that the distances between cofacial porphyrin units are quite different depending upon the spacer as shown in Figure 2-9. The metal-metal separations in $(DPA)Co_2$ (4.53 Å) and $(DPX)Co_2$ (4.58 Å) are virtually almost the same. However, the xanthene spacer of $(DPX)Co_2$ is readily more flexible than the anthracene spacer of $(DPA)Co_2$. It has been shown that dicobalt complexes $(DPD)Co_2$ and $(DPX)Co_2$ are also efficient catalysts for the four-electron reduction of dioxygen to water despite a ca. 4 Å difference in their metal–metal distances. This result suggests that the longitudinal "Pac-Man" flexibility of those cofacial systems allows the distal cavity to

structurally accommodate reaction intermediates during multielectron catalytic processes.[23,58,59] It is also worthy to point out a 'quasi-parallel' geometry of the rings is observed in the case of biphenylenyl and anthracenyl (DPB)H$_4$ and (DPA)H$_4$ bisporphyrins while an 'open mouth' structure is generally observed in the case of the dibenzofuran (DPD)H$_4$ bisporphyrin.[199] The parallel geometry of the rings observed in (DPB)H$_4$ and (DPA)H$_4$ bisporphyrins favor π-π interactions and these interactions can be varied via the use of an appropriate spacer.[199]
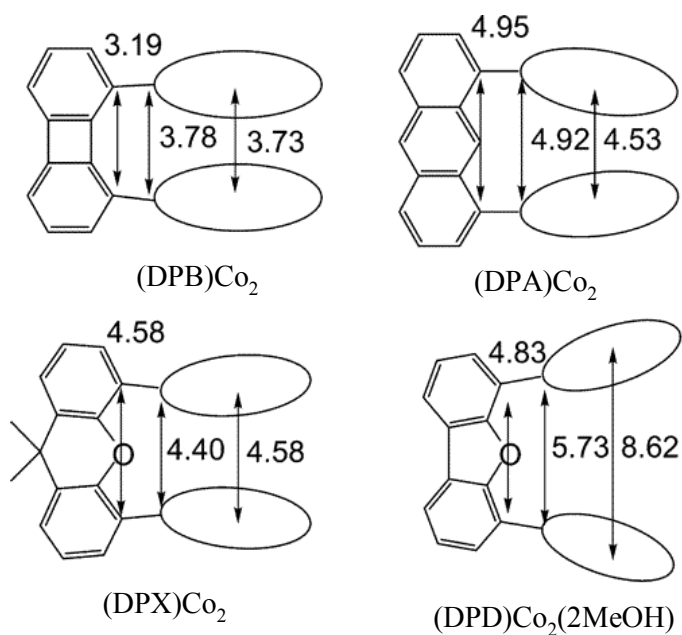
Figure 2-9. Selected distances (Å) in (DPB)Co$_2$,[55] (DPA)Co$_2$,[199] (DPX)Co$_2$,[57,59] and (DPD)Co$_2$(2MeOH).[57,59]

A mechanism for the direct four-electron reduction of O_2 by dicobalt bisporphyrins (DPY)Co_2 (Y = A, B, X or D) adsorbed on graphite electrodes has been suggested[23] where the catalytically active species is a mixed-valence Co(II)/Co(III) complex (Scheme 2-3). Experimental studies have shown that the one- and two-electron oxidized cofacial platforms are capable of binding O_2, whereas the fully reduced [Co_2(bisporphyrin)] complex is unreactive to the O_2 substrate.[55,200,201] The active species, a Co(II)/Co(III) compound, provides entry into the catalytic cycle (Scheme 2-3, Cycle A) and is generated from the stable bis-Co(II) derivative, either electrochemically or chemically. The binding of dioxygen leads to a μ-superoxo species which is stabilized by the two Co(III) atoms. Nocera and co-workers[23] stated that the specific protonation of the μ-superoxo Co(III)–O_2–Co(III) adduct bypasses formation of peroxo-type adducts (Cycle B), resulting in complete O−O bond cleavage upon the two-electron transfer. The subsequent addition of one proton and one electron produce two H_2O molecules. Thus, protonation of the superoxo species is essential for favoring multielectron over single-electron processes for O−O activation and cleavage. This crucial stoichiometry of three electrons and one proton which is needed for O−O bond cleavage is also assumed to take place in cytochrome c oxidase.
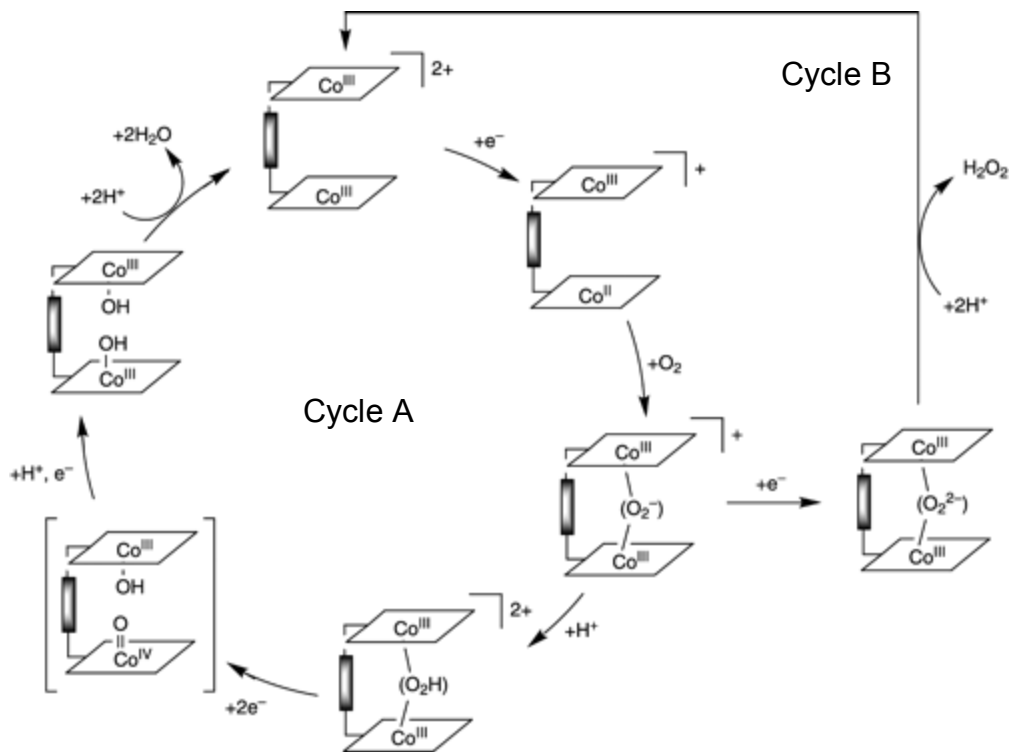
Scheme 2-3. Mechanistic model for the activation and reductive cleavage of the O−O bond by Pacman porphyrins. (Reproduced from ref. 23).

Chapter 3: Experimental Section

3.1 Chemicals and Compounds

Unless otherwise noted, all chemicals were obtained commercially and used without further purification. High purity N_2 gas was purchased from Matheson-Trigas. Organic solvents and mineral acids were of reagent grade and were used as supplied except for benzonitrile (PhCN) which was purified by passage through a column of activated Linde 3 Å molecular sieves followed by distillation under reduced pressure. Aqueous solutions were prepared with deionized water of resistivity not less than 18 MΩ cm. The cobalt complexes used in this study [$(Me_4Ph_5Cor)Co$, $(Me_6Et_2PhP)Co$, $(BCY)Co_2$, $(PCY)Co_2$, $(PMes_2CY)Co_2$, $(PCY)H_2Co$, and $(PCY)MClCoCl$ with Y = anthracene (A), biphenylene (B), 9,9-dimethylxanthene (X), dibenzofuran (O), or dibenzothiophene (S) bridge and M = Fe^{III} or Mn^{III}] were obtained from the group of Dr. Roger Guilard at the Université de Bourgogne, France and were synthesized and purified according to published procedures.[111,112]

3.2 Apparatus and Electrode Preparation

All electrochemical data were collected using a three-electrode cell. The three electrode system consisted of a platinum ring-graphite disk working electrode, a platinum wire as the auxiliary electrode, and a commercial saturated calomel electrode (SCE) as the reference which was separated from the bulk of the solution by means of a salt bridge. The KCl solution in the SCE was changed periodically in order to maintain the correct potential that was checked using a standard solution for redox potential measurements.[202]

An aqueous Ag/AgCl (KCl saturated) reference electrode (–45 mV *vs* SCE) was employed for thin layer experiments.

All electrochemical experiments were conducted at ambient laboratory temperature (22 ± 2 ºC). Cyclic voltammetry and rotating disk experiments were carried out using a Pine Instrument model AFMSR rotator linked to an EG&G Princeton Applied Research (PAR) model 263A potentiostat/galvanostat. The potentiostat was monitored by an IBM compatible PC microcomputer controlled by the software M270 (EG&G PARC). A RDE4 bipotentiostat (Pine Instrument) was employed with a HP 7090A three-channel digital plotter for rotating ring–disk electrochemical experiments. The rotating ring–disk electrode (RRDE), purchased from the Pine Instrument Co., consisted of a platinum ring and a removable graphite disk.

Just before it was coated with the catalyst, the edge-plane pyrolytic graphite disk (A = 0.282 cm^2) was polished to a rough finish with 600 grit SiC paper, rinsed with water and wiped to remove any free graphite particles. The molecular catalyst was irreversibly adsorbed on the electrode surface by means of a dip-coating procedure; the freshly polished electrode was dipped for 5 s in a 0.1 mM solution of the catalyst in $CHCl_3$, transferred rapidly to pure $CHCl_3$ for 1-2 s and then dried following the procedure of Anson.[47] After being coated with the catalyst, the ring–disk electrode was introduced into air-saturated aqueous 1 M $HClO_4$. Particular care was taken to ensure a high reactivity of the Pt ring towards H_2O_2. Immediately prior to use, the Pt surface was cleaned with a 5 μm alumina slurry (Buehler MICROPOLISH II polishing suspension) on a polishing cloth (Buehler MICROCLOTH), rinsed successively with water and methanol, dried, and activated by cycling between 1.20 V and –0.20 V in 1 M $HClO_4$ until reproducible

58

voltammograms were obtained.[203,204] During polishing of the Pt ring, the graphite disk was removed to avoid contamination of the Pt with graphite particles and to preserve the integrity of the graphite surface.

The diffusion-limiting currents for the reduction of O_2 in aqueous solution at the rotating disk electrode were calculated using the following parameters: kinematic viscosity of H_2O at 25 °C, 0.01 cm^2 s^{-1}; solubility of O_2 in air-saturated 1 M $HClO_4$, 0.24 mM; diffusion coefficient of O_2, 1.7×10^{-5} cm^2 s^{-1}.[47] The solubility of dioxygen in 1 M $HClO_4$ was calculated by using the Setschenow equation ($\ln\{m_{O_2}^0 / m_{O_2}\} = k_s \times m$) and the Pitzer equation[205] ($k_S(HClO_4) = 2\lambda_{O_2,H^+} + 2\lambda_{O_2,ClO_4^-}$) where m is the molality (mol kg^{-1}) of $HClO_4$, $m_{O_2}^0$ is the molality of O_2 in pure water,[206] $\lambda_{O_2,H^+} = 0.0353$ and $\lambda_{O_2,ClO_4^-} = -0.007$.[207]

3.3 Electrochemical Techniques

3.3.1 The Edge Plane Pyrolytic Graphite (EPPG) Electrode

An electrode made from pyrolytic graphite will have a surface composed of both edge plane and basal plane graphite, with the basal:edge ratio and graphite monocrystal size depending on the quality of the pyrolytic graphite used.[126] EPPG electrodes are fabricated by taking a piece of high quality highly ordered pyrolytic graphite (HOPG) and cutting the desired electrode geometry such that the layers of graphite lie perpendicular to the surface; conversely, BPPG electrodes are produced by cutting the electrode geometry

such that the graphite layers lie parallel to the surface.
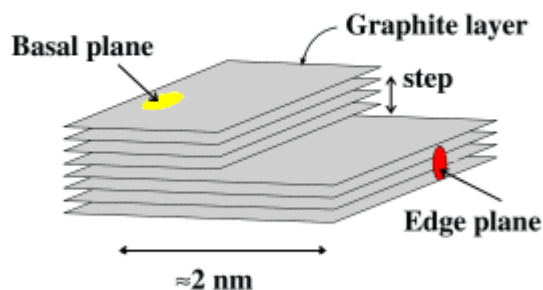
Figure 3-1. Illustration of the heterogeneity of the HOPG surface.
(Reproduced from ref. 208).

The basal plane surface of HOPG electrode, which is the most well defined graphite surface commercially available, consists of layers of graphite (graphene sheets) which lie parallel to the surface and are separated from each other by 3.35 Å. Although a basal plane pyrolytic graphite (BPPG) electrode conducts electricity, it can be considered electrochemically inert.[209] For a large number of redox couples, electron transfer rate constants at basal plane graphite have been found to be over 10^3 times lower than that for the same electrode reaction at edge plane graphite.[210] Recently, Compton and co-workers have shown that the electron transfer rate constant of ferrocyanide at an edge plane pyrolytic graphite (EPPG) electrode was 0.022 cm sec^{-1}, whereas k^0 for the same reaction at a basal plane HOPG electrode was less than 10^{-9} cm s^{-1}.[208] The authors suggested that the observed electrochemical reactivity of basal plane HOPG electrodes is due to an ensemble of edge plane graphite nano-bands arising where there are imperfections (steps)

in the perfectly flat basal plane (Figure 3-1).[209] The basal plane graphite terraces have no influence on the voltammetry and are effectively inert.[209] The same conclusion can be applied to other carbon materials such as carbon nanotubes which are rolled-up graphene sheets.[211]

3.3.2 Rotating Disk Electrode Techniques

3.3.2.1 The Nernst diffusion layer

In the third decade of the twentieth century, Levich and co-workers made great progress in developing the mathematical equations describing fluid dynamics at submerged electrode surfaces of different geometries.[212] One of the electrode systems described by Levich is the rotating disk electrode (RDE) shown in Figure 3-2. This technique provides a well-defined and reproducible laminar flow over the surface of the disk.[213]
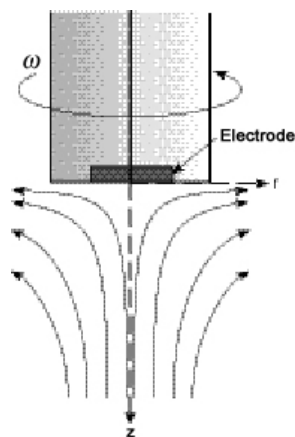
Figure 3-2. Flow profile of solution at a rotating disk electrode.

Because of the electrode rotation, a stagnant layer of solution adheres at the disk

61

surface and rotates at an angular velocity (ω) equal to that of the electrode. The solution at some infinite distance from the disk is also rotating although not at the velocity of the electrode. The centrifugal force upon this fluid causes it to move in a radial direction near the disk surface. The radial fluid displacement is compensated by an axial fluid flow, as shown in the pictorial representation of Figure 3-2. The convective mass transport is negligible within the layer and diffusion alone is responsible for mass transport in this region. The layer of solution at the disk surface where diffusion is the prominent mode of mass transport is called the Nernst diffusion layer.[213] Under these experimental conditions Levich deduced an expression relating the thickness (δ) of the diffusion layer with experimental variables such as the kinematic viscosity of the solution (ν), the diffusion coefficient of the electroactive species in solution (D) and the rotation speed of the electrode (ω):

$$\delta = 1.61 \upsilon^{1/6} D^{2/3} \omega^{-1/2} \qquad \text{(eq. 16)}$$

3.3.2.2 Steady-state voltammetry

Methods involving forced convective mass transport of reactants and products at an electrode in motion such as an RDE are also called hydrodynamic methods. Advantages of rotated disk electrodes include: (i) The rate of mass transport of reactants to a RDE surface is controlled precisely by fixing the rotational velocity (ω) of the electrode; (ii) electrode currents (i) quickly achieve steady-state values ($\partial i/\partial t = 0$) following establishment of applied electrode potential (E_{app}) for moderate-to-high rates of rotational velocity ($\omega > 10$ rad s^{-1}). As a consequence, the voltammetric response ($i - E_{app}$) for a

species transported from the bulk of the solution to the RDE surface is independent of the potential scan rate for low rates scan (v < 0.1 V s^{-1}); (iii) Current response at RDEs is insensitive to incidental vibrations of the apparatus.

Under steady-state conditions, the activities and fluxes of reactants, intermediates, and products in the electrode process remain essentially constant, both at the electrode surface and in the bulk of the solution. The current reaches a steady-state at hydrodynamic electrodes as fresh analyte is being transported to the electrode surface by convection. The kinetic expressions describing the electrode reactions thus reduce to time-independent algebraic equations which may usually be solved analytically for the surface concentrations of the species in question. As a result, exact solutions of the boundary-value problems can be obtained for considerably more complex reaction schemes than is possible for transient voltammetric methods.

Of the forced-flow techniques for which exact solutions of the Navier-Stokes equations of hydrodynamic motion[214] are obtainable, that of the rotating disk electrode is the most suitable for investigation of electrochemical reactions at solid electrodes. The Nernst diffusion layer concept permits a trivial derivation of the current at an RDE when the electrode reaction is mass-transport (diffusion) controlled. Since the surface concentration of the electroactive species is zero, the limiting current (i_{lim}) is given by eq. 17:

$$i_{lim} = nFA\frac{D}{\delta}C \qquad \text{(eq. 17)}$$

where n, F, A, D, δ, and C are, respectively, the number of electrons transferred, the Faraday constant (96485 C eq^{-1}), the electrode surface area (cm^2), the diffusion

coefficient of the electroactive species in solution ($cm^2\ s^{-1}$), the thickness of the diffusion layer (cm), and the concentration of the electroactive species (mol cm^{-3}), respectively. Equations eq. 16 and eq. 17 show that in the region of laminar flow, the flux of electroactive species ($\frac{D}{\delta}C$) is proportional to the square root of the angular velocity of the disk, ω, and that the diffusion layer thickness, δ, is constant over the entire disk surface. The latter significant result implies that the local current density i/A is the same everywhere on the surface and independent of the total area of the electrode.

The use of forced-flow techniques permits the kinetics of electrode reactions to be studied under steady-state conditions as a function of the rate of mass transport of the reaction constituents to or from the electrode surface. By adjustment of the flow rate, the thickness of the diffusion boundary layer can be varied in such a manner so as to alter the relative degree of control of the overall reaction rate by kinetics and mass transport. Thus, by increasing the rate of mass transport of the electroactive species to the surface, it becomes possible to extend appreciably the range of kinetic control. However, with high rotation velocities, the fluid flow at the RDE becomes turbulent and relations based on laminar mass transport are no longer valid.

In the following section, the use of the rotating disk electrode for kinetic studies of heterogeneous first-order catalytic electrode reactions is discussed. It is assumed that for mass transport by convective diffusion, the thickness of the diffusion boundary layer remains constant as a function of time and hence that steady-state conditions prevail.

3.3.2.3 Kinetics studies of ORR by rotating disk electrode (RDE) technique

In order to distinguish the effects of kinetic control by the coupled chemical reaction (C) of heterogeneous catalytic electrode reactions from those of the electrochemical reaction (E) itself, it is necessary to maintain the electrode at a potential where the rate of the latter reaction is controlled solely by the rate of supply of O_2 to the surface, *i.e.*, in the limiting-current region (i_{lim}) (Figure 3-3).
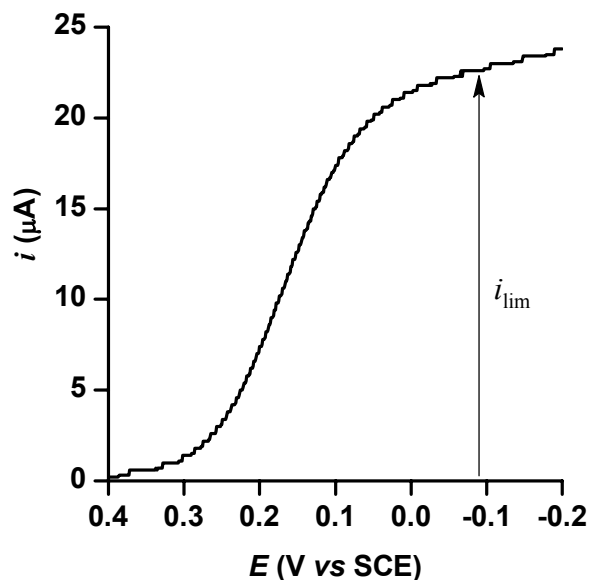
Figure 3-3. Current-potential curve for the reduction of O_2 in 1 M $HClO_4$ at a rotating graphite disk electrode coated with 2.4×10^{-10} mol cm^{-2} of Co(TPP). Rotation rate: 100 rpm. Scan rate: 5 mV sec^{-1}.

To investigate the kinetics of an electrode reaction, mass transport should be fast in comparison to the charge transfer rate.[215] The RDE is uniquely suited to the determination of heterogeneous rate constants for moderately rapid electron transfer

processes because the mass transport rate can be regulated via the disk rotation velocity. For catalyzed dioxygen reduction, the data were acquired at 100, 400, 900, 1600, 2500 and 3600 rpm (rpm = rotation per minute).

If the mass-transport process in the solution controls the reduction of dioxygen at the catalyst-modified electrode, the relationship between the limiting current of the rotating disk voltammogram and rotation rate obeys the Levich equation:

$$i_{lim} = i_{Lev} = 0.62nFAC^*D^{2/3}v^{-1/6}\omega^{1/2}$$ (eq. 18)

where n, A, D, C^*, v and ω represent the number of electrons transferred in the overall electrode reaction, the electrode area (cm^2), the dioxygen diffusion coefficient (cm^2 s^{-1}), the bulk concentration of dioxygen in the solution (mol cm^{-3}), the kinematic viscosity (cm^2 s^{-1}), and the rotation rate (rad s^{-1}), respectively. From eq. 18, the plot of the limiting current i_{lim} as a function of the square root of rotation rate $\omega^{1/2}$ should be a straight line intersecting the origin. A lack of linearity in the Levich plot suggests that the catalytic reaction is limited by chemical kinetics and not by mass transport.

The catalytic current i corresponding to the mediated reaction is a function of the Levich current i_{Lev} representing the mass transport of O_2 in the solution and the kinetic current i_k representing the current in the absence of mass transport effect. For the pseudo-first order catalytic reduction of oxygen (O_2 concentration is in large excess compared to the catalyst) at a chemically modified electrode, the limiting-current measured experimentally at the rotating disk electrode is described by the Koutecky-Levich equation:

$$1/i_{lim} = 1/i_k + 1/i_{Lev}$$ (eq. 19)

The first term on the right-hand side is the inverse of the kinetic current, i_k, as expressed by

$$i_k = nFk\Gamma C^*$$
(eq. 20)

where n is the number of electrons transferred in the overall electrode reaction, k the pseudo-first order rate constant for the catalyzed reaction ($M^{-1}s^{-1}$), Γ the surface concentration of catalyst on the electrode surface (mol cm^{-2}), F the faraday constant (96,487 C eq^{-1}), and C^* the bulk concentration of O_2 (mol cm^{-3}). The second term in eq. 21 is the inverse of the Levich mass transport limited current density for the reduction of O_2.

The kinetic current (i_k) that would have been obtained in the absence of mass transport limitation can also be calculated by transforming eq. 19:

$$i_k = \frac{i \cdot i_{lim}}{i_{lim} - i}$$
(eq. 22)

3.3.2.4 Catalytic reduction of O_2 at a RDE coated with Co(TPP)

The catalytic reduction of O_2 at a RDE coated with Co(TPP) is shown in Figure 3-4a. Limiting current values were taken at a fixed potential on the catalytic wave plateau of Figure 3-4a (−0.2 V). Levich plot[212] of the potential-independent plateau currents vs the electrode (rotation rate)$^{1/2}$ is curved (Figure 3-4b), as is typical for the electroreduction of O_2 catalyzed by adsorbed cobalt porphyrins.[48] The clear lack of linearity in the Levich plot suggests that the catalytic reaction is limited by kinetics and not by mass transport. The slope of the Koutecky–Levich plot[216,217] (Figure 3-4c) shows that the electrocatalytic

reduction of O_2 is a two-electron process. The nonzero intercept of the line drawn through the experimental points in Figure 3-4c shows that the electrocatalytic reduction of oxygen is not mass transport controlled, but is limited by a kinetic controlled process. A chemical step, previously assigned to the formation of a cobalt(III)-O_2 adduct,[72] precedes the electron transfer and limits the current to values below the convection–diffusion limit.
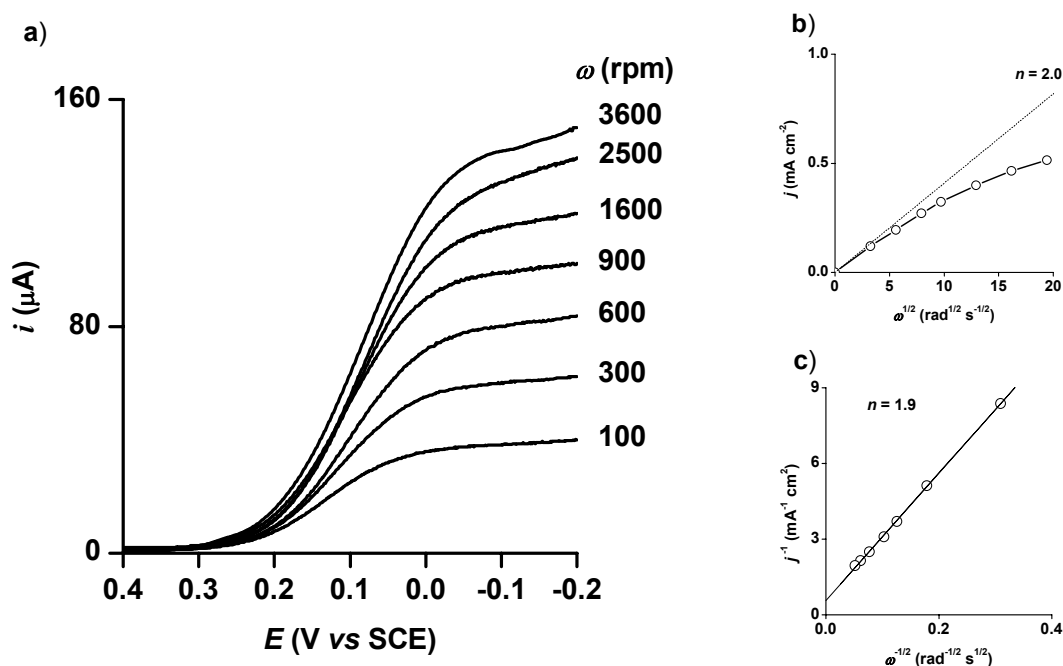
Figure 3-4. (a) Current-potential curves for the reduction of O_2 in 1 M $HClO_4$ at a rotating graphite disk electrode coated with 2.4×10^{-10} mol cm^{-2} of Co(TPP). Values of the rotational velocity (ω) of the electrode in rpm are indicated on each curve. (b) Levich plot of the rotating limiting currents (j) vs square root of rotational velocity (ω)$^{1/2}$. The circle are experimental; the dotted line refers to the theoretical curve for the diffusion-convection-limited reduction of O_2 by two electrons, as indicated in the figure. (c) Koutecky-Levich plot of the reciprocal currents in part b vs (ω)$^{-1/2}$.

3.3.3 Rotating Ring–Disk Electrode Technique

3.3.3.1 Technical aspects

The technique most often used for studying the catalytic reduction of O_2 by metalloporphyrins is rotating ring–disk voltammetry.[214] This electrochemical technique provides a quantitative measurement of any H_2O_2 produced as a product of the O_2 reduction and allows discrimination between the formation of free H_2O_2 as an intermediate and that which is formed as a minor side product in the desired conversion of O_2 to H_2O by 4 electrons. The ring–disk electrode assembly consists of a pyrolytic graphite disk inside a concentric Pt ring. The compound to be tested as a reduction catalyst is applied to the graphite disk by irreversible adsorption. As the assembly is rotated, fresh O_2-saturated electrolyte is drawn vertically toward the disk surface and ejected radially across the disk and ring. The disk potential is controlled by a potentiostat, and the disk current (I_D)-potential (E) profile records the O_2 reduction process. At the same time, the ring is held at a potential where any H_2O_2 reaching it is rapidly oxidized to O_2. The ring current response (I_R) thus monitors H_2O_2 production; and the ratio of disk to ring current, normalized for the collection efficiency, defines the relative contributions of the $4e^-$ and $2e^-$ reduction processes.

The equations used to calculate the average number of electrons transferred n and the percentage of H_2O_2 formed at the electrode are eq. 23 and eq. 24, respectively:

$$n = 4I_D/(I_D + I_R/N) \qquad \text{(eq. 23)}$$

$$\%H_2O_2 = 100(2I_R/N)/(I_D + I_R/N) \qquad \text{(eq. 24)}$$

where I_D is the faradic current at the disk and I_R is the faradic current at the ring.[218] The

value of the collection efficiency, $N = I_R/ I_D$, is determined using a standard redox couple, such as $Fe(CN)_6^{3-/4-}$ in 1 M KCl.

3.3.3.2 Catalytic reduction of O_2 at a RRDE coated with Co(TPP)

Figure 3-5 shows the current–potential curves for the two-electron reduction process of O_2 to H_2O_2 recorded at a rotating graphite disk–platinum ring electrode (RRDE) coated with Co(TPP) in air-saturated 1 M $HClO_4$. The disk potential was scanned from 0.4 V to –0.3 V vs SCE at a rotation speed of 100 rpm while the ring potential was held at +1.0 V to oxidize the H_2O_2 generated by O_2 reduction at the disk electrode. A disk current (I_D) for dioxygen reduction at +0.3 V is observed (see upper curve in Figure 3-5), which attains a limiting diffusion current at more negative potentials. A large anodic ring current (I_R) flows as the reduction of O_2 occurs (lower curve in Figure 3-5). The ratio of the ring to disk limiting current, I_R/I_D, is 0.13 for the Co(TPP)-coated RRDE, which is relatively close the collection efficiency N of 0.15 determined at a bare graphite disk– platinum ring electrode with the use of the $[Fe(CN)_6]^{3-/4-}$ redox couple in 1 M KCl. From the ratio of the ring–disk current, the calculated number of electrons involved in the reduction of O_2 is found to be 2.0 according to eq. 23, which is almost identical to that acquired from the Koutecky-Levich plot (*vide supra*).
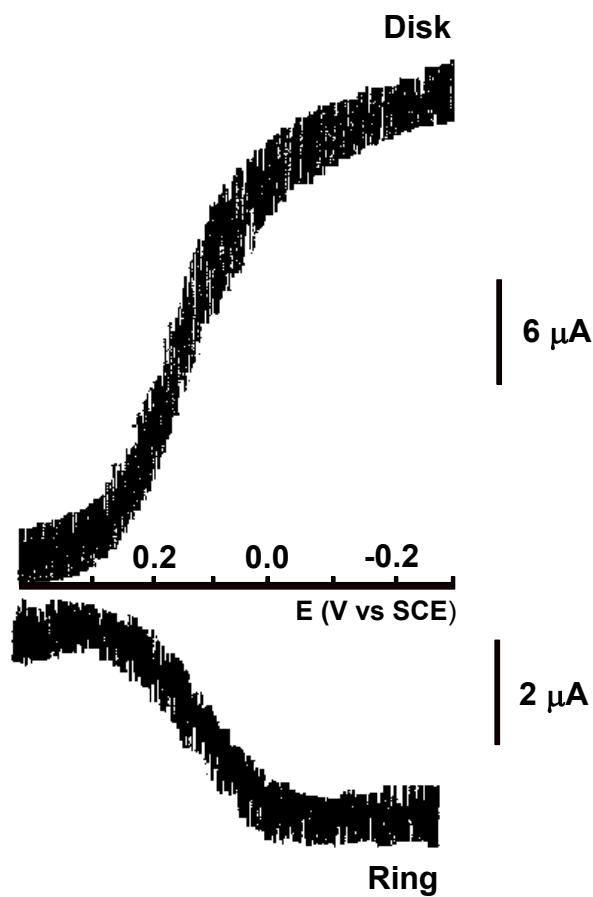
Figure 3-5. Current-potential curves obtained during the reduction of O_2 at a rotating graphite disk–platinum ring electrode. The graphite disk is coated with Co(TPP). Scan rate: 5 mV s^{-1}. Rotation rate: 100 rpm. Supporting electrolyte: air-saturated 1 M $HClO_4$. The potential of the platinum ring electrode was set to 1.0 V to oxidize H_2O_2 to O_2 completely. $I_D = 21.4$ μA and $I_R = 2.9$ μA.

Chapter 4: **Reactivity of Cobalt(III) Complexes of Monocorrole, Biscorroles, and Porphyrin–Corrole Dyads Toward Dioxygen**

4.1 Introduction

Several porphyrin–corrole,[67] biscorrole,[67] and bisporphyrin[23,27,34,201,219-221] dyads linked in a cofacial configuration have been synthesized and examined as to their electrochemical reactivity with small molecules such as O_2 or CO. One such compound is the anthracenyl bridged porphyrin−corrole dyad (PCA)Co$_2$, **1a**, (Chart 4-1) which strongly binds O_2 in air giving a stable bis-Co(III) μ-superoxo complex as evidenced by its 15-line ESR spectrum.[71] A similar dicobalt face-to-face anthracenyl-bridged bisporphyrin[27,54] is able to catalyze the four-electron electroreduction of O_2 in acidic media, and it was of interest to examine catalytic properties of the related mixed oxidation state porphyrin−corrole dyads **1a-1d** and the Co(III) biscorrole dyads **3a-3e** (Chart 4-1) under similar experimental conditions.

Metallocorroles have been examined as to their catalytic properties in oxidation reactions[63,65] and their affinity for dioxygen,[106] but nothing has been reported as to their ability to catalyze the electroreduction of O_2 when adsorbed on an electrode surface. The main difference between the cobalt corroles and previously studied cobalt porphyrins is the oxidation state of the central metal ion. The uncharged cobalt mono- and bisporphyrins contain Co(II) ions while the neutral porphyrin−corrole dyads, **1a-1d**, contains a Co(III) corrole linked to a Co(II) porphyrin. In contrast, the biscorrole dyads (BCY)Co$_2$, **3a-3e**, and the uncharged monocorrole **2** contain only Co(III) ions.

(PCY)Co₂, 1 **(Me₄Ph₅Cor)Co, 2** **(BCY)Co₂, 3**
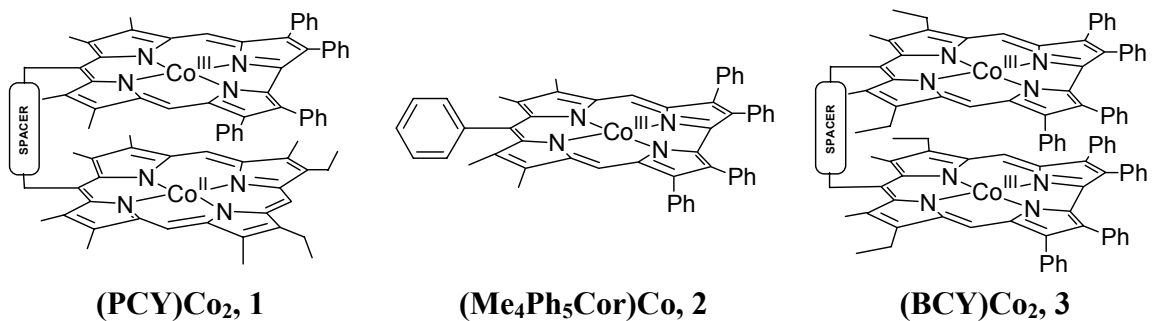
SPACERS (Y)
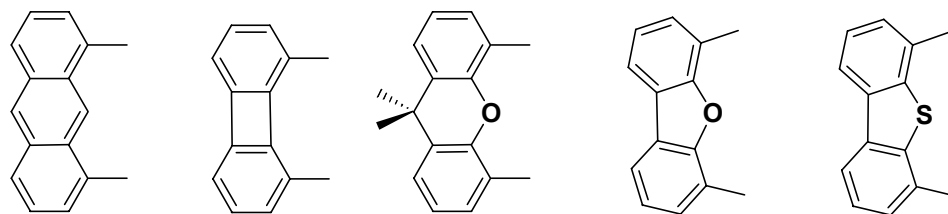
(PCA)Co₂: 1a **(PCB)Co₂: 1b** **(PCX)Co₂: 1c** **(PCO)Co₂: 1d**

(BCA)Co₂: 3a **(BCB)Co₂: 3b** **(BCX)Co₂: 3c** **(BCO)Co₂: 3d** **(BCS)Co₂: 3e**

Chart 4-1

One goal of the present study was to examine the redox properties of the three series of corroles in acidic media and another was to examine their use as catalysts for the reduction of O_2 at a graphite electrode. The four dicobalt porphyrin–corrole dyads, **1a-1d**, the five dicobalt biscorrole dyads, **3a-3e**, and the monocobalt corrole, **2**, examined in this study are well characterized as to their electrochemistry under N_2 in a variety of nonaqueous solvents.[71,92,108,109,111] $(Me_4Ph_5Cor)Co^{III}$, **2**, can be reversibly reduced to its Co(II) form at $E_{1/2}$ = −0.15 V to −0.17 V *vs* SCE in CH_2Cl_2, PhCN or THF.[92] Slightly more negative potentials are observed for the Co(III)/Co(II) process of the biscorroles $(BCY)Co_2$[109,111] and porphyrin−corroles $(PCY)Co_2$[111] under similar experimental conditions.

Of more relevance to the present work are the potentials where the three series of corroles **1**, **2** and **3** are oxidized to their higher, formally Co(IV) and Co(IV) π-cation radical oxidation states. These electrode reactions occur at $E_{1/2}$ = 0.47 and 0.82 V for $(Me_4Ph_5Cor)Co^{III}$, **2**, in PhCN 0.1 M TBAP and at $E_{1/2}$ = 0.53 and 0.73 V in THF giving $[2]^+$ and $[2]^{2+}$ in both solvents.[92] A splitting of the first redox process of **2** is observed in CH_2Cl_2 due to the presence of dimers.[92] As will be described, both series of biscobalt complexes **1** and **3** can serve as catalysts for the four-electron electroreduction of dioxygen in an air-saturated aqueous acidic solution containing 1 M $HClO_4$. The onset potentials of the catalytic reduction for both biscobalt complexes are comparable to the potentials for the formal Co(IV)/Co(III) processes of the catalysts in nonaqueous media. This result is consistent with the binding of O_2 by the Co(III) form of the compounds and is also consistent with the previously described μ-superoxo species that are formed in the reaction between O_2 and $(PCA)Co_2$.[71]

4.2 Results and Discussion

4.2.1 Redox Properties of Complexes and Catalytic Reduction of O_2.

A detailed discussion is given for compounds **1a**, **2** and **3a** and this is followed by data on the other linked derivatives in the two series of biscobalt complexes.

The three series of cobalt complexes were applied to an edge-plane pyrolytic graphite (EPPG) electrode by irreversible adsorption from a dilute chloroform solution. Cyclic voltammograms recorded at a graphite disk coated with complex **1a** are illustrated in Figure 4-1A. In the absence of dioxygen, the response of the modified graphite electrode is characterized by a redox process centered at $E_{1/2} = 0.38$ V in 1 M $HClO_4$ ($E_{pc} = 0.36$ V, $E_{pa} = 0.40$ V). When the solution is saturated with air, a larger cathodic peak is observed at almost the same potential of $E_p = 0.40$ V. The reduction of O_2 at an uncoated graphite electrode occurs at $E_p = -0.34$ V which indicates that complex **1a** catalyzes the electroreduction of dioxygen when adsorbed on graphite.

A catalytic reduction wave of dioxygen is also observed at a rotating platinum ring−graphite disk electrode modified by adsorption of complex **1a** on the disk as illustrated in Figure 4-1B. This RRDE voltammogram was obtained by scanning the disk potential from 0.70 to 0.00 V *vs* SCE at a rotation speed of 100 rpm while holding the ring potential at 1.10 V so that any H_2O_2 formed at the disk could be detected at the ring. Under these conditions, the anodic ring current results from the oxidation of H_2O_2 to O_2.

Figure 4-1. (A) Cyclic voltammograms of **1a** adsorbed on an EPPG electrode. Supporting electrolyte: 1 M HClO$_4$ (a) saturated with argon and (b) saturated with air. Scan rate: 50 mV s^{-1}. (B) Reduction of O$_2$ at a rotating ring (Pt)−disk (EPPG) electrode in air-saturated 1 M HClO$_4$. The potential of the ring electrode was maintained at 1.1 V. Rotation rate: 100 rpm. Scan rate: 5 mV s^{-1}.

As seen in Figure 4-1B, the disk current begins to increase at about 0.60 V and the plateau is reached at 0.30 V. At about 0.26 V, the current begins to decrease slightly and then rises again as the potential is scanned to more negative values. A similar behavior was previously observed for (FTF4)Co$_2$[114,222] (FTF4 = face-to-face porphyrin dimer with a linking group of 4 atoms) and biscobalt "Pacman" type bisporphyrins.[54,57,72] Only a relatively small amount of hydrogen peroxide is detected at the ring electrode in the vicinity of $E_{1/2}$ when the reaction is carried out in air-saturated HClO$_4$ (Table 4-1). The value of the disk current at $E_{1/2}$ corresponds to an apparent number of electrons

transferred of $n = 3.9$. From the data in the figure, we cannot say which of the two cobalt centers is reduced first in (PCA)Co$_2$ (that of the corrole or that of the porphyrin) but there is no doubt that the redox process at $E_{1/2} = 0.38$ V in HClO$_4$ under argon corresponds to the electroreduction of O$_2$ to give H$_2$O at $E_p = 0.40$ V under air.

The electrochemical and electrocatalytic properties of the monocorrole **2** in HClO$_4$ differ from that of the dicobalt porphyrin−corrole **1a** under the same solution conditions. The cyclic voltammogram of **2** adsorbed on a graphite disk in the absence of dioxygen shows three reversible processes located at $E_{1/2} = 0.38$, 0.20 and −0.08 V (Figure 4-2A). The three reactions can be related to similar reactions for the same compound in CH$_2$Cl$_2$ which occur at $E_{1/2} = 0.62$, 0.45 and −0.15 V.[92,109] The electrochemical response at −0.15 V was assigned to the Co(III)/Co(II) couple.[109] In comparison with the same process of a structurally related porphyrin, (OEP)Co[48] ($E_{1/2} = 0.41$ V) where OEP = octaethylporphyrin, the smaller ring size of the macrocyclic cavity[62] of **2** shifts the formal potential of the Co(III)/Co(II) couple by 490 mV to lower values in accordance with the fact that a corrole macrocycle stabilizes the Co(III) oxidation state whereas porphyrins stabilize cobalt in a +2 oxidation state.[62,67,223] The two processes at $E_{1/2} = 0.38$ and 0.20 V for complex **2** suggest reduction via a dimeric species as is also observed in a nonaqueous solvent such as CH$_2$Cl$_2$.[92,108] The first reduction peak at $E_p = 0.35$ V in Figure 4-2A thus probably corresponds to formation of a monooxidized dimer, $[(\mathbf{2})_2]^+$, which is catalytically active toward the reduction of dioxygen as seen in Figure 4-2B by the substantially enhanced peak currents at $E_p = 0.36$ V in the presence of O$_2$.

Table 4-1. Electroreduction of Dioxygen by Adsorbed Dicobalt Porphyrin−Corroles and Biscorroles in Air-Saturated 1 M $HClO_4$.

	Compound	$E_p{}^a$	$E_{1/2}{}^b$	n^c
1a	$(PCA)Co_2$	0.40	0.47	3.9
1b	$(PCB)Co_2$	0.38	0.46	3.7
1c	$(PCX)Co_2$	0.38	0.45	3.7
1d	$(PCO)Co_2$	0.34	0.41	3.5
2	$(Me_4Ph_5Cor)Co$	0.36	0.38	2.9
3a	$(BCA)Co_2$	0.36	0.39	3.4
3b	$(BCB)Co_2$	0.35	0.37	2.4
3c	$(BCX)Co_2$	0.34	0.37	2.9
3d	$(BCO)Co_2$	0.33	0.35	3.4
3e	$(BCS)Co_2$	0.33	0.35	3.1

[a] Peak potential of the dioxygen reduction wave (V *vs* SCE). [b] Half-wave potential (V *vs* SCE) for dioxygen reduction at rotating disk electrode (ω = 100 rpm). [c] The apparent number of electrons transferred per dioxygen molecule (*n*) at $E_{1/2}$ is calculated from $n = 4I_D/(I_D+I_R/N)$ where I_D and I_R are disk and ring currents, respectively, and N (= 0.24) is the collection efficiency of the ring−disk electrode.[218]
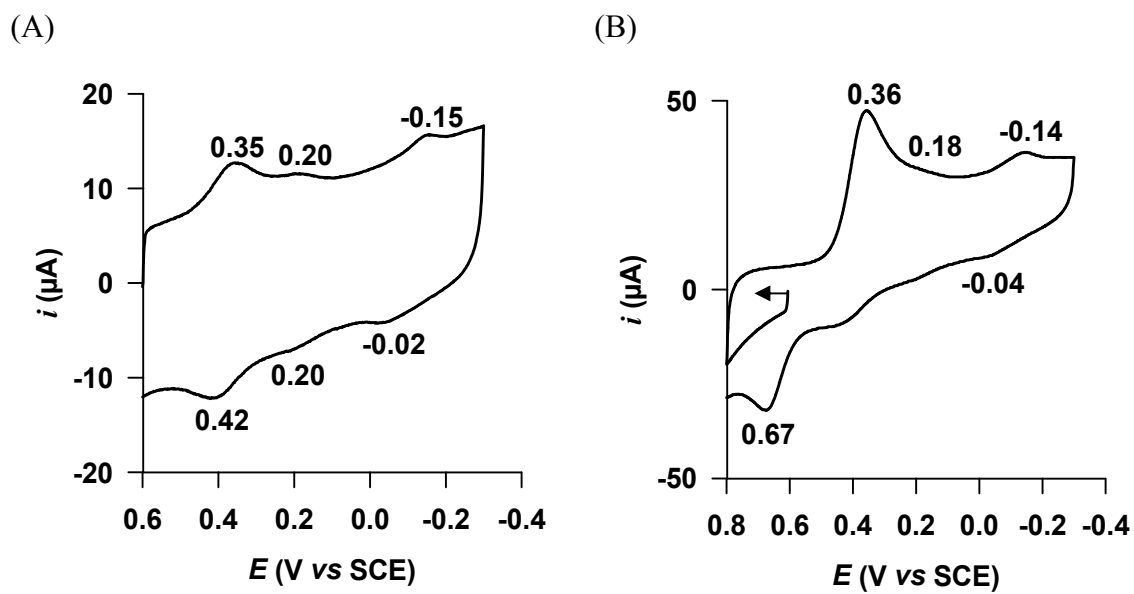
Figure 4-2. Cyclic voltammograms of **2** adsorbed on EPPG electrode. Supporting electrolyte: 1 M $HClO_4$ saturated (A) with argon, (B) with air. Scan rate: 50 mV s^{-1}.

Shown in Figure 4-3 are the cyclic voltammograms and rotating ring−disk electrode voltammograms responses obtained for (BCA)Co_2, **3a**, adsorbed on an EPPG electrode in 1 M $HClO_4$. Results for the biscorrole **3a** parallel what is observed for **1a** except that more H_2O_2 is produced at the $E_{1/2}$ of 0.39 V (30%) than in the case of the porphyrin−corrole mixed oxidation state derivative where only 5% of H_2O_2 was observed. The biscorrole **3a** is thus less selective than the porphyrin−corrole dyad **1a** but more selective than the monocorrole **2** (55% H_2O_2). In comparison with the dicobalt porphyrin−corrole **1a** and biscorrole **3a**, the half-wave potential $E_{1/2}$ of the dioxygen reduction wave is less positive for the monomeric cobalt complex **2** (Table 4-1). Also, in the case of **2**, H_2O_2 is detected at the ring electrode as soon as dioxygen reduction occurs (Figure 4-4). Under these conditions, the value of n calculated from the disk and the ring currents is 2.9 at 0.38 V (Table 4-1). As complex **2** is not catalytically active towards the reduction of H_2O_2 (*vide infra*), this value of n requires that a portion of the dioxygen that reaches the electrode surface be reduced by four electrons to H_2O. The catalytic behavior of **2** is thus similar to what has been reported for cobalt porphyrins with unsubstituted *meso* positions such as (OEP)Co[48] or Co(II) porphine.[46] In both cases, a formation of dimers on the surface of the graphite electrode was proposed to explain the catalytic electroreduction of O_2 to H_2O.
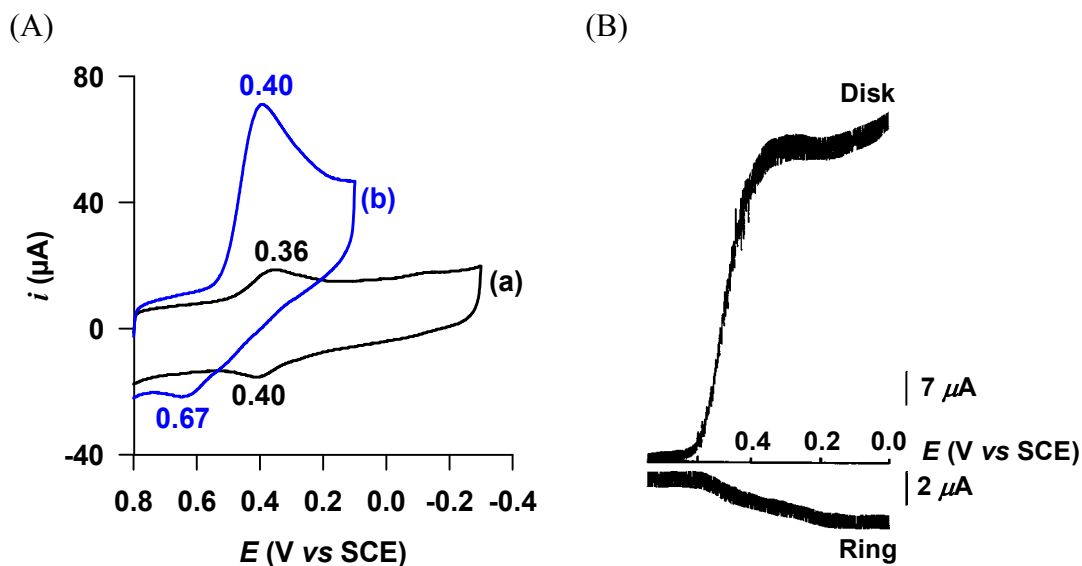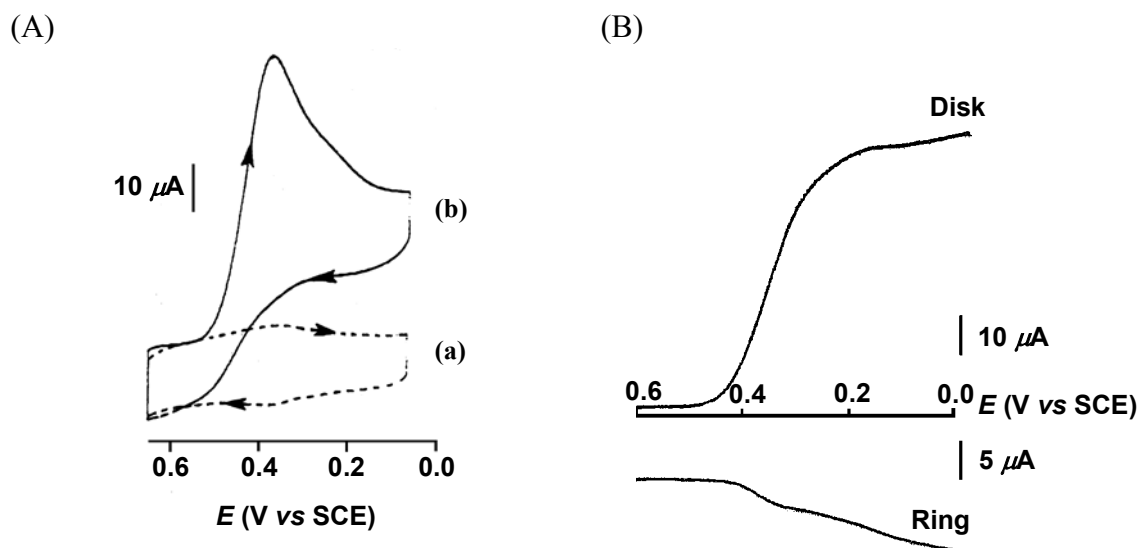
Figure 4-3. (A) Cyclic voltammograms of **3a** adsorbed on an EPPG electrode. Supporting electrolyte: 1 M HClO$_4$ (a) saturated with argon and (b) saturated with air. Scan rate: 50 mV s^{-1}. (B) Reduction of O$_2$ at a rotating ring (Pt)−disk (EPPG) electrode in air-saturated 1 M HClO$_4$. The potential of the ring electrode was maintained at 1.1 V. Rotation rate: 100 rpm. Scan rate: 5 mV s^{-1}.

Disk

0.6   0.4   0.2   0.0 | 7 μA
                       E (V *vs* SCE)
                       | 2 μA
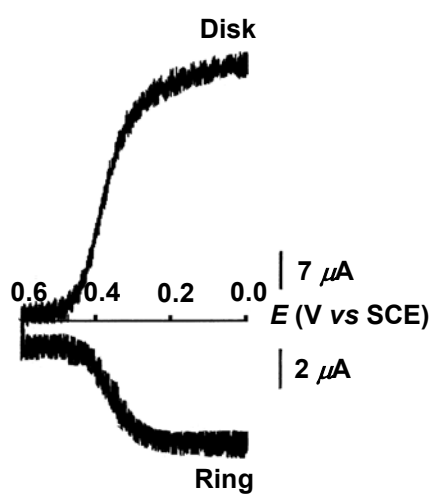
Ring

Figure 4-4. Reduction of O_2 at a rotating ring (Pt)−disk (EPPG) electrode coated with **2** in air-saturated 1 M $HClO_4$. Collection efficiency $N = 0.24$. The potential of the ring electrode was maintained at 1.1 V. Rotation rate: 100 rpm. Scan rate: 5 mV s^{-1}.

4.2.2 Kinetics of O_2 Reduction Catalyzed by $(Me_4Ph_5Cor)Co$ and $(PCA)Co_2$.

Figure 4-5A shows a set of current-potential curves for the reduction of dioxygen at a rotating disk electrode coated with the cobalt monocorrole **2** and porphyrin−corrole **1a** in 1 M $HClO_4$. The corresponding Levich plot of limiting current *vs* the square root of the rotation rate $(\omega)^{1/2}$ and the lines calculated from the Levich equation (eq. 18) for the diffusion-convection-limited two- and four-electron reduction of dioxygen are shown in Figure 4-5B. The Levich plot for monocorrole **2** shows that the steady-state limiting currents exceed the calculated values corresponding to the two-electron reduction of O_2. The nonlinearity of the Levich plot in Figure 4-5B suggests that the catalytic reaction is limited by a rate-determining step that precedes the electronic transfer (*CE* mechanism). This nonlinearity was previously observed for several cobalt(II) porphyrin complexes[47,48,171,175,224-227] and the chemical step was assigned to the formation of a dioxygen adduct[192] which is a reducible species. Kinetic analysis of such systems is facilitated by means of Koutecký-Levich plots[228] of reciprocal current density $(j_{lim})^{-1}$ *vs* reciprocal square root of rotational velocity $(\omega)^{-1/2}$. Typical plots are shown in Figure 4-5C. These plots are interpreted on the basis of equation (1):

$$\frac{1}{j_{lim}} = \frac{1}{j_{lev}} + \frac{1}{j_k} \tag{1}$$

where j_{lim} is the measured limiting current density (mA cm^{-2}). The Levich current, j_{lev}, and j_k, the kinetic current that measure the rate of the current-limiting chemical reaction, are defined by equations (2) and (3), respectively.

$$j_{lev} = 0.62\, nFD^{2/3} \upsilon^{-1/6} C^* \omega^{1/2} \qquad (2)$$

where n is the number of electrons transferred in the overall electrode reaction, F the

Faraday constant (96487 C mol^{-1}), D and C^* are the diffusion coefficient (cm^2 s^{-1}) and

bulk concentration of dioxygen (mol dm^{-3}), respectively, υ is the kinematic viscosity of

water (cm^2 s^{-1}), and ω is the angular rotation speed (rad s^{-1}) of the electrode.

$$j_k = 10^3 nFk\Gamma C^* \qquad (3)$$

where k (M^{-1} s^{-1}) is the second-order rate constant governing the current-limiting reaction

between the reduced catalyst and O$_2$ and Γ (mole cm^{-2}) is the surface concentration of

catalyst on the electrode that participates in catalyzing the reaction. The quantity of

(Me$_4$Ph$_5$Cor)Co present on the electrode ($\Gamma = 2.0 \times 10^{-10}$ mol cm^{-2}) was obtained by

measuring the area under the cyclic voltammogram recorded in dioxygen-free 1 M

HClO$_4$. The value of n determined from the slope of the Koutecký-Levich plot (Figure

4-5C) shows that a portion of dioxygen is reduced to water. This is in agreement with the

value of $n = 2.9$ determined from the ring−disk experiment at a rotation speed of 100 rpm

(Table 4-1). The value of the O$_2$ reduction rate constant k, evaluated at pH = 0, from the

intercept of the Koutecký-Levich plot, is higher than previously reported rate constants

governing the kinetics of the coordination of dioxygen to adsorbed cobalt(II) porphyrin

complexes (Table 4-2).[192]

Complex **2**   Complex **1a**

(A)

(B)

(C)
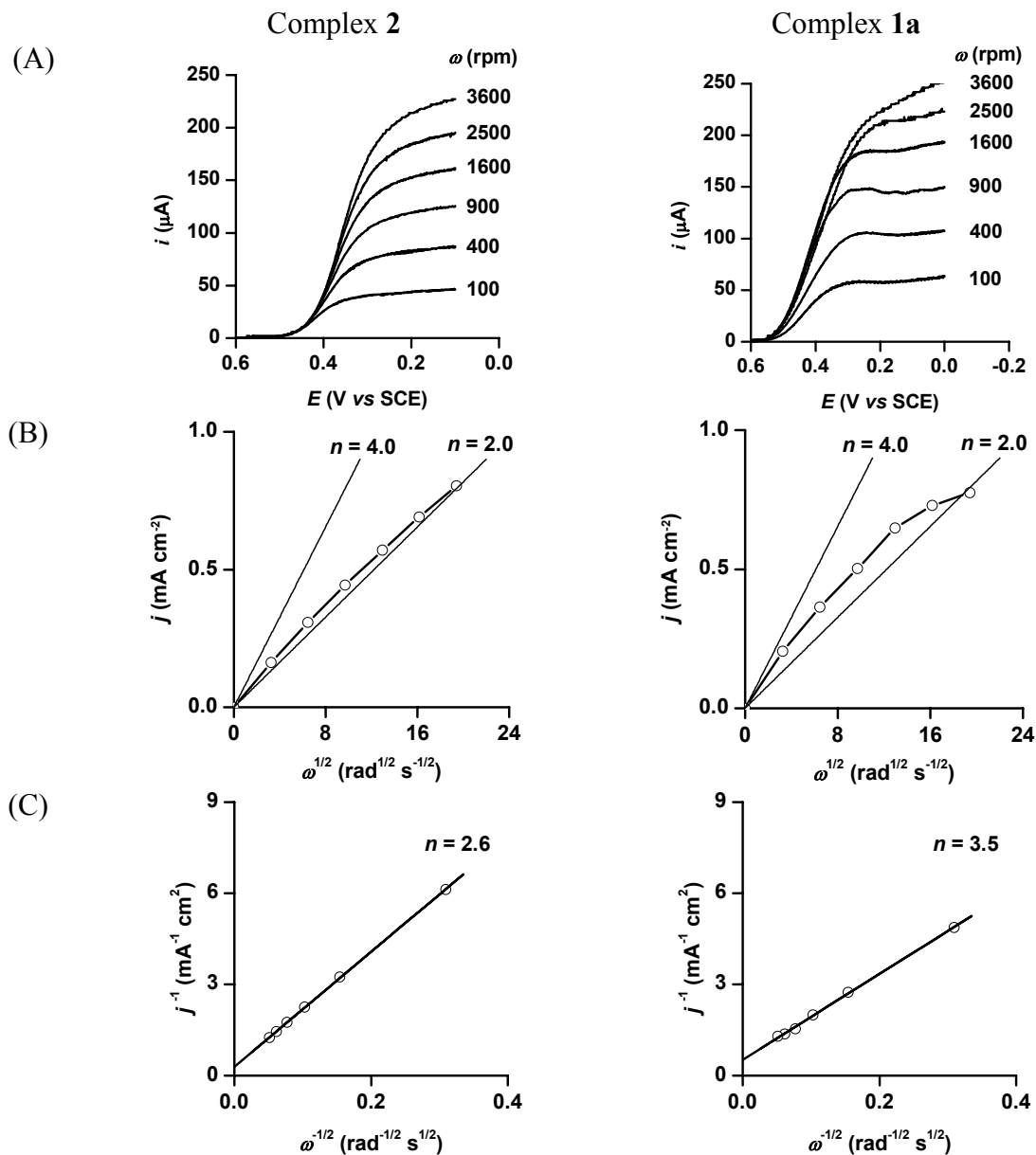
Figure 4-5. (A) Current-potential curves for the reduction of O_2 in 1 M $HClO_4$ at a rotating graphite disk electrode coated with 2.0×10^{-10} mol cm^{-2} of **2** (left) and 11.0×10^{-10} mol cm^{-2} of **1a** (right). Values of the rotational velocity (ω) of the electrode in rpm are indicated on each curve. The disk potential was scanned at 5 mV s^{-1}. (B) Levich plots of the rotating limiting currents (j) of (A) ($\circ$) *vs* square root of rotational velocity $(\omega)^{1/2}$. The lines refer to the theoretical curves for the $2e^-$ and $4e^-$ processes, as indicated in the figures. (C) Koutecký-Levich plots corresponding to B.

86

Table 4-2. Rate Constants (k) for the Electroreduction of O_2 by Adsorbed Catalysts in Air-Saturated 1 M $HClO_4$ (pH = 0).

Catalyst	$10^{-5} k$, M^{-1} s^{-1}	Ref
(PCA)Co$_2$ (**1a**)	0.2	T.W.
(Me$_4$Ph$_5$Cor)Co (**2**)	5.7	T.W.
(FTF4)Co$_2$	3.0	192
(diethylesterMe$_2$Et$_2$P)Co	1.4	192
(DPA)Co$_2$	0.2	72

T.W. = This work.

The rotating disk procedure described above for measuring the rate constant governing the catalytic reaction of **2** with O_2 was also applied to the dicobalt porphyrin−corrole **1a**. An EPPG disk was modified with (PCA)Co$_2$ using a dip-coating procedure. The surface coverage of the disk was calculated from integration of the voltammetric peak recorded in a deoxygenated acidic solution (Figure 4-1A) and was found to be 11.0×10^{-10} mol cm^{-2} of geometric electrode area. The recorded hydrodynamic voltammograms in the presence of dioxygen are shown in Figure 4-5A. The Levich plot in Figure 4-5B is nonlinear, as expected for a reduction in which a current-limiting chemical step precedes the electron transfer. The reciprocal slope of the corresponding Koutecký-Levich plot (Figure 4-5C) corresponds to an apparent n value of 3.5 which suggests that O_2 is reduced to a mixture of H_2O and H_2O_2. This is also consistent with the magnitudes of the anodic ring currents at potentials on the plateau of the disk curent-potential curve in Figure 4-1B. The rate constant, k, for the catalytic reduction of O_2 by (PCA)Co$_2$ was evaluated from the intercept of the Koutecký-Levich plot (Figure 4-5C) and found to be 0.2×10^5 M^{-1} s^{-1} (Table 4-2). This value is lower than that obtained for the monocobalt porphyrin (diethylesterMe$_2$Et$_2$P)Co ($k = 1.4 \times 10^5$ M^{-1} s^{-1})[192] and its related dimer (FTF4)Co$_2$ ($k = 3.0 \times 10^5$ M^{-1} s^{-1})[192] but it is identical to that reported previously for the electrocatalytic reduction of O_2 in 1 M CF$_3$CO$_2$H by a (DPA)Co$_2$-coated graphite electrode where DPA = anthracenyl-bridged diporphyrin ($k = 0.2 \times 10^5$ M^{-1} s^{-1}).[72]

4.2.3 Thin-layer Voltammetry.

Further insight into the catalyzed reduction of dioxygen by **2** was obtained by dissolving the catalyst in a thin layer of benzonitrile next to the electrode instead of adsorbing it directly on the electrode surface. Shown in Figure 4-6 are cyclic voltammograms obtained with an EPPG electrode on which was placed a 30 μm layer of benzonitrile containing $(Me_4Ph_5Cor)Co$. The electrode was immersed in an aqueous solution of 1 M $HClO_4$. The large cathodic peak current at $E_p = 0.20$ V *vs* Ag/AgCl (Figure 4-6A) arises from the reduction of O_2 catalyzed by **2**. The rise in the catalytic current occurs at the same potential where, in the absence of O_2, $[(Me_4Ph_5Cor)Co^{IV}]^+$ is reduced to $[(Me_4Ph_5Cor)Co^{III}]^0$ in 1 M $HClO_4$ (Figure 4-6B). This implicates the cobalt(III) corrole as the catalytically active species. The reversible process observed at more cathodic potentials ($E_p = -0.30$ V *vs* Ag/AgCl) corresponds to the Co(III)/Co(II) redox couple.
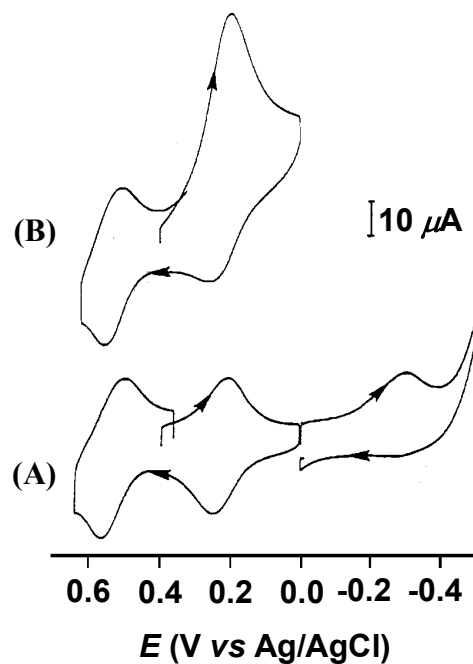
Figure 4-6. Cyclic voltammograms of **2** (0.6 mM) dissolved in a thin layer of acidified PhCN placed on an EPPG electrode that was immersed in 1 M $HClO_4$. (A) In the presence of O_2 and (B) after the aqueous phase (and the equilibrated thin layer of PhCN) was saturated with argon. Scan rate: 50 mV s^{-1}.

4.2.4 Catalytic Activity of Cobalt Corrole Derivatives Towards H_2O_2 at pH = 0.

As shown by the rotating disk electrode voltammograms of $(Me_4Ph_5Cor)Co$ (Figure 4-5A), the reduction of O_2 proceeds in a single step and H_2O_2 is the major product of the reduction at the plateau. In contrast, the larger disk current with $(PCA)Co_2$ (Figure 4-5A) shows that a portion of the O_2 is reduced to H_2O instead of H_2O_2. However, the catalyst may produce H_2O_2 as an intermediate species in the catalytic process. To test this possibility, the solution used to record the cyclic voltammogram in the presence of dioxygen (Figure 4-1) was made 0.5 mM in H_2O_2 and deoxygenated with argon for 20 minutes. The cyclic voltammogram was then recorded with a $(PCA)Co_2$-coated electrode in the presence of hydrogen peroxide and the resulting current-voltage curve is shown in Figure 4-7A where the potential was first scanned from 0.50 to 0.10 V and then from 0.10 to 0.80 V and back to 0.10 V. Under these conditions, a catalytic oxidation peak of H_2O_2 to O_2 was observed at $E_p = 0.65$ V whereas the reduction of the dioxygen formed at the electrode occured at 0.42 V on the reverse scan. No peak corresponding to the reduction of H_2O_2 to H_2O was detected between 0.80 and 0.00 V. The same electrochemical behavior was observed for $(Me_4Ph_5Cor)Co$ (Figure 4-7B) except that the magnitude of the oxidation peak current at $E_p = 0.70$ V was relatively higher than seen in Figure 4-7A for $(PCA)Co_2$. In order to obtain a more quantitative assessment of the catalytic properties of complexes **1a** and **2** towards H_2O_2, current-potential curves were recorded at a rotating disk electrode in 1 M $HClO_4$ saturated with argon (Figure 4-8). Here, both adsorbed complexes catalyze the electrooxidation of H_2O_2 at $E_{1/2} = 0.61$ and 0.65 V, respectively.
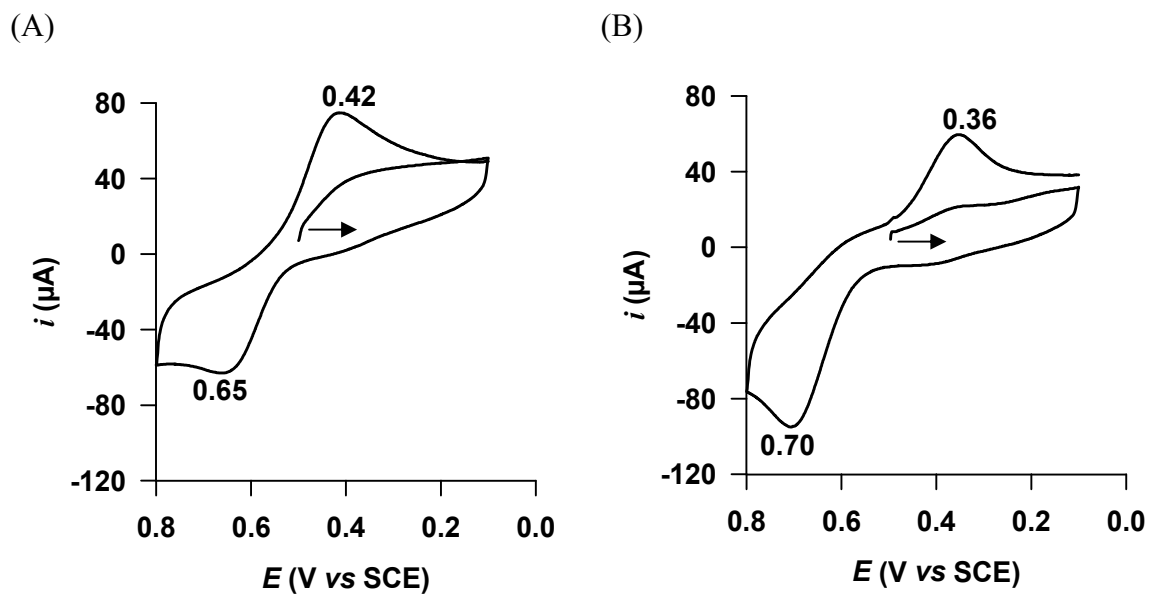
Figure 4-7. Cyclic voltammograms of **1a** (A) and **2** (B) adsorbed on EPPG electrode. Supporting electrolyte: 1 M $HClO_4$ saturated with argon. $[H_2O_2]$ = 0.5 mM. Scan rate: 50 mV s^{-1}.
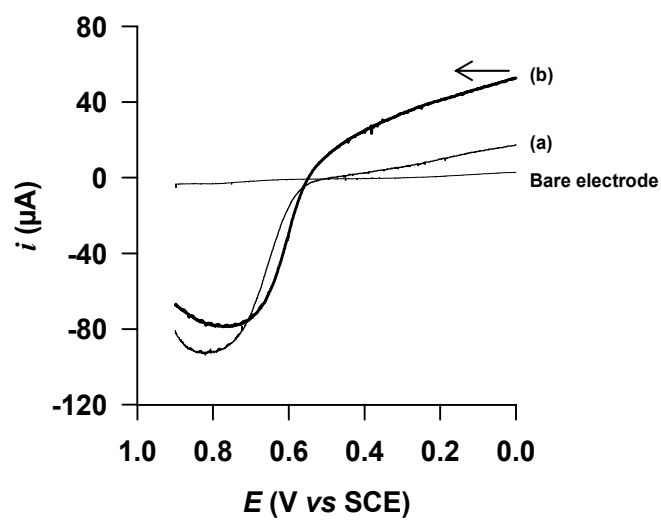
Figure 4-8. Rotating disk voltammograms of **2** (curve a) and **1a** (curve b) adsorbed on EPPG electrode. Supporting electrolyte: 1 M HClO$_4$ saturated with argon. [H$_2$O$_2$] = 0.5 mM. Rotation rate: 100 rpm. Scan rate: 5 mV s^{-1}.

The decrease in limiting currents observed for **1a** and **2** at potentials higher than 0.80 V corresponds to a gradual loss of catalytic activity due to a possible degradation of the compounds at the EPPG surface. The curves for reduction of H_2O_2 at the $(Me_4Ph_5Cor)Co$-coated electrode reveal that cobalt(III) monocorrole **2** reduces H_2O_2 at a much slower rate than it catalyzes its oxidation. The RDE voltammogram recorded in a deoxygenated solution containing 0.5 mM H_2O_2 (curve a, Figure 4-8) shows a slow rise of the disk current from ca. 0.60 to 0.00 V. An analogous RDE experiment with a $(PCA)Co_2$-coated graphite disk (curve b, Figure 4-8) shows a similar behavior of the dicobalt porphyrin−corrole dyad towards the catalytic reduction of H_2O_2. However, the magnitudes of the cathodic currents recorded between 0.60 and 0.00 V are higher than those observed for the monocobalt corrole $(Me_4Ph_5Cor)Co$ (curve a, Figure 4-8). As expected, no oxidations or reductions of H_2O_2 were observed at the bare electrode and this is also evident from the current-voltage curves in Figure 4-8.

Collman *et al.* observed that a graphite electrode coated with $(FTF4)Co_2$ also catalyzes the two-electron reduction of H_2O_2 to H_2O in acidic media.[183] The catalytic reduction of H_2O_2 by $(FTF4)Co_2$ was characterized by rotating disk electrode voltammograms similar to those recorded for complex **1a** (Figure 4-8). A similar catalytic activity toward H_2O_2 was reported by Anson, Chang and coworkers for a dicobalt cofacial diporphyrins, $(DPA)Co_2$, that is structurally similar to complex **1a**.[72] The lack of significant catalytic activity of $(DPA)Co_2$ towards the disproportionation of H_2O_2 was also demonstrated. Both Collman and Anson have stated that the rate of the electrocatalytic reduction of H_2O_2 by $(FTF4)Co_2$ and $(DPA)Co_2$ is very slow compared to

the rate of O_2 reduction.[72,183] From the results shown in Figure 4-8 it is clear that this is also true for (PCA)Co$_2$.

4.2.5 Effect of Different Spacers on O$_2$ Catalysis.

The dioxygen reduction catalytic properties of dicobalt porphyrin−corrole and biscorroles complexes bridged by biphenylene, 9,9-dimethylxanthene, dibenzofuran and dibenzothiophene were compared to those of (PCA)Co$_2$ and (BCA)Co$_2$ (Chart 4-1). The electrochemical data are compiled in Table 4-1. The structural details on complexes with spacers of the type used in this study were reported previously.[94,95,112,229] The rigidity of the anthracene and biphenylene bridges in complexes **1a**, **1b**, **3a** and **3b** minimize ring lateral slippage while maintaining a face-to-face arrangement of both macrocycles.[34] Biphenylene provides a tighter binding cavity than anthracene due to the fewer number of atoms separating the macrocyclic units. However, both single rigid linkers afford a small flexibility along the longitudinal axis of the ligands that allow the molecular clefts to structurally accommodate reaction intermediates during multielectron catalysis ("Pac-Man" effect[34,58]), thus resulting in an efficient catalytic reduction of O_2. The porphyrin−corrole dyads bridged by 9,9-dimethylxanthene (**1c**) and dibenzofuran (**1d**) also efficiently catalyze the direct four-electron reduction of O_2 to H_2O (Table 4-1), despite the structural difference between the two ligands. The xanthene bridge contains the same number of atoms as anthracene whereas the five-membered ether ring in dibenzofuran increases the size of the binding pocket. The presence of an sp^3 oxygen in the latter bridge allows the porphyrin–corrole dyad to open and close its binding pocket

by a longitudinal distance of over 4 Å in the presence of exogineous ligands as reported by Nocera and coworkers[58] This longitudinal flexibility is also observed in complex **1d** since the PCO system displays a four-electron reactivity toward dioxygen (Table 4-1).

Coatings of cobalt(III) biscorroles catalyze O_2 reduction at more negative potentials than do the $(PCY)Co_2$ derivatives under the same experimental conditions (Table 4-1). The $E_{1/2}$ values of **3a-3c** are close to that observed for $(Me_4Ph_5Cor)Co$ ($E_{1/2}$ = 0.38 V), whereas complexes **3d** and **3e** reduce O_2 at more slightly negative potentials ($E_{1/2}$ = 0.35 V). Rotating ring−disk measurements show that reduction of O_2 by the $(BCY)Co_2$ complexes produce a more significant amount of H_2O_2 than porphyrin−corrole derivatives. In comparison with $(PCY)Co_2$ systems, the decrease of catalytic selectivity towards the four-electron reduction of O_2 to H_2O in 1 M $HClO_4$ observed with $(BCY)Co_2$-coated electrodes suggests that the partially reduced dioxygen species is less stabilized. This decrease of selectivity for the direct reduction of O_2 to H_2O might also be explained by a difference of electronic properties between the electron-poor aryl-substituted corrole and the electron-rich alkyl-substituted porphyrin subunits. In comparison with **1**, the presence of a second cobalt(III) corrole unit in **3** may reduce the basicity of the oxygen adduct which strongly disfavors the four-electron reduction pathway.[23]

4.3 Conclusion

In summary, we have shown that cobalt corroles can be used as effective catalysts in the reduction of O_2. The half-wave potentials range from 0.35 to 0.47 V for the ten investigated catalysts when measured by cyclic voltammetry in 1 M $HClO_4$. However, the H_2O/H_2O_2 product ratios of the reduction differ in each case, with the most effective catalyst being the mixed oxidation state derivative **1a-1d** which leads almost exclusively to a four-electron reduction of O_2 at $E_{1/2}$ = 0.41 to 0.47 V *vs* SCE. A four-electron reduction also occurs to some extent in the absence of a porphyrin macrocycle and, under these conditions, O_2 reduction occurs at an $E_{1/2}$ of 0.35-0.39 V as seen in Table 4-1. Finally, reduction of hydrogen peroxide in 1 M $HClO_4$ by the dicobalt porphyrin-corrole **1a** is too slow to account for participation of free H_2O_2 as an intermediate in the four-electron reduction of O_2.

Chapter 5: **Catalytic Activity of Free-Base Porphyrin–Cobalt Corrole Dyads for the Electroreduction of O$_2$**

5.1 Introduction

In Chapter 4, we examined the use of face-to-face bis-Co(III) corroles or dyads containing one Co(III) corrole and one Co(II) porphyrin as catalysts for the electroreduction of O_2 in acid media when adsorbed on a graphite electrode.

In this chapter, three face-to-face dyads where one macrocycle is a cobalt(III) corrole and the other a free-base porphyrin are examined. The present study shows the ability of the three free-base porphyrin−Co(III) corrole dyads to catalyze the electroreduction of dioxygen in 1 M $HClO_4$ or 1 M HCl when adsorbed on a graphite electrode, and these results are compared to what is reported for the series of biscobalt porphyrin−corrole dyads with the same linker groups desribed in Chapter 4. The examined compounds in this chapter are illustrated in Chart 5-1 and are represented as $(PCY)H_2Co$, where P = a porphyrin dianion and C = a corrole trianion. Y is a biphenylenyl (B), 9,9-dimethylxanthenyl (X) or anthracenyl (A) spacer which links the two macrocycles.

Face-to-face bismacrocycles with one cobalt porphyrin and one free-base porphyrin have earlier been examined as to their efficiency in the electrocatalysis of O_2 when adsorbed on a graphite surface in acid media.[72,192] These monocobalt bisporphyrins exhibit four electron reduction pathways, as evidenced by n_{app} values which are much greater than 2.0, and it was, therefore, of interest in the current study to examine the reactivity of the three $(PCY)H_2Co$ dyads toward O_2 electroreduction in 1 M $HClO_4$ as well in 1 M HCl where Cl^- anions were expected, on the basis of previous studies,[70] to bind to the Co(IV) and maybe also the Co(III) form of the complex.

(Me₄Ph₅Cor)Co

(Et₂Me₆PhPor)H₂
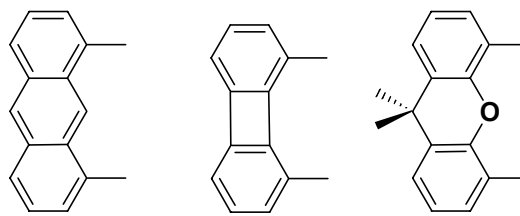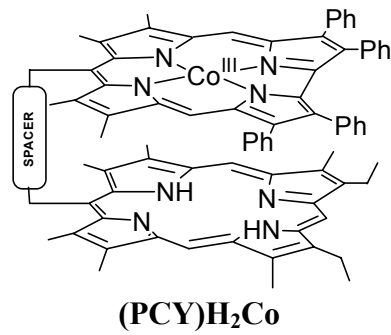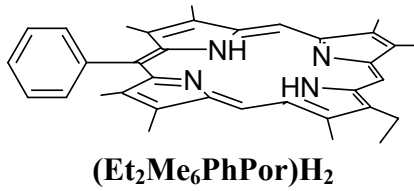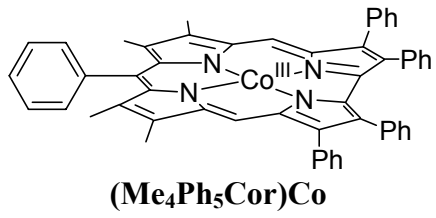
(PCY)H₂Co

SPACERS (Y)   **A**   **B**   **X**

Chart 5-1

5.2 Results and Discussion

5.2.1 Redox Properties of (PCY)H$_2$Co (Y = A, B, and X) and Catalytic Reduction of O$_2$

The catalytic activity of the (PCY)H$_2$Co dyads toward the reduction of O$_2$ was examined by cyclic voltammetry and rotating ring–disk electrode voltammetry in aqueous solutions of 1 M HClO$_4$. Current–potential curves recorded at a graphite disk coated with (PCA)H$_2$Co and (PCB)H$_2$Co are illustrated in Figure 5-1. In the absence of dioxygen, the response of the graphite electrode coated with (PCA)H$_2$Co resembles that obtained with the (PCB)H$_2$Co-coated electrode (Figure 5-1a). The cyclic voltammogram of (PCB)H$_2$Co shows two reversible processes located at $E_{1/2}$ = 0.37 and –0.02 V in 1 M HClO$_4$ whereas the (PCA)H$_2$Co system is characterized by a reversible system at $E_{1/2}$ = 0.36 V and an irreversible reduction peak at E_{pc} = –0.12 V. On the basis of comparisons with the electrochemical response of (Me$_4$Ph$_5$Cor)Co adsorbed on a graphite electrode (Chapter 4) ($E_{1/2}$ = 0.38, 0.20 and –0.08 V), the two processes of (PCB)H$_2$Co at $E_{1/2}$ = 0.37 and –0.02 V can be assigned to the formal potentials of the Co(IV)/Co(III) and Co(III)/Co(II) couples, respectively. The presence of an additional reversible process at $E_{1/2}$ = 0.20 V for (Me$_4$Ph$_5$Cor)Co was earlier explained (see Chapter 4) by the tendency of the corrole to spontaneously dimerize (or to form higher aggregates) on the graphite surface. This electrochemical behavior is not observed for the currently investigated free-base porphyrin-cobalt corrole dyads.
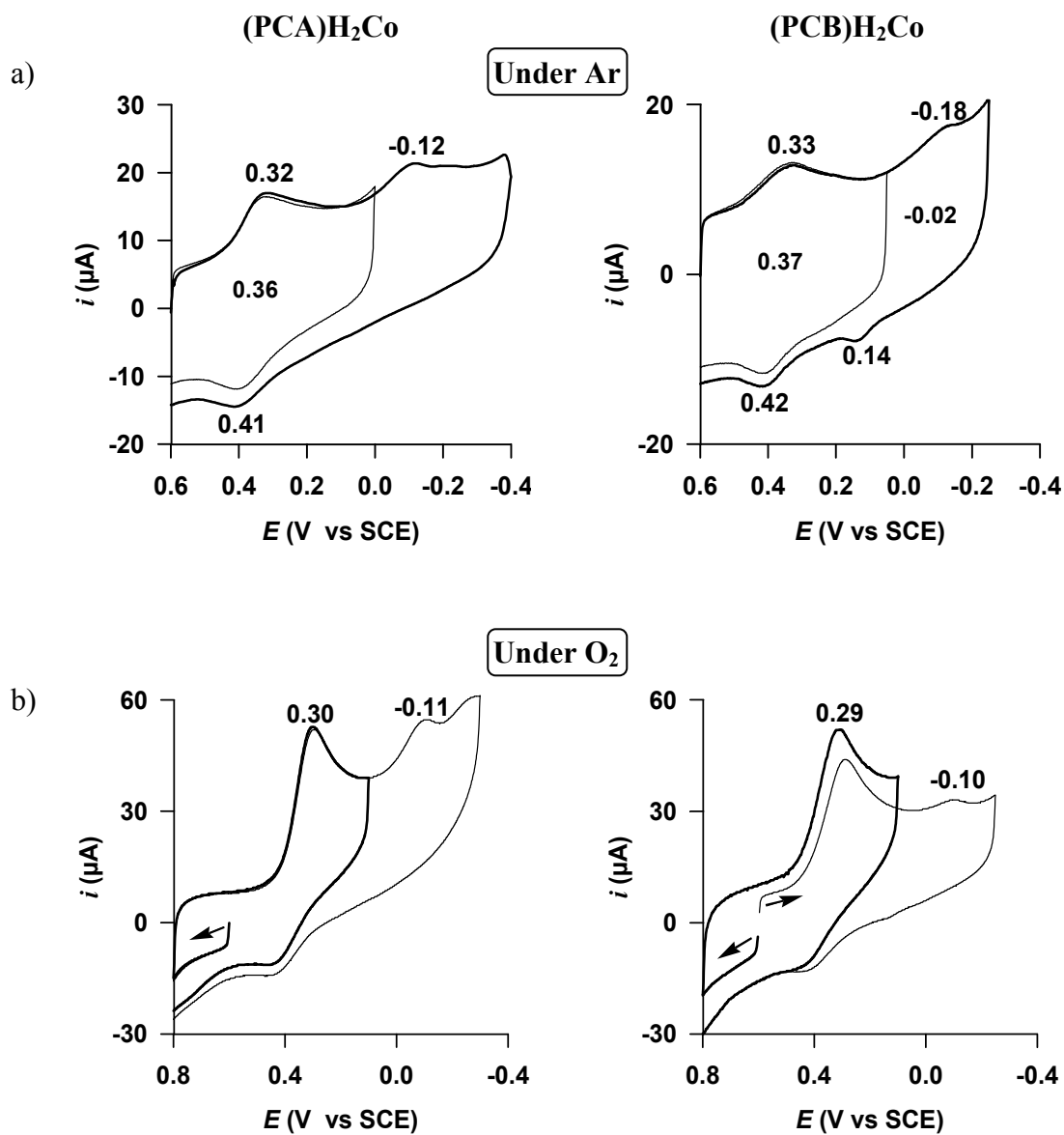
Figure 5-1. (a) Cyclic voltammograms of (PCA)H$_2$Co (left) and (PCB)H$_2$Co (right) adsorbed on an EPPG electrode. Supporting electrolyte: 1 M HClO$_4$ saturated with argon. Scan rate: 50 mV/s. (b) Cyclic voltammograms of (PCA)H$_2$Co (left) and (PCB)H$_2$Co (right) adsorbed on an EPPG electrode. Supporting electrolyte: 1 M HClO$_4$ saturated with argon. [O$_2$] = 0.24 mM. Scan rate: 50 mV/s.

Table 5-1. Electroreduction of Dioxygen by Adsorbed Free-Base Porphyrin−Cobalt Corrole Dyads in Air-Saturated 1 M $HClO_4$ or 1 M HCl.

compound	1 M $HClO_4$			1 M HCl		
	$E_p{}^a$	$E_{1/2}{}^b$	n^c	$E_p{}^a$	$E_{1/2}{}^b$	$\Delta E_{1/2}$ ($HClO_4$-HCl)
(PCA)H$_2$Co	0.30	0.35	2.8	0.21	0.28	0.07
(PCX)H$_2$Co	0.31	0.35	2.5	0.23	0.28	0.07
(PCB)H$_2$Co	0.29	0.35	2.9	0.24	0.29	0.06
(Me$_4$Ph$_5$Cor)Co	0.36	0.38	2.9	0.28	0.33	0.05

[a] Peak potential of the dioxygen reduction wave (V vs SCE). [b] Half-wave potential (V vs SCE) for dioxygen reduction at a rotating disk electrode (w = 100 rpm). [c] The apparent number of electron transferred per dioxygen molecule (n) at $E_{1/2}$ is calculated from $n = 4I_D/(I_D + I_R/N)$ where I_D and I_R are disk and ring currents, respectively, and N (= 0.24) is the collection efficiency of the ring-disk electrode.

When the solution is saturated with air (Figure 5-1b), the response of the (PCY)H_2Co-coated electrodes is characterized by a large reduction peak located at E_{pc} = 0.29-0.31 V, depending upon the spacer (see exact values in Table 5-1). The electroreduction of O_2 by the three (PCY)H_2Co complexes occurs at slightly less positive potentials than that of the related cobalt(III) corrole (Me$_4$Ph$_5$Cor)Co (E_{pc} = 0.36 V), but leaves no doubt that the electrocatalysis proceeds at the potential of the Co(IV)/Co(III) process, with the cobalt(III) center of the dyad being the active site in the electroreduction of O_2.

The rotating ring–disk electrode responses obtained for (PCA)H_2Co and (PCB)H_2Co adsorbed on the graphite electrode in 1 M HClO$_4$ (Figure 5-2) exhibit a single wave for the reduction of O_2 ($E_{1/2}$ = 0.35 V) as does (PCX)H_2Co, and the average number of electrons transferred (n) is higher than 2 (Table 5-1) for all three investigated porphyrin−corrole dyads. The number of electrons transferred in the O_2 electroreduction process ranges from 2.5 to 2.9 for (PCY)H_2Co and (Me$_4$Ph$_5$Cor)Co, indicating that the electrocatalytic reduction of O_2 leads to the formation of H_2O_2 and H_2O through processes involving both 2e$^-$ and 4e$^-$ reactions, as was previously reported for monocoabalt cofacial bisporphyrins.[72] This is clearly different behavior from that of the pophyrin–corrole dyads with two cobalt centers, (PCY)Co$_2$ (Y = O, A, X, and B), where n = 3.5−3.9 and O_2 is mainly reduced to H_2O through a 4e$^-$ process.

The unmetallated porphyrin unit of the (PCY)H_2Co dyads may increase the selectivity for the four-electron reduction of O_2 to H_2O over the two-electron pathway by helping to stabilize the partially reduced dioxygen species.
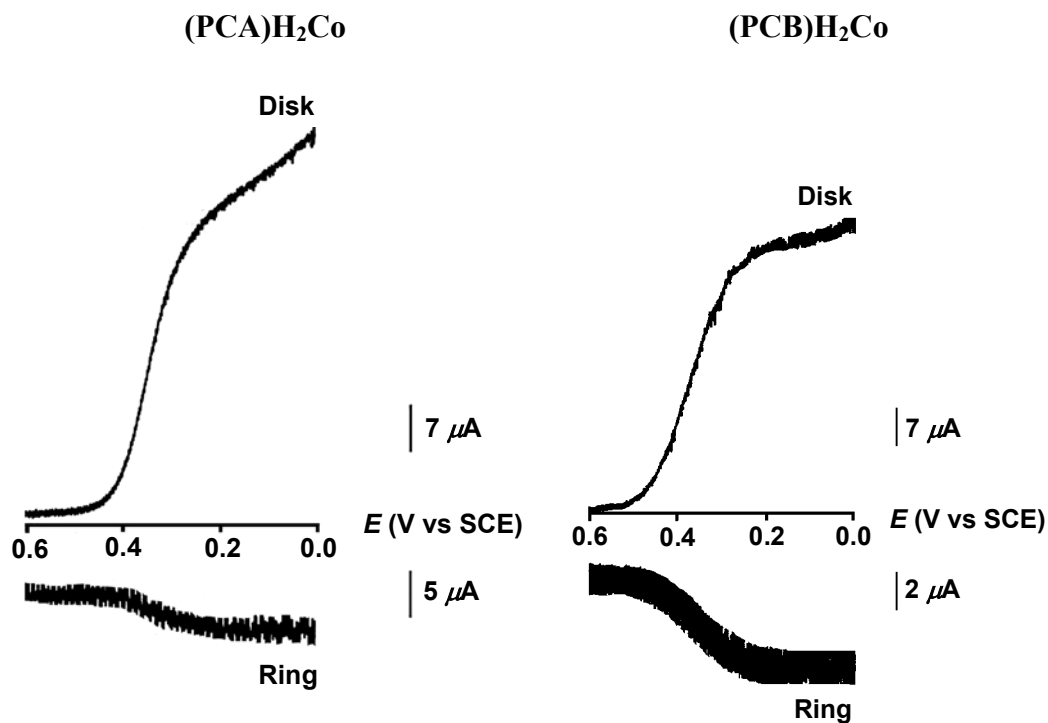
Figure 5-2. Reduction of O_2 at a rotating ring (Pt)−disk (EPPG) electrode coated with

(PCA)H$_2$Co (left) and (PCB)H$_2$Co (right) in air-saturated 1 M HClO$_4$. the potential of

the ring electrode was maintained at 1.1 V. Rotation rate: 100 rpm. Scan rate: 5 mV s^{-1}.

A similar effect has been reported for face-to-face bisporphyrin systems containing one free-base porphyrin and one cobalt porphyrin.[73] Alternatively, the increased value of n above 2.0 may be due to the presence of aggregates or dimers of the dyads on the electrode surface, as was postulated to occur in the case of $(Me_4Ph_5Cor)Co(III)$ (see Chapter 4), $(OEP)Co(II)$,[48] and $Co(II)$ porphine.[46] A dimerization is not detected by electrochemistry of the dyads in HCl or $HClO_4$, but it is clearly evident from the cyclic voltammograms of $(PCX)H_2Co$ and $(PCA)H_2Co$ in CH_2Cl_2 or PhCN.

5.2.2 Catalytic Reduction of O_2 in 1 M HCl.

The catalytic reduction of dioxygen by $(PCY)H_2Co$ and the monocorrole, $(Me_4Ph_5Cor)Co$, was also investigated by cyclic voltammetry and rotating disk electrode voltammetry in 1 M HCl where the ligand Cl^- from the acid would be expected to coordinate to the Co(IV) center of the corrole adsorbed on the electrode surface. As shown in Figure 5-3, the electrocatalytic reduction wave of dioxygen recorded in air-saturated 1 M HCl at a graphite disk coated with $(PCB)H_2Co$ is shifted by 60 mV to more negative potentials, consistent with Cl^- coordinating to the Co(IV) center of the porphyrin−corrole dyad. A similar negative shift is seen for the other two $(PCY)H_2Co$ complexes as well as for $(Me_4Ph_5Cor)Co$ in HCl, and the magnitude of the shift in $E_{1/2}$ is listed in Table 5-1 as $\Delta E_{1/2}$, which ranges from 50 to 70 mV. The fact that $(PCY)H_2Co$ and $(Me_4Ph_5Cor)Co$ both catalyze the reduction of dioxygen in the presence of Cl^- (see Table 5-1) suggests that the anionic axial ligand is released rapidly when the cobalt(IV) center is reduced to Co(III) in the dyad.
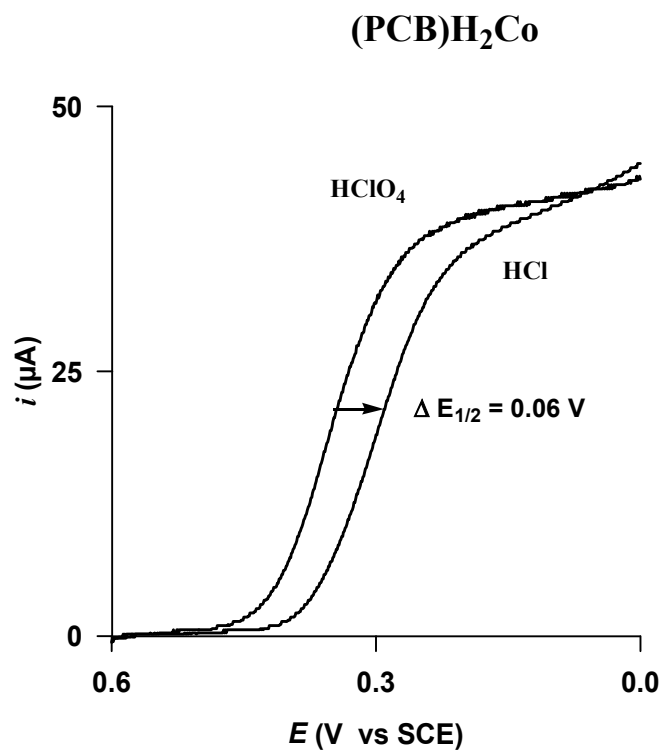
(PCB)H$_2$Co

Figure 5-3. Reduction of O$_2$ at a rotating disk electrode coated with (PCB)H$_2$Co in air-saturated 1 M HClO$_4$ or 1 M HCl. Rotating rate: 100 rpm. Scan rate: 5 mV s^{-1}.

5.3 Conclusion

Three face-to-face linked porphyrin-corrole dyads were investigated as to their ability to catalyze the electroreduction of dioxygen in aqueous 1 M $HClO_4$ or HCl when adsorbed on a graphite electrode. The characterized compounds are represented as $(PCY)H_2Co$, where P = a porphyrin dianion; C = a corrole trianion; and Y = a biphenylenyl, 9,9-dimethylxanthenyl, or anthracenyl spacer, which links the two macrocycles in a face-to-face arrangement. The Co(III) form of the corrole in $(PCY)H_2Co$ appears to be the catalytically active species in the electroreduction of dioxygen, which occurs at potentials associated with the Co(IV)/Co(III) reaction, that is, 0.35 V in 1 M $HClO_4$ as compared to 0.31−0.42 V for the same three dyads in PhCN and 0.1 M TBAP.[104] The potential for the catalytic electroreduction of O_2 in HCl shifts negatively by 60 to 70 mV as compared to $E_{1/2}$ values in 1 M $HClO_4$, consistent with the binding of Cl^- to the Co(IV) form of the corrole and its rapid dissociation after electroreduction to Co(III) at the electrode surface.

Chapter 6: Catalysis of O_2 reduction by heterobimetallic dyads containing a face-to-face linked Fe(III) or Mn(III) porphyrin

6.1 Introduction

In the previous chapters, we demonstrated that cobalt(III) corroles could be used as effective catalysts for the electroreduction of O_2 when adsorbed onto a pyrolytic edge-plane graphite electrode.[104,230] The most efficient electrocatalysts for the production of H_2O from O_2 were shown to be the dicobalt cofacial porphyrin (P)–corrole (C) dyads, $(PCY)Co_2$ where P represented a Co(II) porphyrin linked to a Co(III) corrole (C) by an anthracenyl (A), biphenylene (B), 9,9-dimethylxanthene (X), or a dibenzofuran (O) bridge (represented as Y in the formula). The least efficient of the studied cobalt corrole catalysts where the monomeric cobalt(III) corroles or the dicobalt cofacial biscorrole dyads, $(BCY)Co_2$, which contained two Co(III) corrole units linked in a face-to-face arrangement. The potentials for catalytic O_2 electroreduction in 1 M $HClO_4$ by adsorbed mixed-valent Co(II) porphyrin/Co(III) corrole complexes of the type $(PCY)Co_2$ ranged from 0.41 to 0.47 V vs the saturated calomel electrode (SCE) while the same reaction with dicobalt(III) biscorrole derivatives of the type $(BCY)Co_2$ occurred at more negative $E_{1/2}$ values (0.35–0.39 V) which were close to values obtained when the catalyst was the cobalt(III) monocorrole $(Me_4Ph_5Cor)Co$ under the same experimental conditions ($E_{1/2}$ = 0.38 V). A difference also exists in the number of electrons transferred for the catalytic reduction of O_2 using as catalysts the porphyrin–corrole dyads $(PCY)Co_2$ and the biscorrole dyads $(BCY)Co_2$. A value of $n = 4$ is expected for complete conversion of O_2 to H_2O while an $n = 2$ is expected for the 2e⁻ conversion of O_2 to H_2O_2. Under the same experimental conditions, the average measured value of n ranged from 3.5 to 3.9 for the

biscobalt (PCY)Co$_2$ catalysts, from 2.4 to 3.4 for the biscorrole dyads (BCY)Co$_2$ and from 2.5 to 2.9 for the (PCY)H$_2$Co series of compounds adsorbed on a graphite electrode. These results suggest that the cobalt porphyrin macrocycle not present in (BCY)Co$_2$ or (PCY)H$_2$Co plays a key role in the initial stage of O$_2$ reduction. We were therefore interested in examining the catalytic activity for a similar series of recently characterized[70,112] heterobinuclear face-to-face porphyrin–corrole dyads of the form (PCY)MClCoCl (where Y = A, B, X, or O, M = Fe(III) or Mn(III)), C represents a Co(III) corrole and P an Fe(III) or Mn(III) porphyrin linked by a rigid spacer Y (Chart 6-1). These results are reported in the present chapter and provide a clear picture as to the role of the cobalt porphyrin in the electrocatalytic process.

6.2 Results and discussion

6.2.1 Electrocatalytic Reduction of O$_2$.

The catalytic activity of the heterobimetallic porphyrin–corrole complexes (PCY)MClCoCl (Y = A, B, O, X and M = Fe^{III} or Mn^{III}) towards the reduction of O$_2$ were examined by cyclic voltammetry and rotating ring–disk electrode voltammetry in aqueous solutions of 1 M HClO$_4$. Figure 6-1A displays current–potential responses for the catalytic reduction of O$_2$ at a graphite disk coated with (PCO)MnClCoCl (top of figure) or (PCA)FeClCoCl (bottom). Curves (a) in Figure 6-1A were obtained by cyclic voltammetry, scanning from +0.80 V to –0.30 V and then back to the initial potential whereas the rotating disk electrode voltammograms illustrated by curves (b) show the current–voltage curves only for reduction over the same range of potentials.
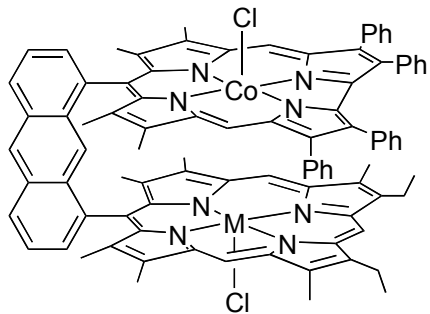
M = Fe, (PCA)FeClCoCl
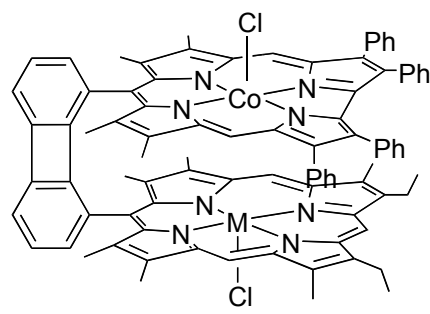
M = Fe, (PCB)FeClCoCl
M = Mn, (PCB)MnClCoCl
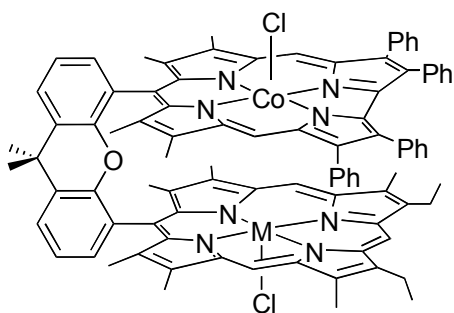
M = Fe, (PCX)FeClCoCl
M = Mn, (PCX)MnClCoCl
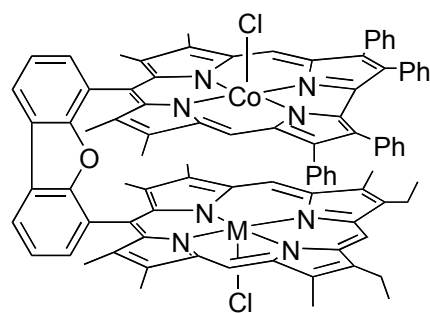
M = Fe, (PCO)FeClCoCl
M = Mn, (PCO)MnClCoCl
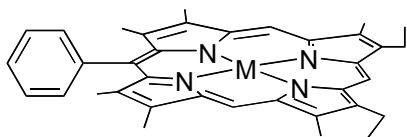
M = Co, (Me$_6$Et$_2$PhP)Co
M = FeCl, (Me$_6$Et$_2$PhP)FeCl
M = MnCl, (Me$_6$Et$_2$PhP)MnCl
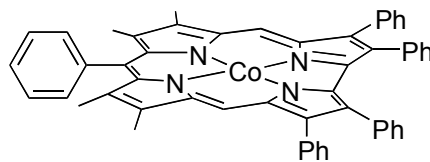
(Me$_4$Ph$_5$Cor)Co

Chart 6-1

The rotating ring–disk electrode (RRDE) voltammograms obtained for the same two compounds, (PCO)MnClCoCl and (PCA)FeClCoCl, are presented in Figure 6-1B. The reduction is carried out at the disk and the products of the reactions, H_2O_2 or H_2O, are monitored at the ring where any H_2O product of reduction will be electrooxidized at an applied potential of 1.10 V vs SCE. H_2O is electroinactive at this potential and thus the magnitude of the ring current provides a direct indication as to the amount of H_2O_2 produced in the electroreduction of O_2. It should also be pointed out that the corrole redox process assigned as Co(IV)/Co(III) in the dyads occurs at $E_{1/2}$ values close to 0.40 V in $HClO_4$[104,230] and at $E_{1/2} = 0.50$ V vs SCE in PhCN.[70,111]

Only the Co(IV) form of the corrole is present in the catalyst on the electrode surface when a negative potential scan is initiated at 0.80 to 0.60 V *vs* SCE as seen in Figure 6-1A. This assignement which is based on the Co(IV)/Co(III) redox potential will be discussed later in this chapter and is important with respect to the fact that $E_{1/2}$ for the electrocatalytic reduction of O_2 occurs at potentials quite close to $E_{1/2}$ values for electrochemical generation of the Co(III) corrole from (PCY)M^{III}ClCo^{IV}Cl or (PCY)H_2Co on the electrode surface.

In the presence of O_2, the current-potential curves obtained at (PCY)MnClCoCl- and (PCY)FeClCoCl-coated graphite electrodes are characterized by two irreversible processes. The cyclic voltammogram of (PCO)MnClCoCl (curve a, Figure 6-1A) shows an initial reduction peak at $E_{pc} = 0.30$ V followed by a second less intense peak at a more cathodic potential ($E_{pc} = -0.06$ V). A similar response is seen for the electrode coated with (PCA)FeClCoCl and here the first reduction peak in the air-saturated solution is
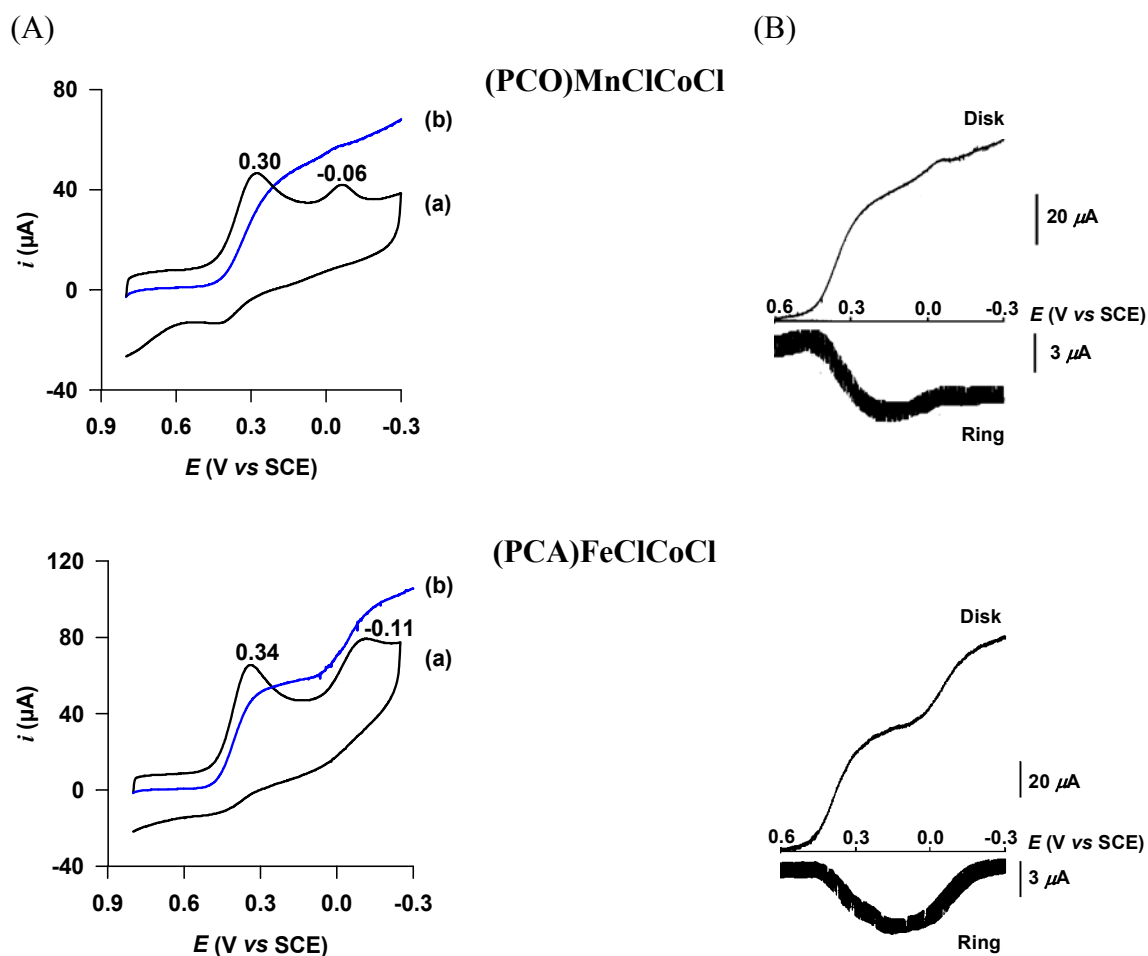
Figure 6-1. (A) Cyclic voltammograms (curves a) and rotating disk electrode voltammograms (curves b) of M–Co porphyrin–corroles adsorbed on EPPG electrode (M = Fe(III)Cl, Mn(III)Cl). Supporting electrolyte: 1 M $HClO_4$ saturated with air. Scan rate: 50 mV s^{-1}. (B) Current-potential curves at a rotating (Pt) ring–(EPPG) disk electrode in air-saturated 1 M $HClO_4$. Scan rate: 5 mV s^{-1}. Rotation rate: 100 rpm. E_{ring} = 1.1 V vs SCE.

located at E_{pc} = 0.34 V and the second at E_{pc} = –0.11 V for a scan rate of 0.05 V/s. At pH 0, the current–potential curves for O_2 reduction at the rotating disk electrode coated with (PCA)FeClCoCl or (PCO)MnClCoCl consists of two distinct waves (curves b, Figure 6-1A). In both cases, the magnitude of the first reduction currents are similar but the plateau currents for the second processes are notably larger at the electrode coated with (PCA)FeClCoCl than the one with (PCO)MnClCoCl. Also, the presence of the (PCA)FeClCoCl dyad on the electrode surface leads to an electroreduction of O_2 at a slightly more positive half-wave potential ($E_{1/2}$ = 0.39 V) than in the case when (PCO)MnClCoCl is used as the catalyst ($E_{1/2}$ = 0.36 V).

The $E_{1/2}$ values for the first reduction wave associated with the catalytic reduction of O_2 by the seven investigated complexes having the formula (PCY)MnClCoCl or (PCY)FeClCoCl range from 0.30 to 0.39 V (see Table 6-1) and are consistent with a cobalt(III) corrole-catalyzed reduction of O_2 based on previous experiments with monocobalt (PCY)H$_2$Co complexes which lack a reducible metal ion in the porphyrin macrocycle and show only a single redox process at $E_{1/2}$ = 0.35 V over the range of investigated potentials (see Chapter 5). In comparison, the Fe(II) form of the "simple" monomeric iron porphyrin macrocycle, (Me$_6$Et$_2$PhP)FeCl, catalyzes the electroreduction of O_2 at $E_{1/2}$ = 0.01 V (see Table 6-1) and this reaction occurs at potentials associated with the Fe(III)/Fe(II) process. A similar catalytic process is not readily observed for the Mn(II) form of (Me$_6$Et$_2$PhP)MnCl, in large part because the Mn(III)/Mn(II) process does not occur until much more negative potentials of –0.40 to –0.60 V vs SCE depending upon the solution conditions.[70,112]

Table 6-1. Catalytic Behavior of Heterodinuclear Porphyrin–Corroles Complexes Towards the Reduction of O_2.

Compound	1st wave		2nd wave	
	$E_{1/2}{}^a$	n^b	$E_{1/2}{}^a$	n^b
(PCA)FeClCoCl	0.39	2.8	−0.04	3.0
(PCO)FeClCoCl	0.35	2.8	−0.03	3.2
(PCX)FeClCoCl	0.33	2.6	−0.08	3.2
(PCB)FeClCoCl	0.30	2.6	−0.06	3.1
(PCO)MnClCoCl	0.36	2.6	−0.02	2.7
(PCX)MnClCoCl	0.33	2.5	−0.16	2.5
(PCB)MnClCoCl	0.32	2.8	−0.14	2.8
(Me$_4$Ph$_5$Cor)Co	0.38^c	2.9^c		
(Me$_6$Et$_2$PhP)Co	0.43	2.6		
(Me$_6$Et$_2$PhP)FeCl	0.01	3.1		

^{a} Half-wave potential (V vs SCE) for dioxygen reduction at rotating graphite disk electrode coated with the catalyst and rotated at 100 rpm in 1 M $HClO_4$ saturated with air. ^{b} The apparent number of electrons transferred per dioxygen molecule (n) at $E_{1/2}$ is calculated from $n = 4I_D/(I_D+I_R/N)$ where I_D and I_R are disk and ring currents, respectively, and N (= 0.24) is the collection efficiency of the ring–disk electrode.[218] ^{c} Data taken from ref. 230.

As seen in Table 6-1, the $E_{1/2}$ values for the catalytic reduction of O_2 vary slightly as a function of the specific bridge linking the porphyrin and corrole macrocycles in the (PCY)FeClCoCl and (PCY)MnClCoCl series. The most positive $E_{1/2}$ values are observed for dyads with the A or O bridges and the most negative for derivatives with the X or B bridges. Coatings of (PCX)FeClCoCl and (PCB)FeClCoCl electrocatalyze the reduction of O_2 at more negative potentials ($E_{1/2}$ = 0.33 and 0.30 V) than do the (PCA)FeClCoCl, (PCO)FeClCoCl and (Me$_4$Ph$_5$Cor)Co complexes (Table 6-1). However, there appears to be no effect of the porphyrin metal ion in influencing the $E_{1/2}$ values for oxygen reduction using as catalysts the (PCY)MnClCoCl or (PCY)H$_2$Co derivatives. For example, (PCO)MnClCoCl and (PCY)H$_2$Co all show an identical $E_{1/2}$ of 0.35-0.36 V within experimental error.

Measurements with a rotating (Pt) ring–(EPPG) disk electrode coated with (PCY)MnClCoCl or (PCY)FeClCoCl show that the number of electrons transferred (n) at the half-wave potential of the first electroreduction process ranges from 2.5 to 2.8 (Table 6-1), indicating that the electrocatalytic reduction of O_2 by the Co(III) center of the heterobimetallic complexes leads to the formation of both H_2O_2 ($n = 2$) and H_2O ($n = 4$).

A second reduction is also observed for the (PCY)FeClCoCl dyads in air-saturated solutions. This reduction is located at the same potential as in solutions containing added H_2O_2 (*vide infra*) and, as discussed below, is assigned to an iron(II) porphyrin catalyzed reduction of H_2O_2 or O_2 to H_2O. This reaction is responsible for the decrease in anodic ring current which accompanies the increase in disk current observed for (PCA)FeClCoCl (Figure 6-1B). The RRDE voltammogram of (PCO)MnClCoCl (Figure 6-1B) shows a slight increase of the disk current as well as a decrease of the ring current

starting at 0.10 V which suggests a slow reduction of H_2O_2 or a disproportionation of a portion of H_2O_2 by the manganese porphyrin since no decrease of the ring current is observed below 0.10 V for the series of dyads with one cobalt corrole macrocycle linked to a free-base porphyrin, *i.e.* $(PCY)H_2Co.$[104] This second reduction process of $(PCY)MnClCoCl$ occurs at a slightly more negative half-wave potential for $(PCB)MnClCoCl$ ($E_{1/2}$ = −0.16 V) than for $(PCX)MnClCoCl$ ($E_{1/2}$ = −0.14 V), again consistent with the small influence of the bridge on the redox potentials for O_2 electrocatalysis.
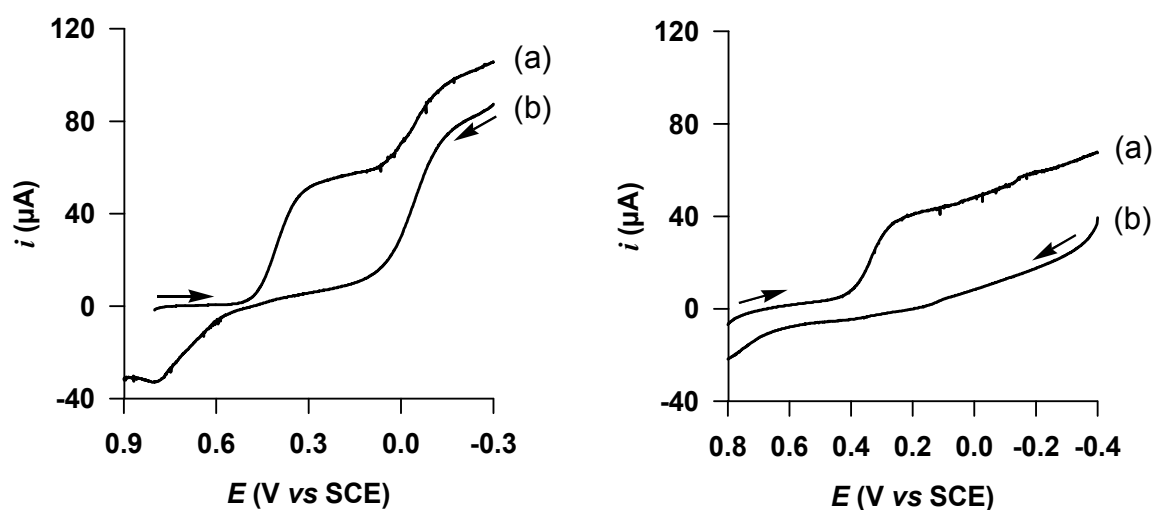
Figure 6-2. Rotating disk voltammograms of $(PCA)FeClCoCl$ (left) and $(PCB)MnClCoCl$ (right) adsorbed on EPPG. Supporting electrolyte: 1 M $HClO_4$ (a) saturated with air; (b) saturated with argon and in the presence of H_2O_2. $[H_2O_2]$ = 0.25 mM. Scan rate: 5 mV s^{-1}. Rotation rate: 100 rpm.

Shown in Figure 6-2 (curves b) are rotating disk voltammograms recorded with (PCO)MnClCoCl- or (PCA)FeClCoCl-coated electrodes in dioxygen-free 1 M $HClO_4$ containing 0.25 mM H_2O_2. The voltammogram of (PCA)FeClCoCl under these conditions shows a well-defined reduction wave at $E_{1/2} = -0.04$ V. The same $E_{1/2}$ value is obtained for the second reduction when the air-saturated solution has no added H_2O_2, thus giving further evidence that the second catalytic process is initiated after formation of an Fe(II) porphyrin. This redox reaction in air-saturated solutions is assigned in part to a catalytic reduction of H_2O_2 formed in the first step of O_2 reduction[173] but it may also involve a direct 4e⁻ reduction of O_2 by the heterobimetallic dyad which contains a Co(III) corrole linked to an Fe(II) porphyrin at potentials where the Fe(III)/Fe(II) reaction occurs. In contrast to what is observed for (PCA)FeClCoCl, the voltammogram obtained at the (PCO)MnClCoCl-coated electrode in $HClO_4$ solutions with H_2O_2 shows only a slow rise of the disk current from 0.20 to –0.40 V. An analogous RDE experiment (data not shown) carried out with a Mn(III) porphyrin, $(Me_6Et_2PhP)MnCl$, as a catalyst exhibits a similar "sluggish" redox behavior towards H_2O_2 and the small increase in the plateau current observed at $E_{1/2} = -0.02$ V for (PCO)MnClCoCl is attributed to a slow reaction between H_2O_2 and the reduced manganese center of the porphyrin–corrole.

The Co(III) corrole units of (PCA)FeClCoCl and (PCO)MnClCoCl both catalyze the electrooxidation of H_2O_2 at anodic potentials (see Figure 6-2, curves b) and this was also earlier reported in the case of $(Me_4Ph_5Cor)Co$.[230] As seen in Figure 6-2, the electrooxidation of H_2O_2 at a (PCA)FeClCoCl-coated electrode proceeds in a single step at $E_{1/2} = 0.69$ V. The current-potential curve obtained with a (PCB)MnClCoCl-coated

electrode, also shown in this figure, exhibits a less intense catalytic wave which might be due to degradation of the modified graphite electrode during H_2O_2 oxidation.

Because surface poisoning of the Pt ring by impurities in solution easily deactivates the electrode towards H_2O_2 oxidation,[183] the collection efficiency of the ring–disk electrode is always lower than the theoretical value and this could result in an overestimation of the catalytic selectivities. Therefore, linear Koutecky–Levich plots (K–L) of (plateau current)$^{-1}$ vs (rotation rate)$^{-1/2}$ for (PCA)FeClCoCl were used to confirm the apparent numbers of electrons (n) determined in the RRDE experiments (Table 6-1) and were compared with the K–L plot of the iron-free derivative (PCA)H_2Co (Figure 6-3). The catalyzed reduction of O_2 by the latter complex occurs in one step whereas a two steps reduction is clearly observed with (PCA)FeClCoCl (Figure 6-3A). For both complexes, the plateau currents do not increase linearly with (rotation rate)$^{1/2}$ (Figure 6-3B), indicating that the coordination of O_2 with the cobalt(III) center in the catalyst is the current-limiting step, as previously reported for (Me$_4$Ph$_5$Cor)Co and (PCA)Co$_2$.[230] The reciprocal intercept of the K–L plot corresponds to a kinetic current which depends upon the rate of oxygen-adduct formation. However, due to uncertainties in determining the quantities of the initially deposited catalyst, we did not attempt to calculate the second-order rate constant for the current-limiting reaction. Also, in the case of (PCA)FeClCoCl, the deviations of the plateau currents are too small to produce a measurable intercept in the K–L plots (Figure 6-3C).
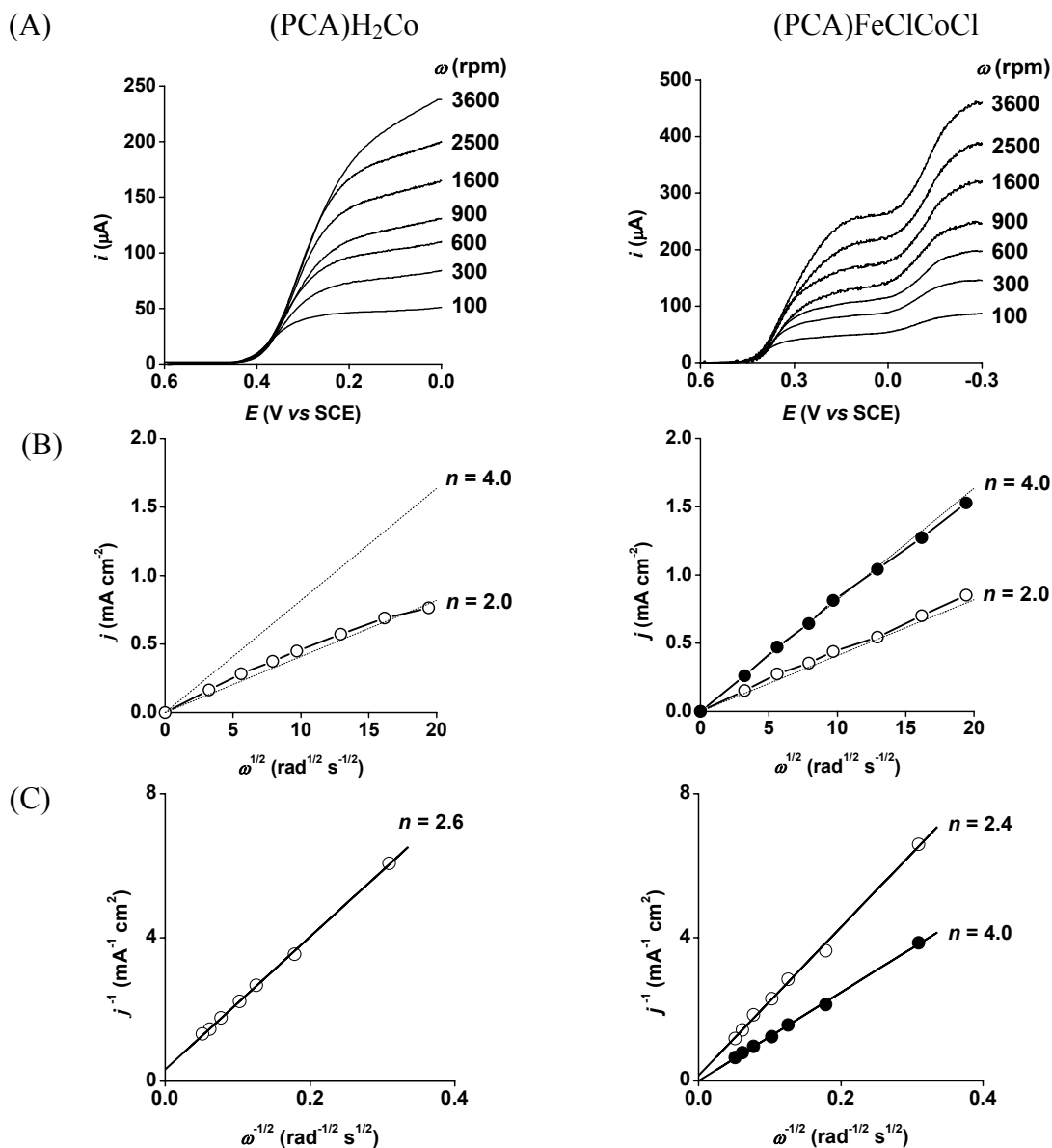
Figure 6-3. Catalyzed reduction of O_2 in 1 M $HClO_4$ at a rotating graphite disk electrode coated with (PCA)H_2Co (left) and (PCA)FeClCoCl (right). (A) Values of the rotation rates of the electrode (ω) are indicated on each curve. The disk potential was scanned at 5 mV s^{-1}. (B) Levich plots of the plateau currents of (A) vs (rotation rate)$^{1/2}$. (○) First current plateau for (PCA)H_2Co and (PCA)FeClCoCl; (●) final current plateau for (PCA)FeClCoCl. The lines refer to the theoretical curves expected for the diffusion-convection limited reduction of O_2 by 2e$^-$ or 4e$^-$, as indicated in the figures. (C) Koutecky-Levich plots of the reciprocal plateau currents vs (rotation rates)$^{-1/2}$. Supporting electrolyte: 1 M $HClO_4$ saturated with air.

For (PCA)FeClCoCl, the values of n calculated from the slopes of the lines in Figure 6-3C were 2.4 and 4.0 on the first and the second current plateau, respectively. These values confirm that a portion of O_2 that reaches the electrode surface (20%) is reduced by four electrons to H_2O on the initial current plateau whereas 100% of the O_2 reaching the electrode is reduced to H_2O on the plateau of the second wave. In comparison, the (PCA)H_2Co dyad with a free-base porphyrin exhibits less efficient catalytic behavior since only 30% of the O_2 reaching the electrode surface ($n = 2.6$) is reduced to H_2O on the plateau of the wave.

6.2.2 Comparison Between Catalytic Behavior of Homo- and Heterobimetallic Cofacial Porphyrin–Corrole and Biscorrole Dyads.

As explained in the introduction, our initial objective was to examine the extent to which the presence of iron or manganese porphyrins in the dyads could affect the electrocatalytic activity of the resulting derivatives towards the catalytic electroreduction of O_2. All seven of the heterobimetallic porphyrin–corrole dyads examined in this study act as electrocatalysts for the reduction of O_2. In the first step of the reaction, the (PCY)MClCoCl catalysts reduce O_2 to a mixture of H_2O_2 and H_2O and these reactions occur at $E_{1/2}$ values close to half-wave potentials for the conversion of (PCY)M^{III}ClCo^{IV}Cl to (PCY)M^{III}ClCo^{III}, *i.e.* the Co(IV)/Co(III) process of the corrole in the absence of dioxygen. A similar catalytic behavior is observed for the (PCY)H_2Co dyads which catalyze the electroreduction of O_2 by more than two electrons.[104] Again, as in the case of (PCY)MClCoCl, the $E_{1/2}$ values for the electrocatalytic reduction of O_2 are

close to the $E_{1/2}$ values for the Co(IV)/Co(III) process of (PCY)H$_2$Co in the absence of O$_2$.

The most illuminating comparison between the previously investigated (PCY)Co$_2$ catalysts and the other three series of related porphyrin-corrole dyads, (PCY)H$_2$Co, (PCY)FeClCoCl and (PCY)MnClCoCl is given in Table 6-2 and Figure 6-4 which summarize half-wave potentials for the catalytic electroreduction of O$_2$ and the overall measured number of electrons transferred in the process which should range from 2.0 for exclusive formation of H$_2$O$_2$ to 4.0 for the complete reduction of O$_2$ to H$_2$O. Also included in Table 6-2 are data on the dicobalt biscorrole catalysts with the same bridges, (BCY)Co$_2$.[230]

Clear differences exist between the porphyrin-corrole dyads containing a Co(II) porphyrin central ion and those without this central metal ion. As seen in Figure 6-4B, the average $E_{1/2}$ value for the electroreduction of O$_2$ by (PCY)Co$_2$ is 0.45 V while the ten other dyads in the three series of compounds show an average $E_{1/2}$ of 0.34 V for O$_2$ electroreduction. This latter value is close to $E_{1/2}$ for the electroreduction of O$_2$ using as catalyst the simple monocorrole (Me$_4$Ph$_5$Cor)Co (0.38 V). It is also close to the measured $E_{1/2}$ for the Co(IV)/Co(III) process of the monocorrole in the absence of dioxygen.[230] This latter fact clearly establishes that the cobalt corrole is in its +3 oxidation state in the catalytically active form of the (PCY)MClCoCl and (PCY)H$_2$Co dyads. In this regard, it should be noted that quite similar $E_{1/2}$ values, averaging 0.37 V for electroreduction of O$_2$, have previously been measured for four (BCY)Co$_2$ dyads in acid media (see Table 6-2), thus providing strong evidence for a similar initial site of electron transfer step in these catalysts.

Table 6-2. Half-Wave Potentials and Measured n Values at $E_{1/2}$ for the Electroreduction of O_2 by the Different Dyads Adsorbed on a Rotating Graphite Disk Electrode in Contact with Air-Saturated 1 M $HClO_4$.

Bridge (Y)	Monomer	PCY Complexes				BCY Complexes
		Co/Co	H_2/Co	Fe/Co	Mn/Co	Co/Co
A		0.47 (3.9)	0.35 (2.8)	0.39 (2.8)	-	0.39 (3.4)
O		0.41 (3.5)	-	0.35 (2.8)	0.35 (2.6)	0.35 (3.4)
X		0.45 (3.7)	0.35 (2.5)	0.33 (2.6)	0.33 (2.5)	0.37 (2.9)
B		0.46 (3.7)	0.35 (2.9)	0.30 (2.6)	0.32 (2.8)	0.37 (2.4)
None (P)	0.43 (2.6)	[Me$_6$Et$_2$PhP]Co		-	-	-
None (C)	0.38 (2.9)	[Me$_4$Ph$_5$Cor]Co		-	-	-
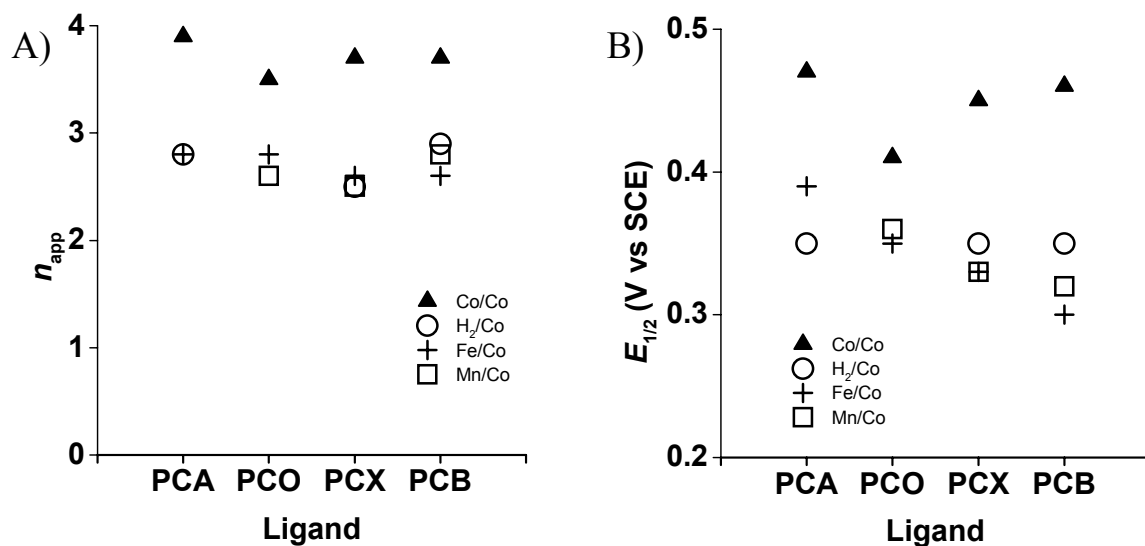
Figure 6-4. (A) apparent numbers of electrons transferred (n_{app}) vs Ligand and (B) Half-wave potentials ($E_{1/2}$) for O_2 reduction vs Ligand. (▲) $(PCY)Co_2$, (○) $(PCY)H_2Co$, (+) $(PCY)FeClCoCl$, (□) $(PCY)MnClCoCl$ with Y = A, B, X or O.

In contrast to $(PCY)H_2Co$ and $(PCY)MClCoCl$, the four $(PCY)Co_2$ dyads catalyze the electroreduction of O_2 at much more positive potentials and here the average $E_{1/2}$ value for this process is 0.45 V, close to the $E_{1/2}$ of 0.43 V for O_2 reduction by the analogous cobalt monoporphyrin $(Me_6Et_2PhP)Co$ in the absence of a second macrocycle (see Table 6-2). The O_2 electrocatalysis half-wave potentials of 0.41 to 0.47 V for $(PCY)Co_2$ in Table 6-2 are also close to the related Co(III)/Co(II) process of the monoporphyrin in the absence of O_2 ($E_{1/2} = 0.41$ V), thus providing strong evidence that the first step in the electrocatalysis with $(PCY)Co_2$ is initiated by a reduction of the porphyrin and not the corrole unit of the dyad since the Co(IV)/Co(III) corrole redox process occurs at significantly more negative half-wave potentials ($E_{1/2} = 0.38$ V). The large difference in O_2 reduction potentials ($\Delta E_{1/2} \sim 110$ mV) observed between dicobalt $(PCY)Co_2$ dyads and the monocobalt $(PCY)MClCoCl$ and $(PCY)H_2Co$ dyads indicates that the cobalt(II) porphyrin unit of $(PCY)Co_2$ catalyzes the electroreduction of O_2 whereas the cobalt corrole unit remains catalytically inactive towards O_2. The bulkiness of the aryl-substituents attached to the corrole subunit in $(PCY)Co_2$ may decrease the non-covalent π-π interaction of this macrocycle with the graphite surface, favoring the adsorption of the alkyl-substituted cobalt porphyrin unit on the electrode surface as well as its catalytic activity toward O_2.[19] The existence of stronger interactions between the carbon surface and the porphyrin ring[19] could also explain the positive potential shift observed ($\Delta E_{1/2} = 50$ mV) when $(Me_6Et_2PhP)Co$ is used as a catalyst instead of $(Me_4Ph_5Cor)Co$ (Table 6-2).

A) Porphyrin Centered Reduction

(PCY)Co₂ → $(PCY)Co_2$

reaction 1:
$\xrightarrow{e^-}$ 0.45 V

$(PCY)Co_2$

reaction 2:
$\xrightarrow{e^-}$ 0.43 V

$(Me_6Et_2PhP)Co$

Legend:
Co = corrole

M = porphyrin

$M = FeCl, MnCl \text{ or } 2H$
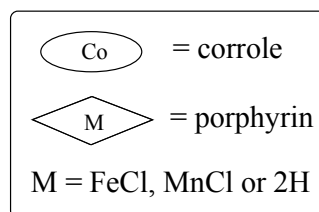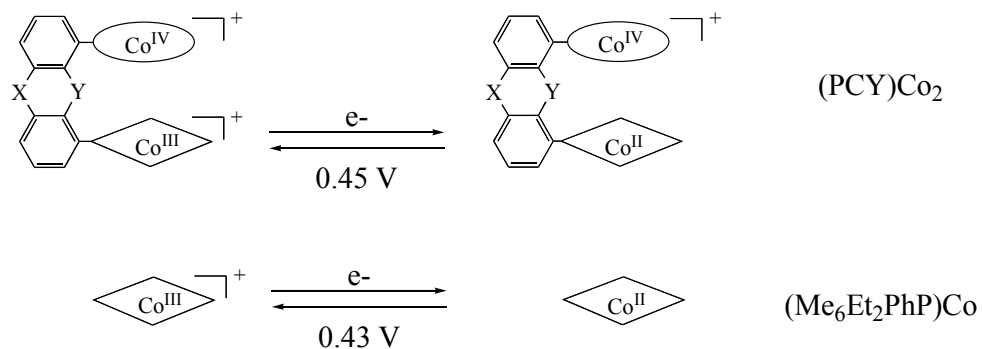
B) Corrole Centered Reduction

$\xrightarrow{e^-}$ 0.34 V

$(PCY)H_2Co$
$(PCY)MnClCoCl$
$(PCY)FeClCoCl$

$\xrightarrow{e^-}$ 0.35 V

$(BCY)Co_2$

$\xrightarrow{e^-}$ 0.38 V

$(Me_4Ph_5Cor)Co$
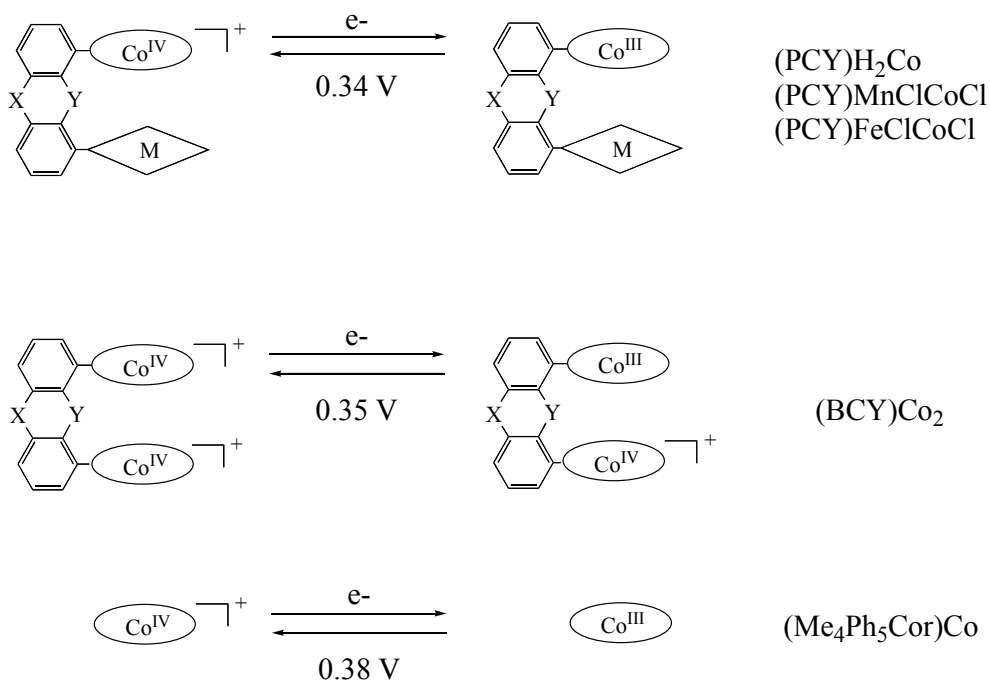
Scheme 6-1

The proposed initial site of electron transfer in the different types of porphyrin–corrole dyads is shown schematically in Scheme 6-1. Under an applied potential of 0.60 to 0.80 V where the negative potential sweep is initiated, the dyads all exist with the corrole in its Co^{IV} oxidation state. The cobalt porphyrin from $(PCY)Co_2$ is also oxidized to its Co(III) form at a potential of 0.60 to 0.80 V and thus the catalyst on the surface for $(PCY)Co_2$ is actually doubly oxidized $[(PCY)Co_2]^{2+}$ which contains a Co(IV) corrole and a Co(III) porphyrin. The other dyads also contain a Co(IV) corrole before starting the potential sweep, *i.e.* $[(PCY)H_2Co]^+$, $(PCY)MnClCoCl$ and $(PCY)FeClCoCl$. The above mentioned compounds are all inactive towards the electroreduction of O_2 as is doubly oxidized $[(BCY)Co_2]^{2+}$ which contains two Co(IV) corrole macrocycles under an applied potential of 0.8 V in $HClO_4$.

As indicated earlier, the initial site of electron transfer involves the cobalt porphyrin center in the case of $(PCY)Co_2$ and the cobalt corrole center in the case of all other compounds. This is shown in Scheme 6-1 which also includes the electrode reaction corresponding to the first reduction of $[(BCY)Co_2]^{2+}$ at the electrode surface. It is suggested that only one of the two Co(IV) centers is converted to Co(III) which is not an unreasonable assumption given the similar values of $E_{1/2}$ for $(BCY)Co_2$, $(PCY)H_2Co$ and $(PCY)MClCoCl$ in the catalytic electroreduction of O_2 (see Table 6-2) and the known tendency of bisporphyrins and biscorroles to undergo redox reactions at different half-wave potentials due to the interactions which occur between two equivalent redox active sites in the molecules.[23,27,55,57,86,192,201,221]

The different metal oxidation states of the four singly reduced dyads in the $(PCY)Co_2$ series as compared to the 14 other compounds in Table 6-2 must be associated with

different mechanisms for the catalytic reduction of O_2 at potentials of 0.30 to 0.47 V and this is reflected in quite different values of n which range from 3.5 to 3.7 for (PCY)Co$_2$, 2.9 to 3.4 for (BCY)Co$_2$ and 2.5 to 2.8 for the ten compounds in the three series of dyads containing a free-base, Mn(III) or Fe(III) porphyrin macrocycle. The average n value for these latter ten compounds is 2.7 electrons transferred in the reduction of O_2 as compared to an average $n = 3.0$ for the four (BCY)Co$_2$ dyads and $n = 2.9$ for the simple monocorrole under the same experimental conditions (see Table 6-2).

The fact that all of the experimentally determined n values at $E_{1/2} = 0.30 - 0.39$ V are larger than 2.0 for the (PCY)H$_2$Co and (PCY)MClCoCl complexes requires that a portion of the O_2 reaching the electrode surface must be reduced by four electrons to H$_2$O since cobalt(III) corroles are weak catalysts for the reduction of H$_2$O$_2$.[230] All of the dyads in the three monocobalt series of catalysts (PCY)FeClCoCl, (PCY)MnClCoCl and (PCY)H$_2$Co exhibit higher selectivities for the direct reduction of O_2 to H$_2$O over the two-electron, two-proton pathway to give H$_2$O$_2$. There is a slight dependence of $E_{1/2}$ on the bridge but there is no significant difference in the measured n value as a function of bridge type or porphyrin metal ion as shown graphically in Figure 6-4A. Although not shown in Figure 6-4, the measured n value for the (BCY)Co$_2$ catalysts with X and B bridges fit well with the other B- and X-bridged compounds in the (PCY)MClCoCl and (PCY)H$_2$Co series and (Me$_4$Ph$_5$Cor)Co also fits this trend.

A number of different schemes have been proposed in the literature for related porphyrin μ-superoxo intermediates in the catalytic O_2 reduction cycle,[23,34,61,73,201] some of which may be operative for the present series of compounds. We have not investigated the prevailing mechanism of O_2 reduction for the monocorrole or the heterobimetallic

porphyrin–corrole dyads but in both cases there must be two competing catalytic processes to give an n value larger than 2.0. The data indicates that the catalytic active species in $(PCY)H_2Co$, $(PCY)MnClCoCl$ and $(PCY)FeClCoCl$ contains the $Co(III)$ corrole generated at the electrode surface at a half-wave potential associated with the $Co(IV)/Co(III)$ process measured in the absence of O_2. All three series of porphyrin–corrole dyads are proposed to follow the same initial pathway with the only difference being that $(PCY)FeClCoCl$ undergoes a second catalytic process after the $Fe(III)/Fe(II)$ reaction of the porphyrin to give at the electrode surface a dyad having a $Co(III)$ corrole linked to an $Fe(II)$ porphyrin. As we have demonstrated in this chapter, a monomeric $Fe(II)$ porphyrin can efficiently reduce O_2 at a half-wave potential of 0.01 V giving an n = 3.1 (Table 6-1) or it can reduce H_2O_2 to give H_2O at the same half-wave potential (Figure 6-2). The catalytic reduction of H_2O_2 to H_2O by monomeric iron porphyrins is well documented in the literature[27,86] and thus any H_2O_2 generated in the first catalytic step would be quantitatively removed to give only H_2O and an overall $4e^-$ reduction of O_2 to H_2O at the plateau of the second reduction, as is experimentally observed.

On the other hand, the experimentally measured value of $n = 3.1$ for O_2 reduction by $(Me_6Et_2PhP)FeCl$ at 0.01 V (see Table 6-1), combined with the availability of a second metal ion able to bind O_2 in the electrogenerated $Co(III)/Fe(II)$ dyad should in theory lead to the direct $4e^-$ reduction of any O_2 reaching the electrode by a process similar to that observed for $(PCY)Co_2$ which contains one $Co(III)$ corrole and one $Co(II)$ porphyrin. However, more detailed studies must still be carried out in order to definitively elucidate this point.

6.3 Conclusion

In summary, we have examined the catalytic behavior of a series of heterobimetallic porphyrin–corrole dyads towards O_2 electroreduction. The results of our studies indicate that O_2 is initially reduced by the cobalt(III) corrole unit of the complexes. Although the second metal (Fe or Mn) of the (PCY)MClCoCl systems has some influence on the potential where O_2 is reduced, these systems are no more effective towards O_2 catalysis than the monocobalt derivatives (PCY)H$_2$Co, indicating that a bimetallic system is not indispensable for the four-electron reduction of oxygen as previously observed for monomeric iron porphyrins.[27,40,41,43,231] However, the introduction of a second cobalt atom into (PCY)H$_2$Co produces Co–Co catalysts with significantly higher selectivities toward the four-electron reduction of O_2 than the (PCY)MClCoCl systems. Coatings of (PCY)Co$_2$ also catalyze the electroreduction of O_2 at more positive potentials than do the monocobalt derivatives (PCY)MClCoCl and (PCY)H$_2$Co, indicating that the active form of the catalyst contains the cobalt(II) porphyrin moiety.

Chapter 7: *Meso*-substituted cobalt corroles and porphyrin-corrole dyads as catalysts for the electroreduction of molecular oxygen

7.1 Introduction

We have reported in the previous chapters that potentials for the catalytic O_2 electroreduction in 1 M $HClO_4$ by adsorbed mixed-valent Co(II) porphyrin/Co(III) corrole complexes of the type (PCY)Co$_2$ (Y = A, B, X, or O) range from 0.41 to 0.47 V vs the saturated calomel electrode (SCE) while the average number of electrons transferred, n, ranges from 3.5 to 3.9. Under the same experimental conditions, the average value of n ranges from 2.5 to 2.9 for the dyads with a single Co(III) corrole macrocycle linked to a free-base porphyrin, (PCY)H$_2$Co, and from 2.6 to 2.8 for the heterobimetallic porphyrin–corrole complexes (PCY)MClCoCl where a Co(IV) corrole is linked in a face-to-face arrangement with an Fe(III) or Mn(III) porphyrin. The catalytic electroreduction of O_2 by the porphyrin–corrole dyads (PCY)H$_2$Co and (PCY)MClCoCl occurs at an average $E_{1/2}$ value of 0.34 V with the cobalt(III) center of the dyads being the active site in the electroreduction of O_2. In comparison, the biscobalt dyads, (PCY)Co$_2$, catalytze O_2 electroreduction at potentials more positive by an average of 110 mV and the catalytically active form of the biscobalt dyad contains a Co(II) porphyrin and a cobalt(IV) corrole.

This present chapter expands upon our studies of dicobalt porphyrin-corrole dyads (PCY)Co$_2$ (Chapter 4) and here examines how *meso*-substitution of the corrole ring will affect the catalytic efficiency of the biscobalt complexes for the electroreduction of O_2. The examined compounds are shown in Chart 7-1.
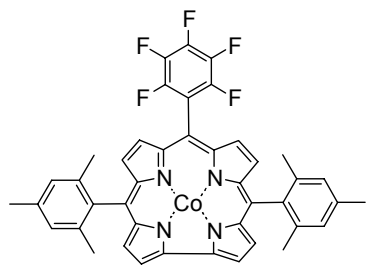
(F₅PhMes₂Cor)Co
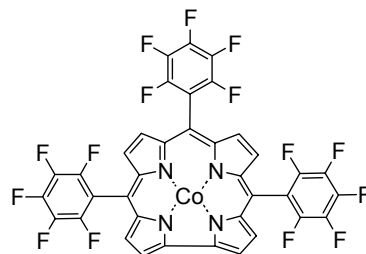
(TPFCor)Co
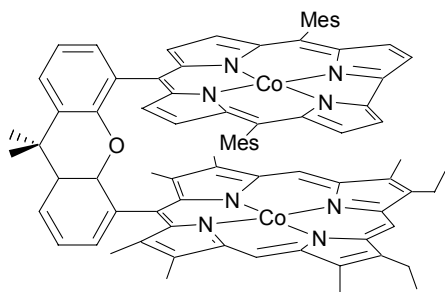
(PMes₂CX)Co₂
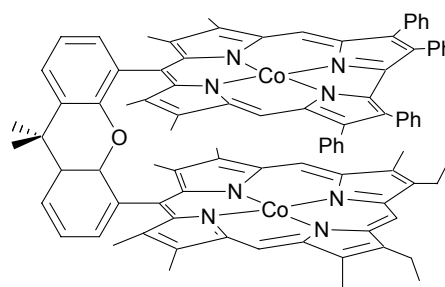
(PCX)Co₂
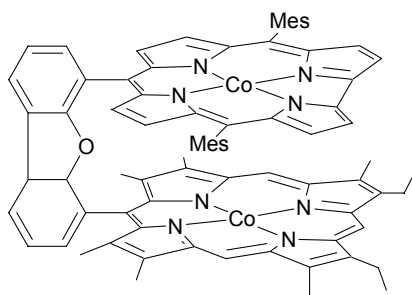
(PMes₂CO)Co₂
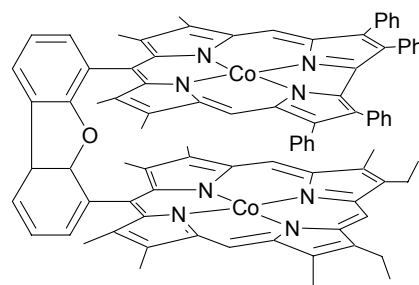
(PCO)Co₂
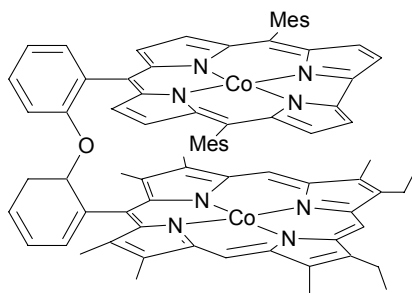
(PMes₂COx)Co₂
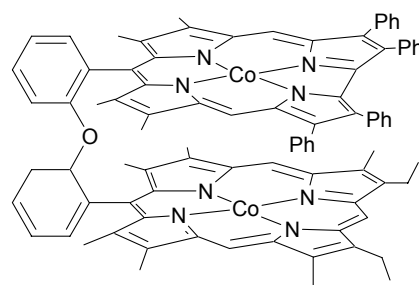
(PCOx)Co₂

Chart 7-1

The dyads are represented as $(PMes_2CY)Co_2$ where Y = 9,9-dimethylxanthene (X), dibenzofuran (O), or diphenylether (Ox). The catalytic behavior of the these three compounds is compared to that of two cobalt corrole mononuclear complexes possessing different *meso*-substituents, $(F_5PhMes_2Cor)Co$ and $(TPFCor)Co$ with F_5PhMes_2Cor = 10-(pentafluorophenyl)-5,15-bis(2,4,6-trimethylphenyl)corrole and $TPFCor$ = 5,10,15-tris(pentafluorophenyl)corrole, respectively. As before, the catalytic activity of each species towards the electroreduction of O_2 was studied by cyclic voltammetry and rotating disk voltammetry in aqueous solutions 1 M $HClO_4$.

7.2 Results and Discussion

Since it has been previously shown that the highest activity of adsorbed cobalt porphyrins and corroles towards oxygen reduction is obtained in acidic media,[114,192,232] we examined all compounds in aqueous solutions containing 1 M $HClO_4$. Each of the examined complexes adsorbs strongly and irreversibly on an EPPG electrode.

7.2.1 Redox Properties of $(F_5PhMes_2Cor)Co$ and $(TPFCor)Co$ and the Catalytic Reduction of O_2 in 1 M $HClO_4$

Figure 7-1 illustrates a series of cyclic voltammograms obtained with an EPPG electrode modified with the cobalt corroles $(F_5PhMes_2Cor)Co$ and $(TPFCor)Co$. In the absence of dioxygen (curves a), both $(F_5PhMes_2Cor)Co$ and $(TPFCor)Co$ exhibit a single redox process centered at $E_{1/2}$ = 0.33 V and $E_{1/2}$ = 0.34 V, respectively, which is assigned to the formal potential of the Co(IV)/Co(III) couple.[104] Reduction of the Co(IV) center in

(TPFCor)Co to Co(III) occurs at a slightly higher potential (E_{pc} = 0.29 V) than $E_{1/2}$ for the reduction of (F_5PhMes_2Cor)Co (E_{pc} = 0.26 V) due to the electron-withdrawing effect of the pentafluorophenyl groups which decrease the electron density on the metal center. It should be pointed out that this electron-withdrawing effect is more pronounced in nonaqueous solvent since the half-wave potentials for the Co(IV)/Co(III) process of (F_5PhMes_2Cor)Co and (TPFCor)Co in PhCN are 0.57 V and 0.74 V, respectively.[233]
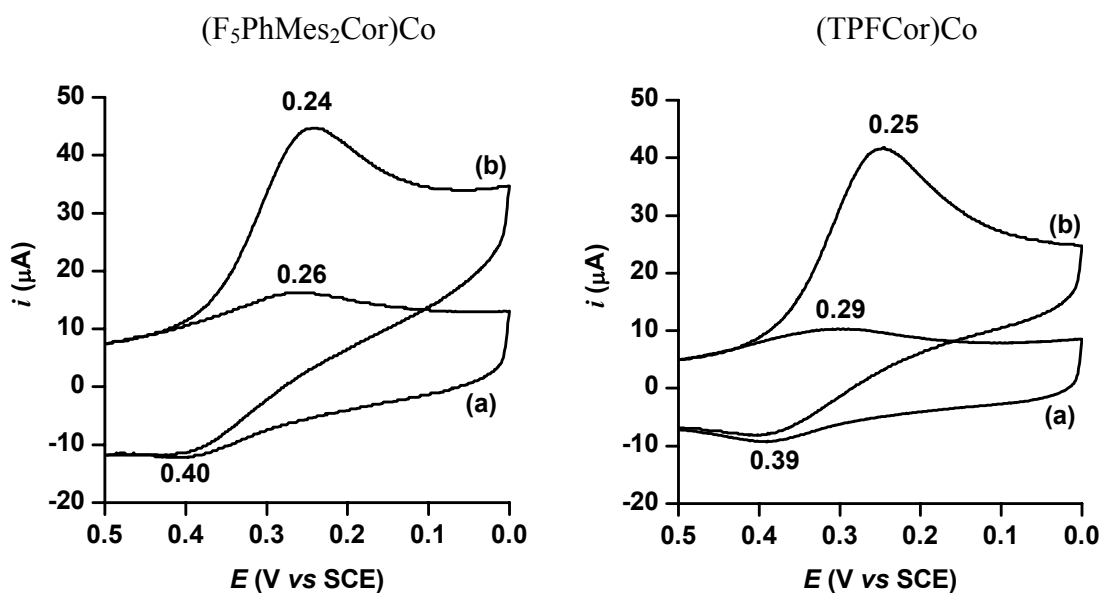
Figure 7-1. Cyclic voltammograms of cobalt corroles adsorbed on EPPG electrode. Supporting electrolyte: 1 M $HClO_4$ (a) saturated with argon and (b) saturated with air. Scan rate: 50 mV s^{-1}.

When the same solutions are saturated with air (curves b), the responses of both (F_5PhMes_2Cor)Co- and (TPFCor)Co-coated graphite electrodes are similar and characterized by a large irreversible reduction peak located at E_{pc} = 0.24–0.25 V for a

scan rate of 50 mV s^{-1} (Figure 7-1 and Table 7-1). In comparison, the reduction of O_2 at an uncoated graphite electrode occurs at a much more negative potential ($E_p = -0.41$ V) which clearly indicates that the reactivity of the electrode upon modification has to be attributed to the adsorbed cobalt corroles. The catalyzed electroreduction of O_2 by ($F_5PhMes_2Cor)Co$ and (TPFCor)Co occur at potentials similar to those where Co(IV) is reduced to Co(III) ($E_{1/2} = 0.33$ V and $E_{1/2} = 0.34$ V, respectively), thus indicating that the reduced form of the cobalt corrole catalyzed the reduction of O_2 as previously reported (Chapters 4, 5 and 6). In comparison to the peak potentials observed for solutions of ($F_5PhMes_2Cor)Co$ and (TPFCor)Co in the absence of dioxygen (Figure 7-1, curves a), the slightly less positive peak potential for O_2 reduction (curves b) may reflect either a slow formation of the O_2 adducts, a less positive reduction potentials of the O_2 adducts, or perhaps both. The half-wave potentials for O_2 reduction at the rotating disk electrode (Table 7-1) are similar for the two corrole catalysts ($E_{1/2} = 0.30$ V) and indicate that the catalytic reduction of O_2 is not strongly influenced by the difference in the substitution pattern between ($F_5PhMes_2Cor)Co$ and (TPFCor)Co. However, both *meso*-substituted corroles catalyze the O_2 reduction at significantly lower potentials than those observed for the previous examined monocobalt corrole with β-pyrrole substituents, *i.e.* ($Me_4PhCor)Co$ ($E_{1/2} = 0.38$ V) and the potentials are also lower than observed for the porphyrin–corrole dyads (PCY)H$_2$Co, (PCY)FeClCoCl and (PCY)MnClCoCl, which show an average $E_{1/2}$ of 0.34 V for O_2 electroreduction (Chapter 6). The redox potential shift in the formal Co(IV)/Co(III) process may be explained by the bulkiness and orientation of the *meso*-substituents on ($F_5PhMes_2Cor)Co$ and (TPFCor)Co. For both complexes, the methyl and fluoro groups at the ortho position prevent rotation of the

137

Table 7-1. Electroreduction of Dioxygen by Cobalt Corroles in Air-Saturated 1 M $HClO_4$.

Monomer	$E_p{}^a$	$E_{1/2}{}^b$	n^c	ref[d]
(F_5PhMes_2Cor)Co	0.24	0.30	2.0	T.W.
(TPFCor)Co	0.25	0.30	2.0	T.W.
(Me_4Ph_5Cor)Co	0.36	0.38	2.9	230

[a] Peak potential of the dioxygen reduction wave (V *vs* SCE). [b] Half-wave potential (V *vs* SCE) for dioxygen reduction at rotating disk electrode (ω = 100 rpm). [c] Electrons consumed in the reduction of O_2 as estimated from the slope of the Koutecky−Levich plots. [d] T.W. = This Work.

phenyl rings at the *meso* position due to a strong repulsion by the pyrrole hydrogens.[19,234] As pointed out by Yamazaki *et al.*,[19] the bulkiness and orientation of these substituents decrease the π–π interaction between the macrocycles and the electrode surface which results in a negative shift of the half-wave potential for O_2 reduction.

To quantify the stoichiometry of the catalyzed reduction of dioxygen, voltammetric measurements at a rotating disk electrode (RDE) were also performed. The RDE responses obtained for $(F_5PhMes_2Cor)Co$ adsorbed on the graphite electrode in 1 M $HClO_4$ (Figure 7-2) show a single wave for the reduction of O_2. A similar behavior is also observed for the pentafluorophenyl derivative $(TPFCor)Co$ (data not shown). The half-wave potential is identical for $(F_5PhMes_2Cor)Co$ and $(TPFCor)Co$, $E_{1/2} = 0.30$ V, (at $i = 0.5i_{max}$ where i_{max} is the limiting current measured at 100 rpm), and becomes more negative at higher rotation rate. The number of electrons transferred during oxygen reduction was calculated from the magnitude of the steady-state limiting current values which were taken at a fixed potential on the catalytic wave plateaus of the different current-voltage curves in Figure 7-2A (–0.1 V). If mass-transport alone controls the reduction of dioxygen at the $(F_5PhMes_2Cor)Co$-modified electrode, then the relationship between the limiting current and rotation rate should obey the Levich equation:[214]

$$i_{Lev} = 0.62nFA\upsilon^{-1/6}D^{2/3}[O_2]\omega^{1/2} \qquad \text{(eq. 25)}$$

where n is the number of electrons transferred, F is the Faraday constant (96485 C mol^{-1}), A is the electrode area (cm^2), ν the kinematic viscosity of the solution (cm^2 s^{-1}), D the

(F$_5$PhMes$_2$Cor)Co   (PMes$_2$CO)Co$_2$
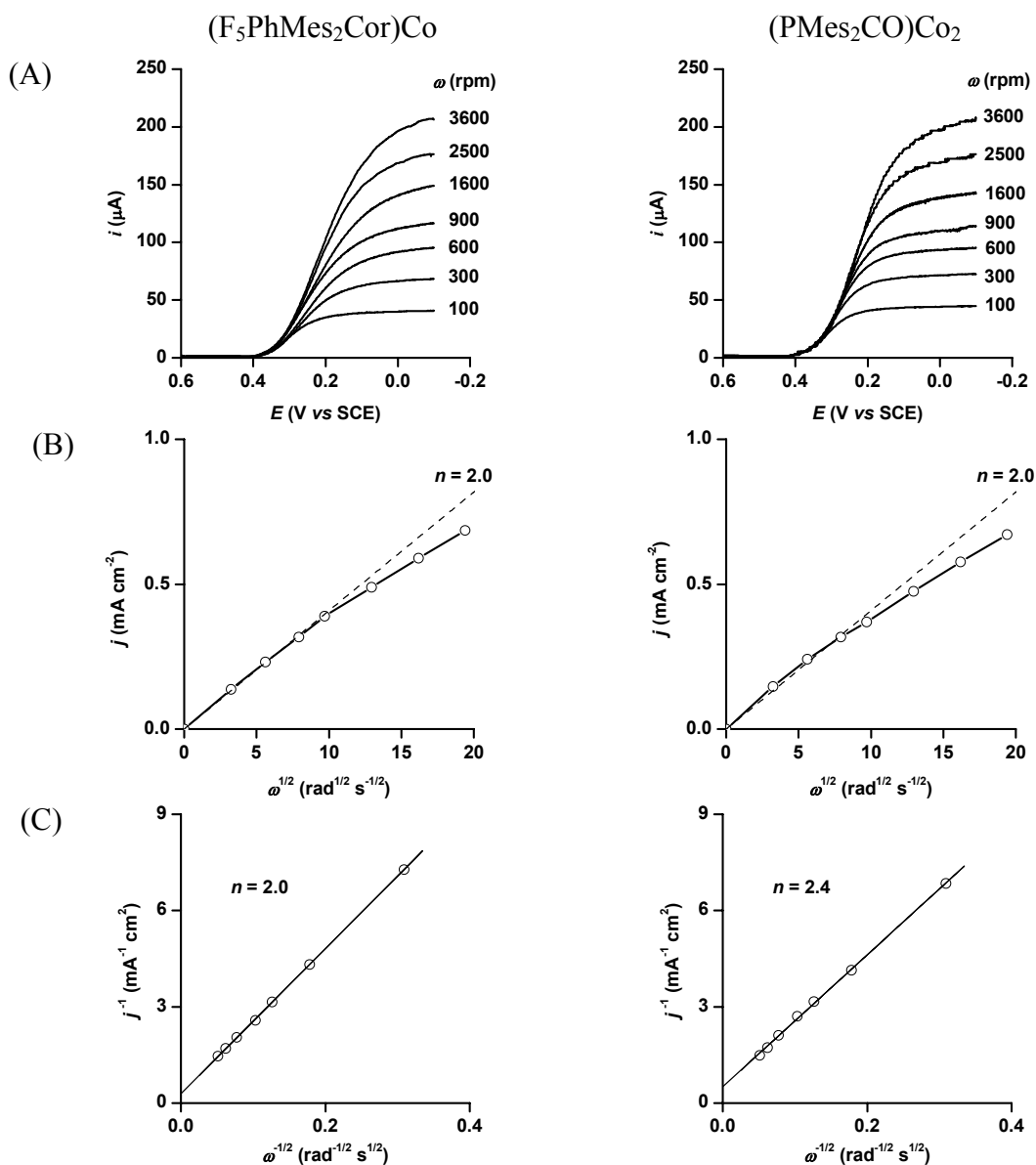
Figure 7-2. Catalyzed reduction of O$_2$ in 1 M HClO$_4$ at a rotating graphite disk electrode coated with (F$_5$PhMes$_2$Cor)Co (left) and (PMes$_2$CO)Co$_2$ (right). (A) Values of the rotation rates of the electrode (ω) are indicated on each curve. The disk potential was scanned at 5 mV s^{-1}. (B) Levich plots of the plateau currents of (A) vs (rotation rate)$^{1/2}$. The dashed line refers to the theoretical curve expected for the diffusion-convection limited reduction of O$_2$ by 2e$^-$, as indicated in the figures. (C) Koutecky-Levich plots of the reciprocal plateau currents vs (rotation rates)$^{-1/2}$. Supporting electrolyte: 1 M HClO$_4$ saturated with air.

140

dioxygen diffusion constant ($cm^2\ s^{-1}$), [O_2] the bulk concentration of oxygen (mol dm^{-3}), and ω the rate of rotation (rad s^{-1}). From eq. 25, the plot of the limiting current density j ($j = i/A$) as a function of the square root of the electrode rotation rate $\omega^{1/2}$ should be a straight line intersecting the origin. Figure 7-2B shows that the Levich plot[212] of the plateau currents vs $\omega^{1/2}$ is curved as is typical for the electroreduction of O_2 catalyzed by adsorbed cobalt complexes.[72] The clear lack of linearity in the Levich plot suggests that the catalytic reaction is limited by kinetics and not by mass transport. A chemical step, previously assigned to the formation of a cobalt(III)-O_2 adduct (Chapter 5), precedes the electron transfer and limits the current to values below the convection–diffusion limit.

The reciprocal of the limiting current density was plotted against the reciprocal of the square root of the rotation rate (Figure 7-2C). The straight line obeys the Koutecky-Levich equation:[216,217]

$$\frac{1}{j} = \frac{1}{nFk[O_2]} + \frac{1}{0.62nF\upsilon^{1/6}D^{2/3}[O_2]}\frac{1}{\omega^{1/2}} \qquad \text{(eq. 26)}$$

For large values of $\omega^{1/2}$ ($\omega \rightarrow \infty$), the current is controlled by the kinetic process and reaches an asymptotic maximum value, j_k (mA cm^{-2}), which can be obtained experimentally from the intercept of the Koutecky–Levich line in Figure 7-2C.

$$j_k = 10^3 nF\Gamma k[O_2] \qquad \text{(eq. 27)}$$

where k is the second-order rate constant of the reaction ($M^{-1}\ s^{-1}$) which limits the plateau current and Γ (mol cm^{-2}) is the surface concentration of (F_5PhMes_2Cor)Co and the other terms have their usual significance as described previously. The slope of the Koutecky–Levich plot shows that the catalytic electroreduction of O_2 by (F_5PhMes_2Cor)Co is a two-electron process. The Koutecky–Levich plot for (TPFCor)Co (not shown) also indicates a

141

two-electron reduction of O_2 to H_2O_2 (Table 7-1) as previously reported in the literature.[232] In comparison, the number of electrons transferred is 2.9 for $(Me_4Ph_5Cor)Co$ (Table 7-1) indicating that the catalytic electroreduction of O_2 by the cobalt complex leads to formation of H_2O and H_2O_2 through processes involving both two-electron and four-electron reactions. The catalytic activity of $(Me_4Ph_5Cor)Co$ was attributed in Chapter 5 to the spontaneous dimerization (and higher aggregation) of this complex on the electrode surface. Such a van der Waals-driven association has also been reported for unsubstituted cobalt porphyrins[47,48] and is believed to create cobalt–cobalt separations that are small enough to permit O_2 molecules to coordinate simultaneously to two cobalt centers. One result of such orientation at the electrode surface is a weakening of the O−O bond which favors its breaking during the four-electron reduction of O_2 to H_2O.[46,47] For $(F_5PhMes_2Cor)Co$ and $(TPFCor)Co$, the two-electron reduction of O_2 clearly indicates that a dimerization (or oligomerization) does not occur for either complex because of steric interactions among the bulky phenyl *meso*-substituents.[48]

The j_k value obtained from the intercept of Figure 7-2 was used to calculate the second-order rate constant k for the formation of the $[(F_5PhMes_2Cor)Co^{III}O_2]$ complex on the electrode surface. The value calculated at pH = 0 using eq. 27 is $k = 1.7 \times 10^5$ M^{-1} s^{-1}, which is lower than that reported in Chapter 5 for the catalytic electroreduction of dioxygen at the $(Me_4Ph_5Cor)Co$-modified electrode ($k = 5.7 \times 10^5$ M^{-1} s^{-1}), but it is identical to the value reported for the electrocatalytic reduction of O_2 by the monocobalt porphyrin $(diethylesterMe_2Et_2P)Co$ ($k = 1.4 \times 10^5$ M^{-1} s^{-1}).[192]

7.2.2 Catalysis of O_2 Reduction by Dicobalt Porphyrin-Corrole Dyads Containing Aryl *Meso*-Substituents

We next sought to examine the eletrocatalytic properties of the dicobalt porphyrin–corrole dyads (PMes$_2$CX)Co$_2$, (PMes$_2$CO)Co$_2$ and (PMes$_2$COx)Co$_2$ under the same solution conditions. The catalytic activity of the dicobalt complexes towards the reduction of O_2 was examined by cyclic voltammetry as well as by rotating disk electrode voltammetry and the results are summarized in Table 7-2. When the solution is saturated with air, the cyclic voltammograms obtained at (PMes$_2$CY)Co$_2$-coated electrodes are characterized by a large reduction peak located at E_{pc} = 0.25–0.27 V, depending upon the spacer (see exact potential in Table 7-2). (PMes$_2$CX)Co$_2$, (PMes$_2$CO)Co$_2$ and (PMes$_2$COx)Co$_2$ catalyze the electroreduction of O_2 at potentials close to those observed for (F$_5$PhMes$_2$Cor)Co and (TPFCor)Co (E_{pc} = 0.24–0.25 V). Also, the average $E_{1/2}$ value for the electroreduction of O_2 at a rotating disk electrodes coated with (PMes$_2$CY)Co$_2$ is 0.32 V (Table 7-2) while (F$_5$PhMes$_2$Cor)Co and (TPFCor)Co show an average $E_{1/2}$ of 0.30 V (Table 7-1). The former value is also close to the measured $E_{1/2}$ for the Co(IV)/Co(III) process of the monocorroles (F$_5$PhMes$_2$Cor)Co and (TPFCor)Co in the absence of dioxygen (*vide supra*). This latter fact indicates that the cobalt corrole is in its +3 oxidation state in the catalytically active form of the (PMes$_2$CY)Co$_2$ dyads. A similar catalytic behavior was also observed for the free-base porphyrin–cobalt corrole dyads (PCY)H$_2$Co and the heterobimetallic porphyrin–corrole dyads (PCY)MClCoCl (M = Fe^{III}, Mn^{III}) which both catalyze the electroreduction of O_2 by more than two electrons at an average half-wave potential of 0.34 V (Chapters 5 and 6). Comparisons between the

Table 7-2. Electroreduction of Dioxygen by Adsorbed Dicobalt Porphyrin–Corrole Dyads in Air-Saturated 1 M $HClO_4$.

Bridge (Y)	$(PMes_2CY)Co_2$			$(PCY)Co_2$		
	$E_p{}^a$	$E_{1/2}{}^b$	n^c	$E_p{}^a$	$E_{1/2}{}^b$	n^c
X	0.25	0.32	2.5	0.38	0.45	3.7
O	0.25	0.32	2.4	0.34	0.41	3.5
Ox	0.27	0.33	2.5	0.35	0.40	3.1

Bridge

X   **O**   **Ox**

[a] Peak potential (V *vs* SCE) of the dioxygen reduction wave obtained by cyclic voltammetry (scan rate = 50 mV s^{-1}). [b] Half-wave potential (V *vs* SCE) for O_2 reduction at rotating disk electrode (ω = 100 rpm). [c] Electrons consumed in the reduction of O_2 as estimated from the slope of the Koutecky−Levich plots.

two series of porphyrin–corrole dyads (PCY)MClCoCl and (PMes$_2$CY)Co$_2$ suggest that the cobalt(III) corrole unit in the latter dyad may catalyze the electroreduction of O$_2$ whereas the cobalt porphyrin unit remains catalytically inactive towards O$_2$. This catalytic behavior contrasts with that observed for the unsubstituted derivatives (PCY)Co$_2$ which were shown to efficiently electrocatalyze the direct reduction of O$_2$ to H$_2$O at an average potential E$_{1/2}$ of 0.45 V (Chapter 4), thus indicating that the active form of the catalyst contains the cobalt(II) porphyrin moiety.

The number of electrons transferred in the O$_2$ electroreduction process determined by rotating disk voltammetry for (PMes$_2$CX)Co$_2$, (PMes$_2$CO)Co$_2$ and (PMes$_2$COx)Co$_2$ ranges from 2.4 to 2.5 (Table 7-2), indicating that the electrocatalytic reduction of O$_2$ by the dicobalt porphyrin–corrole dyads leads to the formation of H$_2$O$_2$ and H$_2$O through processes involving both 2e$^-$ and 4e$^-$ reactions. This catalytic behavior is similar to what is observed for the (PCY)H$_2$Co and (PCY)MClCoCl complexes (Chapters 5 and 6). The average n value for these latter compounds is 2.7 electrons transferred in the reduction of O$_2$ as compared to an average of $n = 2.5$ for the three (PMes$_2$CY)Co$_2$ dyads under the same experimental conditions. This is clearly different from the porphyrin–corrole dyads (PCY)Co$_2$ (Y = X and O), where $n = 3.5$–3.7 (Table 7-2) and O$_2$ is mainly reduced to H$_2$O through a four-electron, four-proton process. By replacing the rigid PCO spacer by the more flexible one, PCOx, the number of electrons transferred is still higher ($n = 3.1$) than that observed for (PMes$_2$COx)Co$_2$ ($n = 2.5$). One possible explanation about the low catalytic efficiency of mesityl-containing porphyrin–corrole dyads (PMes$_2$CY)Co$_2$ in the direct reduction of O$_2$ to H$_2$O is that steric interactions between the bulky substituents of the corrole and the porphyrin macrocycle induce ring lateral slippage[234] which could

disfavor the accommodation of oxygen intermediates during multielectron catalysis. The presence of electron-withdrawing *meso*-substituents in $(PMes_2CY)Co_2$ may also disfavor cleavage of the two formal O−O bonds required for the direct reduction of O_2 to H_2O. This substituent effect was proposed by Nocera *et al*. to explain the low catalytic efficiency toward O_2 by cofacial Pacman porphyrins bearing an aryl group trans to the spacer.[23] The authors also reported that the presence of aryl *meso*-substitutents in cofacial bisporphyrins lower the potential of O_2 reduction by an average of 130 mV compared to the unsubstituted derivatives which is in accord with the decrease in potential observed between $(PCY)Co_2$ ($E_{1/2}$ = 0.43 V) and $(PMes_2CY)Co_2$ ($E_{1/2}$ = 0.32 V) (Table 7-2).

7.3 Conclusion

The results of the present study have demonstrated that the catalytic behavior of cobalt porphyrin–corrole dyads toward the catalytic electroreduction of dioxygen is strongly influenced by the presence of substituents attached to the *meso* positions of the corrole ring. Cyclic voltammetry and rotating disk voltammetry demonstrate that the $(PMes_2CY)Co_2$ dyads exhibit a lower efficiency and a more negative potential for dioxygen reduction in acidic media than the unsubstituted derivatives $(PCY)Co_2$. The results of our studies indicate that O_2 is initially reduced by the cobalt(III) unit of $(PMes_2CY)Co_2$ whereas electroreduction of O_2 by $(PCY)Co_2$ is catalyzed by the cobalt(II) porphyrin unit in the dyad.

146

Chapter 8: General Conclusion

This dissertation presents the investigation of twenty-nine cobalt corrole complexes as catalysts for the electroreduction of dioxygen to water at a graphite electrode. Cyclic voltammetry and rotating ring–disk voltammetry were both used to examine the redox properties and the catalytic activity of the cobalt complexes in acidic media.

The mixed valent Co(II)/Co(III) complexes, (PCY)Co$_2$, where P represents a Co(II) porphyrin linked to a Co(III) corrole (C) by an anthracenyl (A), biphenylene (B), 9,9-dimethylxanthene (X), or a dibenzofuran (O) bridge, and the dicobalt biscorrole complexes, (BCY)Co$_2$, which contain two Co(III) ions in their air-stable forms, all provide a direct four-electron pathway for the reduction of O$_2$ to H$_2$O in aqueous acidic media when adsorbed on a graphite electrode. The half-wave potentials for dioxygen reduction range from 0.35 to 0.47 V for the (PCY)Co$_2$ and (BCY)Co$_2$ complexes when measured by rotating ring–disk voltammetry in 1 M HClO$_4$. The H$_2$O/H$_2$O$_2$ product ratios of the reduction differ for each set of compounds, with the most effective catalysts being (PCY)Co$_2$ which is in the mixed oxidation state Co(II)/Co(III) and gives almost exclusively a four-electron reduction of O$_2$ at $E_{1/2}$ = 0.41 to 0.47 V vs SCE. A four-electron reduction also occurs to some extent at the (BCY)Co$_2$-coated graphite electrodes and under these conditions O$_2$ reduction occurs at an $E_{1/2}$ of 0.35-0.39 V. The efficiency of the O$_2$ catalysis by (PCY)Co$_2$ and (BCY)Co$_2$ is slightly dependent upon the nature of the spacer Y. The most efficient process is observed in the case of complexes having an anthracene spacer. A relatively small amount of hydrogen peroxide (5%) was detected at the Pt ring electrode in the vicinity of $E_{1/2}$ which was located at 0.47 V vs SCE for the anthracene-bridge porphyrin-corrole (PCA)Co$_2$. In comparison, a larger amount of H$_2$O$_2$ is produced at the $E_{1/2}$ of 0.39 V (30%) in the case of (BCA)Co$_2$. The biscorrole is thus

148

less selective towards the four-electron reduction of O_2 to H_2O than the porphyrin–corrole dyad but more selective than the monocorrole $(Me_4Ph_5Cor)Co$, where 55% of H_2O_2 is produced from O_2 at $E_{1/2} = 0.38$ V. The electrocatalytic reduction of O_2 by this latter complex leads to the formation of H_2O and H_2O_2 through processes involving both two-electron and four-electron reactions. The catalytic activity of $(Me_4Ph_5Cor)Co$ was attributed to a spontaneous dimerization (and higher aggregation) of this complex on the electrode surface. This association would lead to cobalt–cobalt separations that are small enough to permit O_2 molecules to coordinate simultaneously to two cobalt centers and thus favor O−O bond cleavage during the four-electron reduction of O_2 to H_2O.

In the absence of dioxygen, the cyclic voltammogram of $(Me_4Ph_5Cor)Co$ adsorbed on a graphite disk shows three reversible processes located at $E_{1/2} = 0.38$, 0.20 and −0.08 V. The two redox processes at $E_{1/2} = 0.38$ V and 0.20 V corresponds to the reduction of a dioxidized and a monoxidized dimer, respectively, the latter being catalytically active towards the reduction of dioxygen. The presence of two redox processes is not observed for the porphyrin–corrole derivatives, $(PCY)H_2Co$, where one macrocycle is a cobalt(III) corrole and the other a free-base porphyrin. In comparison with $(Me_4Ph_5Cor)Co$, the reduction of $(PCY)H_2Co$ is characterized by a single redox process centered at $E_{1/2} = 0.37$ V which may be indicative of a weak dimerization of the dyads on the surface of the graphite electrode.

As part of this dissertation, we also examined the redox properties and catalytic reactivity towards O_2 of heterobimetallic face-to-face complexes of porphyrin–corrole dyads, $(PCY)MClCoCl$, M being either an iron(III) or manganese (III) ion and Y being an anthracenyl (A), biphenylene (B), 9,9-dimethylxanthene (X), or a dibenzofuran (O)

bridge. The (PCY)MClCoCl catalysts reduce O_2 to a mixture of H_2O_2 and H_2O and these reactions occur at $E_{1/2}$ values close to half-wave potentials for the conversion of (PCY)M^{III}ClCo^{IV}Cl to (PCY)M^{III}ClCo^{III}, *i.e.* the Co(IV)/Co(III) process of the corrole in the absence of dioxygen. A similar catalytic behavior is observed for the (PCY)H$_2$Co dyads which catalyze the electroreduction of O_2 by more than two electrons. The half-wave potentials for the catalytic reduction of O_2 by the heterobimetallic complexes range from 0.30 to 0.39 V and vary slightly as function of the specific bridge linking the porphyrin and corrole macrocycles. The most positive $E_{1/2}$ values are observed for dyads with the A or O bridges and the most negative for dyads with the X or B bridges.

In contrast to (PCY)H$_2$Co and (PCY)MClCoCl, the (PCY)Co$_2$ dyads catalyze the electroreduction of O_2 at an average potential which is much more positivie ($E_{1/2}$ = 0.45 V). The large difference in O_2 reduction potentials ($\Delta E_{1/2} \sim 110$ mV) observed between the dicobalt (PCY)Co$_2$ dyads and the monocobalt (PCY)MClCoCl and (PCY)H$_2$Co dyads indicates that the cobalt(II) porphyrin unit of (PCY)Co$_2$ catalyzes the electroreduction of O_2 whereas the cobalt corrole unit remains catalytically inactive towards O_2 since the Co(IV)/Co(III) corrole redox process occurs at significantly more negative half-wave potentials ($E_{1/2}$ = 0.38 V).

Finally, a series of *meso*-substituted cobalt corroles and dicobalt porphyrin-corroles were also investigated as part of this dissertation. The presence of bulky phenyl groups at the *meso* position of the corrole ring in (F$_5$PhMes$_2$Cor)Co and (TPFCor)Co has a significant effect on the catalytic electroreduction of O_2, shifting the reduction potentials negatively by about 80 mV as compared to the O_2 reduction potential observed for (Me$_4$Ph$_5$Cor)Co. This difference in reduction potentials was explained by the bulkiness

and orientation of the *meso*-subtituents which decrease the interaction between the corrole macrocyle and graphite. This effect is also observed for dicobalt porphyrin–corrole dyads (PMes$_2$C)Co$_2$ containing two mesityl groups at the *meso* positions of the corrole ring. These catalysts reduce O$_2$ at an average E$_{1/2}$ potential similar to those measured for Co(IV)/Co(III) process of the monocorroles (F$_5$PhMes$_2$C)Co and (TPFCor)Co. In comparison to (PCY)Co$_2$, the mesityl-substituted dyads also exhibit markedly reduced selectivities for the direct reduction of O$_2$ to H$_2$O over the two-proton, two-electron pathway to H$_2$O. One possible explanation of this catalytic behavior is that mesityl subsituents may sterically prevent a face-to-face arrangement of the two macrocycles and disfavor the accomodation of oxygen intermediates during multielectron catalysis. The electron-withdrawing effect of the *meso*-substituents in (PMes$_2$CY)Co$_2$ may also disfavor cleavage of the two formal O−O bonds required for the direct reduction of O$_2$ to H$_2$O.

BIBLIOGRAPHY

(1)   Lipkowski, J.; Ross, P. N., *Electrocatalysis*. Wiley, John & Sons, Inc.: 1998.

(2)   Ferguson-Miller, S.; Babcock, G.T., *Chem. Rev.* **1996,** 96, 2889-2907.

(3)   Wang, J. X.; Markovic, N. M.; Adzic, R. R., *J. Phys. Chem. B* **2004,** 108, 4127-4133.

(4)   Adzic, R., In *Electrocatalysis*, Lipkowski, J.; Ross, P. N., Eds. Wiley-VCH: New-York, 1998; p 197.

(5)   Chen, S.; Kucernak, A., *J. Phys. Chem. A* **2004,** 108, (10), 3262-3276.

(6)   Deronzier, A.; Moutet, J.-C., In *Comprehensive Coordination Chemistry II*, McCleverty, J. A.; Meyer, T. J., Eds. Elsevier: Oxford, 2004; Vol. 9, pp 471-507.

(7)   Goux, A.; Pauporté, T.; Lincot, D., *Electrochim. Acta* **2006,** 51, 3168-3172.

(8)   Fernández, J. L.; Walsh, D. A.; Bard, A. J., *J. Am. Chem. Soc.* **2005,** 127, (1), 357-365.

(9)   Léger, J.-M., *Electrochim. Acta* **2005,** 50, 3123-3129.

(10)   Stamenkovic, V.; Mun, B. S.; Mayrhofer, K. J. J.; Ross, P. N.; Markovic, N. M.; Rossmeisl, J.; Greeley, J.; Nørskov, J. K., *Angew. Chem., Int. Ed. Engl.* **2006,** 45, 2897-2901.

(11)   Mano, N.; Fernandez, J. L.; Kim, Y.; Shin, W.; Bard, A. J.; Heller, A., *J. Am. Chem. Soc.* **2003,** 125, 15290-15291.

(12)   Soukharev, V.; Mano, N.; Heller, A., *J. Am. Chem. Soc.* **2004,** 126, 8366-8369.

(13)   Zawisza, I.; Rogalski, J.; Opallo, M., *J. Electroanal. Chem.* **2006,** 588, 244-252.

(14)   Tammeveski, K.; Kontturi, K.; Nichols, R. J.; Potter, R. J.; Schiffrin, D. J., *J. Electroanal. Chem.* **2001,** 515, 101-112.

(15)   Manisankar, P.; Gomathi, H., *Electroanalysis* **2005,** 17, (12), 1051-1057.

(16)   Vaik, K.; Mäeorg, U.; Maschion, F. C.; Maia, G.; Schiffrin, D. J.; Tammeveski, K., *Electrochim. Acta* **2005,** 50, 5126-5131.

(17)   Wang, R.; Okajima, T.; Kitamura, F.; Kawauchi, S.; Matsumoto, N.; Thiemann, T.; Mataka, S.; Ohsaka, T., *J. Phys. Chem. A* **2004,** 108, (11), 1891-1899.

(18)   Andrieux, C. P.; Hapiot, P.; Saveant, J.-M., *J. Electroanal. Chem.* **1985,** 189, (1), 121-133.

(19)   Yamazaki, S.-I.; Yamda, Y.; Ioroi, T.; Fujiwara, N.; Siroma, Z.; Yasuda, K.; Miyazaki, Y., *J. Electroanal. Chem.* **2005,** 576, (2), 253-259.

(20)   Kang, C.; Anson, F. C., *Inorg. Chem.* **1995,** 34, 2771-2780.

(21)   Bhugun, I.; Anson, F. C., *Inorg. Chem.* **1996,** 35, 7253-7259.

(22)   Anson, F. C.; Shi, C.; Steiger, B., *Acc. Chem. Res.* **1997,** 30, (11), 437-444.

(23)   Chang, C. J.; Loh, Z.-H.; Shi, C.; Anson, F. C.; Nocera, D. G., *J. Am. Chem. Soc.* **2004,** 126, (32), 10013-10020.

(24)   Fukuzumi, S.; Okamoto, K.; Gros, C. P.; Guilard, R., *J. Am. Chem. Soc.* **2004,** 126, (33), 10441-10449.

(25)   Fukuzumi, S.; Okamoto, K.; Tokuda, Y.; Gros, C. P.; Guilard, R., *J. Am. Chem. Soc.* **2004,** 126, (51), 17059-17066.

(26)   Jasinski, R., *Nature* **1964,** 201, 1212-1213.

(27)   Collman, J. P.; Boulatov, R.; Sunderland, C. J., In *The Porphyrin Handbook*, Kadish, K. M.; Smith, K. M.; Guilard, R., Eds. Academic Press: Boston, 2003; Vol. 11, pp 1-50.

(28)   Bertini, I.; Cavallaro, G.; Rosato, A., *Chem. Rev.* **2006,** 106, 90-115.

(29)   Collman, J. P.; Fu, L.; Herrmann, P. C.; Wang, Z.; Rapta, M.; Bröring, M.; Schwenninger, R.; Boitrel, B., *Angew. Chem., Int. Ed. Engl.* **1998,** 37, (24), 3397-3400.

(30)   Kim, E.; Chufan, E. E.; Kamaraj, K.; Karlin, K. D., *Chem. Rev.* **2004,** 104, 1077-1133.

(31)   Tsukihara, T.; Aoyama, H.; Yamashita, E.; Tomizaki, T.; Yamaguchi, H.; Shinzawa-Itoh, K.; Nakashima, R.; Yahono, R.; Yoshikawa, S., *Science* **1995,** 269, (5227), 1069-1074.

(32)   Tsukihara, T.; Aoyama, H.; Yamashita, E.; Tomizaki, T.; Yamaguchi, H.; Shinzawa-Itoh, K.; Nakashima, R.; Yahono, R.; Yoshikawa, S., *Science* **1996,** 272, 1136-1144.

(33)   Yoshikawa, S.; Shinzawa-Itoh, K.; Nakashima, R.; Yaono, R.; Yamashita, E.; Inoue, E.; Yao, M.; Jei-Fei, M.; Libeu, C. P.; Mizushima, T.; Yamagushi, H.; Tomizaki, T.; Tsukihara, T., *Science* **1998,** 280, 1723-1729.

(34)   Collman, J. P.; Wagenknecht, P. S.; Hutchison, J. E., *Angew. Chem., Int. Ed. Engl.* **1994,** 33, 1537-1554.

(35)   Collman, J. P., *Inorg. Chem.* **1997,** 36, 5145-5155.

(36)   Collman, J. P.; Fu, L.; Herrmann, P. C.; Zhang, X., *Science* **1997,** 275, (5302), 949-951.

(37)   Collman, J. P.; Boulatov, R.; Sunderland, C. J.; Fu, L., *Chem. Rev.* **2004,** 104, 561-588.

(38)   Collman, J. P.; Herrmann, P. C.; Boitrel, B.; Zhang, X. M.; Eberspacher, T. A.; Fu, L.; Wang, J. L.; Rousseau, D. L.; Williams, E. R., *J. Am. Chem. Soc.* **1994,** 116, 9783.

(39)   Collman, J. P.; Rapta, M.; Broring, M.; Raptova, L.; Schwenninger, R.; Boitrel, B.; Fu, L.; L'Her, M., *J. Am. Chem. Soc.* **1999,** 121, 1387-1388.

(40)   Boulatov, R.; Collman, J. P.; Shiryaeva, I. M.; Sunderland, C. J., *J. Am. Chem. Soc.* **2002,** 124, 11923-11935.

(41)   Ricard, D.; Andrioletti, B.; Boitrel, B.; L'Her, M., *Chem. Commun.* **1999**, 1523-1524.

(42)   Ricard, D.; Didier, A.; L'Her, M.; Boitrel, B., *ChemBioChem* **2001,** 2, 144.

(43)   Ricard, D.; L'Her, M.; Richard, P.; Boitrel, B., *Chem. Eur. J.* **2001,** 7, (15), 3291-3297.

(44)   Boulatov, R.; Collman, J. P.; Shiryaeva, I. M.; Sunderland, C. J., *J. Am. Chem. Soc.* **2002,** 124, 11923-11935.

(45)   Shin, H.; Lee, D.-H.; Kang, C.; Karlin, K. D., *Electrochim. Acta* **2003,** 48, (27), 4077-4082.

(46)   Shi, C.; Steiger, B.; Yuasa, M.; Anson, F. C., *Inorg. Chem.* **1997,** 36, (20), 4294-4295.

(47)   Shi, C.; Anson, F. C., *Inorg. Chem.* **1998,** 37, (5), 1037-1043.

(48)   Song, E.; Shi, C.; Anson, F. C., *Langmuir* **1998,** 14, (15), 4315-4321.

(49)   Yuasa, M.; Nishihara, R.; Shi, C.; Anson, F. C., *Polym. Adv. Technol.* **2001,** 12, 266-270.

(50)   Yuasa, M.; Oyaizu, K.; Yamaguchi, H.; Kuwakado, M., *J. Am. Chem. Soc.* **2004,** 126, 11128-11129.

(51)   Yuasa, M.; Yamaguchi, A.; Oyaizu, K.; Fujito, Y.; Kitao, M.; Sato, T., *Polym. Adv. Technol.* **2005,** 16, 702-705.

(52)   Collman, J. P.; Boulatov, R.; Sunderland, C. J., In *The Porphyrin Handbook*, Academic Press: Boston, 2003; Vol. 11, pp 1-49.

(53)   Chang, C. K.; Abdalmuhdi, I., *Angew. Chem., Int. Ed. Engl.* **1984,** 96, (2), 154-155.

(54)   Chang, C. K.; Liu, H.-Y.; Abdalmuhdi, I., *J. Am. Chem. Soc.* **1984,** 106, 2725-2726.

(55)   Collman, J. P.; Hutchison, J. E.; Lopez, M. A.; Tabard, A.; Guilard, R.; Seok, W. K.; Ibers, J. A.; L'Her, M., *J. Am. Chem. Soc.* **1992,** 114, 9869-9877.

(56)   Chang, C. J.; Deng, Y.; Heyduk, A. F.; Chang, C. K.; Nocera, D. G., *Inorg. Chem.* **2000,** 39, (5), 959-966.

(57)   Chang, C. J.; Deng, Y.; Shi, C.; Chang, C. K.; Anson, F. C.; Nocera, D. G., *Chem. Commun.* **2000**, 1355-1356.

(58)   Deng, Y.; Chang, C. J.; Nocera, D. G., *J. Am. Chem. Soc.* **2000,** 122, 410-411.

(59)   Chang, C. K.; Baker, E. A.; Bradford, J. P.; Deng, Y.; Loh, Z.-H.; Miller, S. E.; Carpenter, S. D.; Nocera, D. G., *Inorg. Chem.* **2002,** 41, (12), 3102-3109.

(60)   Guilard, R.; Brandes, S.; Tabard, A.; Bouhmaida, N.; Lecomte, C.; Richard, P.; Latour, J.-M., *J. Am. Chem. Soc.* **1994,** 116, 10202-10211.

(61)   Guilard, R.; Brandes, S.; Tardieux, C.; Tabard, A.; L'Her, M.; Miry, C.; Gouerec, P.; Knop, Y.; Collman, J. P., *J. Am. Chem. Soc.* **1995,** 117, (47), 11721-11729.

(62)   Erben, C.; Will, S.; Kadish, K. M., In *The Porphyrin Handbook*, Kadish, K. M.; Smith, K. M.; Guilard, R., Eds. Academic Press: Boston, 2000; Vol. 2, pp 233-300.

(63)   Collman, J. P.; Zeng, L.; Decreau, R. A., *Chem. Commun.* **2003,** 24, 2974-2975.

(64)   Simkhovich, L.; Mahammed, A.; Goldberg, D. P.; Gross, Z., *Chem. Eur. J.* **2001,** 7, 1041-1055.

(65)   Mahammed, A.; Gray, H. B.; Meier-Callahan, A. E.; Gross, Z., *J. Am. Chem. Soc.* **2003,** 125, 1162-1163.

(66)   Jérome, F. Synthese et reactivite de derives bimacrocycliques face-a-face de type biscorrole et porphyrine-corrole. Universite de Bourgogne, Dijon, 2000.

(67)   Guilard, R.; Barbe, J.-M.; Stern, C.; Kadish, K. M., In *The Porphyrin Handbook*, Kadish, K. M.; Smith, K. M.; Guilard, R., Eds. Academic Press: Boston, 2003; Vol. 18, pp 303-349.

(68)   Burdet, F. Porphyrin-corrole homo- et heterobimetallaiques. Universite de Bourgogne, Dijon, 2004.

(69)   Barbe, J.-M.; Burdet, F.; Espinosa, E.; Guilard, R., *Eur. J. Inorg. Chem.* **2005**, (6), 1032-1041.

(70)   Guilard, R.; Burdet, F.; Barbe, J.-M.; Gros, C. P.; Espinosa, E.; Shao, J.; Ou, Z.; Zhan, R.; Kadish, K. M., *Inorg. Chem.* **2005,** 44, (11), 3972-3983.

(71)   Guilard, R.; Jérome, F.; Gros, C. P.; Barbe, J.-M.; Ou, Z.; Shao, J.; Kadish, K. M., *C. R. Acad. Sci., Ser. IIc: Chim.* **2001,** 4, (3), 245-254.

(72)   Liu, H.-Y.; Abdalmuhdi, I.; Chang, C. K.; Anson, F. C., *J. Phys. Chem.* **1985,** 89, 665-670.

(73)   Ni, C.-L.; Abdalmuhdi, I.; Chang, C. K.; Anson, F. C., *J. Phys. Chem.* **1987,** 91, 1158-1166.

(74)   Moss, G. P., *Pure Appl. Chem.* **1976,** 48, 495-502.

(75)   Moss, G. P., *Eur. J. Biochem.* **1988,** 178, (2), 277-328.

(76)   Johnson, A. W.; Kay, I. T., *J. Chem. Soc.* **1965**, 1620-1629.

(77)   Gouterman, M., *J. Mol. Spec.* **1961,** 6, 138-163.

(78)   Suslick, K. S.; Watson, R. A., *New J. Chem.* **1992,** 16, 633-642.

(79)   Anderson, H. L., *Chem. Commun.* **1999**, 2323-2330.

(80)   Kadish, K. M.; Van Caemelbecke, E.; Royal, G., In *The Porphyrin Handbook*, Kadish, K. M.; Guilard, R.; Smith, K. M., Eds. Academic Press: Boston, 2000; Vol. 8, pp 1-114.

(81)   Kadish, K. M.; Van Caemelbecke, E., *J. Solid State Electrochem.* **2003,** 7, 254-258.

(82)   Fukuzumi, S.; Nakanishi, I.; Barbe, J.-M.; Guilard, R.; Van Caemelbecke, E.; Guo, N.; Kadish, K. M., *Angew. Chem., Int. Ed. Engl.* **1999,** 38, (7), 964-966.

(83)   Ghosh, A.; Wondimagegn, T.; Parusel, A. B. J., *J. Am. Chem. Soc.* **2000,** 122, 5100-5104.

(84)   Weaver, J. J. Corroles. Ph.D., California Institute of Technology, Pasadena, 2005.

(85)   Kadish, K. M.; Smith, K. M.; Guilard, R., *The Porphyrin Handbook*. Academic Press: Boston, 2000 and 2003; Vol. 1-20.

(86)   Fukuzumi, S., In *The Porphyrin Handbook*, Kadish, K. M.; Smith, K. M.; Guilard, R., Eds. Academic Press: Boston, 2000; Vol. 8, pp 115-151.

(87)   Guilard, R.; Van Caemelbecke, E.; Tabard, A.; Kadish, K. M., In *The Porphyrin Handbook*, Kadish, K. M.; Guilard, R.; Smith, K. M., Eds. Academic Press: Boston, 2000; Vol. 3, pp 295-345.

(88)   Kadish, K. M.; Royal, G.; Van Caemelbecke, E.; Gueletti, L., In *The Porphyrin Handbook*, Kadish, K. M.; Guilard, R.; Smith, K. M., Eds. Academic Press: Boston, 2000; Vol. 9, pp 1-212.

(89)   Kadish, K. M.; Koh, W.; Tagliatesta, P.; Sazou, D.; Paolesse, R.; Licoccia, S.; Boschi, T., *Inorg. Chem.* **1992,** 31, (12), 2305-2313.

(90)   Paolesse, R., In *The Porphyrin Handbook*, Kadish, K. M.; Smith, K. M.; Guilard, R., Eds. Academic Press: Boston, 2000; Vol. 2, pp 201-232.

(91)   Nardis, S.; Monti, D.; Paolesse, R., *Mini-Rev. Org. Chem* **2005,** 2, 546-564.

(92)   Kadish, K. M.; Shao, J.; Ou, Z.; Gros, C. P.; Bolze, F.; Barbe, J.-M.; Guilard, R., *Inorg. Chem.* **2003,** 42, 4062-4070.

(93)   Barbe, J.-M.; Canard, G.; Brandès, S.; Jérôme, F.; Dubois, G.; Guilard, R., *J. Chem. Soc., Dalton Trans.* **2004**, 1208-1214.

(94)   Barbe, J.-M.; Stern, C.; Pacholska, E.; Espinosa, E.; Guilard, R., *J. Porphyrins Phthalocyanines* **2004,** 8, 301-312.

(95)   Guilard, R.; Gros, C. P.; Barbe, J.-M.; Espinosa, E.; Jerome, F.; Tabard, A.; Latour, J.-M.; Shao, J.; Ou, Z.; Kadish, K. M., *Inorg. Chem.* **2004,** 43, (23), 7441-7455.

(96)   Barbe, J.-M.; Canard, G.; Brandes, S.; Guilard, R., *Angew. Chem., Int. Ed. Engl.* **2005,** 44, 3103-3106.

(97)   Kadish, K. M.; Shao, J.; Ou, Z.; Zhan, R.; Burdet, F.; Barbe, J.-M.; Gros, C. P.; Guilard, R., *Inorg. Chem.* **2005,** 44, 9023-9038.

(98)   Rovira, C.; Kunc, K.; Hutter, J.; Parinello, M., *Inorg. Chem.* **2001,** 40, (1), 11-17.

(99)   Rovira, C.; Kunc, K.; Hutter, J.; Ballone, P.; Parrinello, M., *J. Phys. Chem. A* **1997,** 101, 8914-8925.

(100)   Liao, M.-S.; Watts, J. D.; Huang, M.-J., *J. Phys. Chem. A* **2005,** 109, 7988-8000.

(101)   Evangelio, E.; Ruiz-Molina, D., *Eur. J. Inorg. Chem.* **2005**, 2957-2971.

(102)   Will, S.; Lex, J.; Vogel, E.; Adamian, V. A.; Van Caemelbecke, E.; Kadish, K. M., *Inorg. Chem.* **1996,** 35, (19), 5577-5583.

(103)   Harmer, J.; Van Dorslaer, S.; Gromov, I.; Broring, M.; Jeschke, G.; Schweiger, A., *Journal of Physical Chemistry B* **2002,** 106, 2801-2811.

(104)   Kadish, K. M.; Shao, J.; Ou, Z.; Frémond, L.; Zhan, R.; Burdet, F.; Barbe, J.-M.; Gros, C. P.; Guilard, R., *Inorg. Chem.* **2005,** 44, (19), 6744-6754.

(105)   Hunter, C. A.; Sanders, J. K. M., *J. Am. Chem. Soc.* **1990,** 112, 5525-5534.

(106)   Ramdhanie, B.; Telser, J.; Caneschi, A.; Zakharov, L. N.; Rheingold, A. L.; Goldberg, D. P., *J. Am. Chem. Soc.* **2004,** 126, (8), 2515-2525.

(107)   Kadish, K. M.; Adamian, V. A.; Van Caemelbecke, E.; Gueletii, E.; Will, S.; Erben, C.; Vogel, E., *J. Am. Chem. Soc.* **1998,** 120, 11986.

(108)   Guilard, R.; Gros, C. P.; Bolze, F.; Jérome, F.; Ou, Z.; Shao, J.; Fischer, J.; Weiss, R.; Kadish, K. M., *Inorg. Chem.* **2001,** 40, 4845-4855.

(109)   Guilard, R.; Jérome, F.; Barbe, J.-M.; Gros, C. P.; Ou, Z.; Shao, J.; Fischer, J.; Weiss, R.; Kadish, K. M., *Inorg. Chem.* **2001,** 40, 4856-4865.

(110)   Jérome, F.; Barbe, J.-M.; Gros, C. P.; Guilard, R.; Fischer, J.; Weiss, R., *New J. Chem.* **2001,** 25, 93-101.

(111)   Kadish, K. M.; Ou, Z.; Shao, J.; Gros, C. P.; Barbe, J.-M.; Jérome, F.; Bolze, F.; Burdet, F.; Guilard, R., *Inorg. Chem.* **2002,** 41, 3990-4005.

(112)   Barbe, J.-M.; Burdet, F.; Espinosa, E.; Gros, C. P.; Guilard, R., *J. Porphyrins Phthalocyanines* **2003,** 7, (4 & 5), 365-374.

(113)   L'Her, M., In *Encyclopedia of Electrochemistry*, Bard, A. J.; Stratmann, M., Eds. Wiley-VCH: Weinheim, 2006; Vol. 7a, pp 119-142.

(114)   Collman, J. P.; Denisevich, P.; Konai, Y.; Marrocco, M.; Koval, C.; Anson, F. C., *J. Am. Chem. Soc.* **1980,** 102, 6027-6036.

(115)   Zagal, J. H., *Coord. Chem. Rev.* **1992,** 119, 89-136.

(116)   Fridowich, I., *Biosci.* **1977,** 27, (7), 462-466.

(117)   Hyman, M. P.; Medlin, J. W., *J. Phys. Chem. B* **2006,** 110, 15338-15344.

(118)   Shi, Z.; Zhang, J.; Liu, Z.-S.; Wang, H.; Wilkinson, D. P., *Electrochim. Acta* **2006,** 51, 1905-1916.

(119)   Maciá, M. D.; Campina, J. M.; Herrero, E.; Feliu, J. M., *J. Electroanal. Chem.* **2004,** 564, 141-150.

(120)   Kim, J.; Gewirth, A. A., *J. Phys. Chem. B* **2006,** 110, 2565-2571.

(121)   Shao, M.-H.; Liu, P.; Adzic, R. R., *J. Am. Chem. Soc.* **2006,** 128, 7408-7409.

(122)   Sode, A.; Li, W.; Yang, Y.; Wong, P. C.; Gyenge, E.; Mitchell, K. A. R.; Bizzotto, D., *J. Phys. Chem. B* **2006,** 110, (17), 8715-8722.

(123)   Hsueh, K.-L.; Chin, D.-T.; Srinivasan, S., *J. Electroanal. Chem.* **1983,** 153, (1-2), 79-95.

(124)   Šljukić, B.; Banks, C. E.; Compton, R. G., *J. Iranian Chem. Soc.* **2005,** 2, (1), 1-25.

(125)   Yeager, E.; Krouse, P.; Rao, K. V., *Electrochim. Acta* **1964,** 9, (8), 1057-1070.

(126)   McCreery, R. L., In *Electroanalytical Chemistry*, Bard, A. J., Ed. Marcel Dekker, Inc.: New York, 1990; Vol. 17, pp 221-374.

(127)   Xu, J.; Huang, W.; McCreery, R. L., *J. Electroanal. Chem.* **1996,** 410, 235-242.

(128)   Yang, H.-H.; McCreery, R. L., *J. Electroanal. Chem.* **2000,** 147, (9), 3420-3428.

(129)   Morcos, I.; Yeager, E., *Electrochim. Acta* **1970,** 15, 953-975.

(130)   Yang, J.; Huang, P., *Chem. Mater.* **2000,** 12, (9), 2693-2697.

(131)   Maldonado, S.; Stevenson, K. J., *J. Phys. Chem. B* **2004,** 108, (31), 11375-11383.

(132)   Maldonado, S.; Stevenson, K. J., *J. Phys. Chem. B* **2005,** 109, 4707-4716.

(133)   Kobayashi, N.; Nevin, W. A., *Appl. Organometal. Chem.* **1996,** 10, (8), 579-590.

(134)   Durand, R. R., Jr.; Collman, J. P.; Anson, F. C., *J. Electroanal. Chem.* **1983,** 151, (1-2), 289-294.

(135)   Le Mest, Y.; L'Her, M.; Collman, J. P.; Hendricks, N. H.; McElwee-White, L., *J. Am. Chem. Soc.* **1986,** 108, (3), 533-535.

(136)   Geiger, T.; Anson, F. C., *J. Am. Chem. Soc.* **1981,** 103, 7489-7496.

(137)   Kang, C.; Xie, Y.; Anson, F. C., *J. Electroanal. Chem.* **1996,** 413, 165-174.

(138)   Wong, C.-L.; Switzer, J. A.; Balakrishnan, K. P.; Endicott, J. F., *J. Am. Chem. Soc.* **1980,** 102, (17), 5511-5518.

(139)   Wong, C.-L.; Endicott, J. F., *Inorg. Chem.* **1981,** 20, (7), 2233-2239.

(140)   Kumar, K.; Endicott, J. F., *Inorg. Chem.* **1984,** 23, (16), 2447-2452.

(141)   Wang, W.-D.; Bakac, A.; Espenson, J. H., *Inorg. Chem.* **1995,** 34, (16), 4049-4056.

(142)   Fukuzumi, S.; Okamoto, K.; Gros, C. P.; Guilard, R., *J. Am. Chem. Soc.* **2004,** 126, 10441-10449.

(143)   Fukuzumi, S.; Okamoto, K.; Tokuda, Y.; Gros, C. P.; Guilard, R., *J. Am. Chem. Soc.* **2004,** 126, 17059-17066.

(144)   Murray, R. W., *Molecular design of electrode surfaces*. Wiley, John and Sons: 1992.

(145)   Durst, R. A.; Baumner, A. J.; Murray, R. W.; Buck, R. P.; Andrieux, C. P., *Pure Appl. Chem.* **1997,** 69, (6), 1317-1323.

(146)   Kutner, W.; Wang, J.; L'Her, M.; Buck, R. P., *Pure Appl. Chem.* **1998,** 70, (6), 1301-1318.

(147)   Johnson, M. J.; Peters, D. G., In *Encyclopedia of Electrochemistry*, Bard, A. J.; Stratmann, M., Eds. Wiley-VCH: Weinheim, 2006; Vol. 7a, pp 531-555.

(148)   Elliot, C. M.; Murray, R. W., *Anal. Chem.* **1976,** 48, (8), 1247-1254.

(149)   Murray, R. W., *Acc. Chem. Res.* **1980,** 13, (5), 135-141.

(150)   Murray, R. W., In *Electroanalytical Chemistry*, Bard, A. J., Ed. Dekker, M.: New York, 1984; Vol. 13, pp 191-368.

(151)   Murray, R. W.; Ewing, A. G.; Durst, R. A., *Anal. Chem.* **1987,** 59, (5), 379A-389A.

(152)   Zen, J.-M.; Kumar, A. S.; Tsai, D.-M., *Electroanalysis* **2003,** 15, (13), 1073-1087.

(153)   Lever, A. B. P.; Ma, Y., In *Trends in Molecular Electrochemistry*, Pombeiro, A. J. L.; Amatore, C., Eds. FontisMedia S.A.: Lausanne, 2004; pp 99-126.

(154)   Andrieux, C. P.; Saveant, J.-M., *J. Electroanal. Chem.* **1978,** 93, 163-168.

(155)   Laviron, E., *J. Electroanal. Chem.* **1982,** 131, 61-75.

(156)   Aoki, K.; Tokuda, K.; Matsuda, H., *J. Electroanal. Chem.* **1986,** 199, 69-79.

(157)   Xie, Y.; Anson, F. C., *J. Electroanal. Chem.* **1995,** 384, 145-153.

(158)   Xie, Y.; Anson, F. C., *J. Electroanal. Chem.* **1995,** 396, 441-449.

(159)   Xie, Y.; Anson, F. C., *J. Electroanal. Chem.* **1996,** 404, 209-213.

(160)   Lyons, M. E. G., *Sensors* **2001,** 1, 215-228.

(161)   Lyons, M. E. G., *Sensors* **2002,** 2, 314-330.

(162)   Lyons, M. E. G., *Sensors* **2002,** 2, (12), 473-506.

(163)   Lyons, M. E. G., *J. Electroanal. Chem.* **2003,** 3, 19-42.

(164)   Sarapuu, A.; Vaik, K.; Schiffrin, D. J.; Tammeveski, K., *J. Electroanal. Chem.*
2003, 541, 23-29.

(165)   Hossain, M. S.; Tryk, D.; Yeager, E., *Electrochim. Acta* **1989,** 34, (12), 1733-
1737.

(166)   Mirkhalaf, F.; Tammeveski, K.; Schiffrin, D. J., *Phys. Chem. Chem. Phys.* **2004,**
6, (6), 1321-1327.

(167)   Vaik, K.; Sarapuu, A.; Tammeveski, K.; Mirkhalaf, F.; Schiffrin, D. J., *J.
Electroanal. Chem.* **2004,** 564, (1-2), 159-166.

(168)   Sarapuu, A.; Helstein, K.; Schiffrin, D. J.; Tammeveski, K., *Electrochem. Solid-
State Lett.* **2005,** 8, (2), E30-E33.

(169)   Golabi, S. M.; Raoof, J. B., *J. Electroanal. Chem.* **1996,** 416, 75-82.

(170)   Salimi, A.; Eshghi, H.; Sharghi, H.; Golabi, S. M.; Shamsipur, M.,
Electroanalysis **1999,** 11, (2), 114-119.

(171)   Durand, R. R., Jr.; Anson, F. C., *J. Electroanal. Chem.* **1982,** 134, 273-289.

(172)   Shigehara, K.; Anson, F. C., *J. Phys. Chem.* **1982,** 86, 2776-2783.

(173)   Shi, C.; Anson, F. C., *Inorg. Chem.* **1990,** 29, (21), 4298-4305.

(174)   Khorasani-Motlagh, M.; Noroozifar, M.; Ghaemi, A.; Safari, N., *J. Electroanal. Chem.* **2004,** 565, (1), 115.

(175)   D'Souza, F.; Hsieh, Y.-Y.; Deviprasad, G. R., *Chem. Commun.* **1998**, 1027-1028.

(176)   Steiger, B.; Anson, F. C., *Inorg. Chem.* **1997,** 36, 4138-4140.

(177)   Winnischofer, H.; Otake, V. Y.; Dovidauskas, S.; Nakamura, M.; Toma, H. E.; Araki, K., *Electrochim. Acta* **2004,** 49, (22-23), 3711-3718.

(178)   Collman, J. P.; Shiryaeva, I. M.; Boulatov, R., *Inorg. Chem.* **2003,** 42, 4807.

(179)   Collman, J. P.; Chong, A. O.; Jameson, G. B.; Oakley, R. T.; Rose, E.; Schmittou, E. R.; Ibers, J. A., *J. Am. Chem. Soc.* **1981,** 103, (3), 516-533.

(180)   Hatada, M. H.; Tulinsky, A.; Chang, C. K., *J. Am. Chem. Soc.* **1980,** 102, 7115.

(181)   Collman, J. P.; Anson, F. C.; Barnes, C. E.; Bencosme, C. S.; Geiger, T.; Evitt, E. R.; Kreh, R. P.; Meier, K.; Pettman, R. B., *J. Am. Chem. Soc.* **1983,** 105, (9), 2694-2699.

(182)   Collman, J. P.; Bencosme, C. S.; Barnes, C. E.; Miller, L. L., *J. Am. Chem. Soc.* **1983,** 105, 2704-2710.

(183)   Collman, J. P.; Hendricks, N. H.; Leidner, C. R.; Ngameni, E.; L'Her, M., *Inorg. Chem.* **1988,** 27, 387-393.

(184)   Karaman, R.; Seungwon, J.; Almarsson, O.; Bruice, T. C., *J. Am. Chem. Soc.* **1992,** 114, 4899-4905.

(185)   Collman, J. P.; Hutchison, J. E.; Lopez, M. A.; Guilard, R., *J. Am. Chem. Soc.* **1992,** 114, 8066-8073.

(186)   Guilard, R.; Lopez, M. A.; Tabard, A.; Richard, P.; Lecomte, C.; Brandes, S.; Hutchison, J. E.; Collman, J. P., *J. Am. Chem. Soc.* **1992,** 114, (25), 9877-9889.

(187)   Barbe, J.-M.; Guilard, R., In *The Porphyrin Handbook*, Kadish, K. M.; Smith, K. M.; Guilard, R., Eds. Academic Press: Boston, 2000; Vol. 3, pp 211-244.

(188)   Collman, J. P.; Anson, F. C.; Barnes, C. E.; Bencosme, C. S.; Geiger, T.; Evitt, E. R.; Kreh, R. P.; Meier, K.; Pettman, R. B., *J. Am. Chem. Soc.* **1983,** 105, 2694-2699.

(189)   Le Mest, Y.; L'Her, M.; Courtot-Coupez, J.; Collman, J. P.; Evitt, E. R.; Bencosme, C. S., *J. Chem. Soc., Chem. Commun.* **1983**, 1286.

(190)   Le Mest, Y.; L'Her, M.; Collman, J. P.; Kim, K.; Hendricks, N. H.; Helm, S., *J. Electroanal. Chem.* **1987,** 234, 277-295.

(191)   Collman, J. P.; Hendricks, N. H.; Leidner, C. R.; Ngameni, E.; L'Her, M., *Inorg. Chem.* **1988,** 27, 387-393.

(192)   Durand, R. R., Jr.; Bencosme, C. S.; Collman, J. P.; Anson, F. C., *J. Am. Chem. Soc.* **1983,** 105, 2710-2718.

(193)   Hutchison, J. E.; Postlethwaite, T. A.; Chen, C.-H.; Hathcock, K. W.; Ingram, R. S.; Ou, W.; Linton, R. W.; Murray, R. W., *Langmuir* **1997,** 13, 2143.

(194)   Collman, J. P.; Hutchison, J. E.; Lopez, M. A.; Guilard, R.; Reed, R., *J. Am. Chem. Soc.* **1991,** 113, 2794-2796.

(195)   Liu, H.-Y.; Weaver, M. J.; Wang, C. B.; Chang, C. K., *J. Electroanal. Interfacial Electrochem.* **1983,** 145, (2), 439-447.

(196)   Chang, C. K.; Abdalmuhdi, I., *Angew. Chem., Int. Ed. Engl.* **1984,** 23, 164-165.

(197)   Chang, C. J.; Deng, Y.; Heyduk, A. F.; Chang, C. K.; Nocera, D. G., *Inorg. Chem.* **2000,** 39, 959-966.

(198)   Collman, J. P.; Hutchison, J. E.; Lopez, M. A.; Tabard, A.; Guilard, R.; Seok, W. K.; Ibers, J. A.; L'Her, M., *J. Am. Chem. Soc.* **1992,** 114, (25), 9869-9877.

(199)   Bolze, F.; Gros, C. P.; Drouin, M.; Espinosa, E.; Harvey, P. D.; Guilard, R., *J. Organomet. Chem.* **2002,** 643-644, 89-97.

(200)   Chang, C. K., *J. Chem. Soc., Chem. Commun.* **1977**, 800.

(201)   Le Mest, Y.; Inisan, C.; Laouenan, A.; L'Her, M.; Talarmin, J.; El Khalifa, M.; Saillard, J.-Y., *J. Am. Chem. Soc.* **1997,** 119, 6095-6106.

(202)   Light, T. S., *Anal. Chem.* **1972,** 44, (6), 1038-1039.

(203)   Conway, B. E.; Angerstein-Kozlowska, H.; Sharp, W. B. A.; Criddle, E. E., *Anal. Chem.* **1973,** 45, (8), 1331-1336.

(204)   Hsueh, K.-L.; Gonzalez, E. R.; Srinivasan, S., *Electrochim. Acta* **1983,** 28, (5), 691-697.

(205)   Millero, F. J.; Huang, F., *J. Chem. Eng. Data* **2003,** 48, 1050-1054.

(206)   Millero, F. J.; Huang, F.; Laferiere, A. L., *Geochim. Cosmochim. Acta* **2002,** 66, (13), 2349-2359.

(207)   Clegg, S. L.; Brimblecombe, P., *Geochim. Cosmochim. Acta* **1990,** 54, 3315-3328.

(208)   Davies, T. J.; Moore, R. R.; Banks, C. E.; Compton, R. G., *J. Electroanal. Chem.* **2004,** 574, 123-152.

(209)   Davies, T. J.; Hyde, M. E.; Compton, R. G., *Angew. Chem., Int. Ed. Engl.* **2005,** 44, 5121-5126.

(210)   Kneten, K. R.; McCreery, R. L., *Anal. Chem.* **1992,** 64, (21), 2518-2524.

(211)   Banks, C. E.; Davies, T. J.; Wildgoose, G. G.; Compton, R. G., *Chem. Commun.* **2005**, 829-841.

(212)   Levich, V. G., *Physicochemical Hydrodynamics*. Prentice Hall: Englewood Cliffs, NJ, 1962.

(213)   Nikolic, J.; Expósito, E.; Iniesta, J.; González-Garcia, J.; Montiel, V., *J. Chem. Educ.* **2000,** 77, (9), 1191-1194.

(214)   Bard, A. J.; Faulkner, L. R., *Electrochemical Methods: Fundamentals and Applications*. 2nd ed.; John Wiley & Sons, Inc: New York, 2001.

(215)   Galus, Z.; Adams, R. N., *J. Phys. Chem.* **1963,** 67, 866-871.

(216)   Koutecky, J.; Levich, V. G., *Zh. Fiz. Khim.* **1956,** 32, 1565.

(217)   Oyama, N.; Anson, F. C., *Anal. Chem.* **1980,** 52, 1192-1198.

(218)   Lefevre, M.; Dodelet, J.-P., *Electrochim. Acta* **2003,** 48, 2749-2760.

(219)   Le Mest, Y.; L'Her, M.; Hendricks, N. H.; Kim, K.; Collman, J. P., *Inorg. Chem.* **1992,** 31, 835-847.

(220)   Le Mest, Y.; L'Her, M., *J. Chem. Soc., Chem. Commun.* **1995**, 1441-1442.

(221)   Le Mest, Y.; L'Her, M.; Saillard, J.-Y., *Inorg. Chim. Acta* **1996,** 248, 181-191.

(222)   Collman, J. P.; Marrocco, M.; Denisevich, P.; Koval, C.; Anson, F. C., *J. Electroanal. Chem.* **1979,** 101, 117-122.

(223)   Licoccia, S.; Paolesse, R., *Structure and Bonding* **1995,** 84, 71-133.

(224)   Anson, F. C.; Ni, C.-L.; Saveant, J.-M., *J. Am. Chem. Soc.* **1985,** 107, 3442-3450.

(225)   Yuasa, M.; Steiger, B.; Anson, F. C., *J. Porphyrins Phthalocyanines* **1997,** 1, 181-188.

(226)   Steiger, B.; Anson, F. C., *Inorg. Chem.* **2000,** 39, 4579-4585.

(227)   Shi, C.; Anson, F. C., *Inorg. Chem.* **2001,** 40, 5829-5833.

(228)   Treimer, S.; Tang, A.; Johnson, D. C., *Electroanalysis* **2002,** 14, (3), 165-171.

(229)   Kadish, K. M.; Burdet, F.; Jerome, F.; Barbe, J.-M.; Ou, Z.; Shao, J.; Guilard, R.,
J. Organomet. Chem. **2002,** 652, 69.

(230)   Kadish, K. M.; Frémond, L.; Ou, Z.; Shao, J.; Shi, C.; Anson, F. C.; Burdet, F.;
Gros, C. P.; Barbe, J.-M.; Guilard, R., *J. Am. Chem. Soc.* **2005,** 127, 5625-5631.

(231)   Didier, A.; L'Her, M.; Boitrel, B., *Org. Biomol. Chem.* **2003**, 1274-1276.

(232)   Collman, J. P.; Kaplun, M.; Decréau, R. A., *Dalton Trans.* **2006**, 554-559.

(233)   Unpublished Work

(234)   Gros, C. P.; Brisach, F.; Meristoudi, A.; Espinosa, E.; Guilard, R.; Harvey, P. D.,
Inorg. Chem. **2007,** 46, (1), 125-135.